

## 4.11 Dynamic Triggering

DP Hill, US Geological Survey, Volcano Science Center, Menlo Park, CA, USA

SG Prejean, US Geological Survey, Alaska Volcano Observatory, Anchorage, AK, USA

© 2015 Elsevier B.V. All rights reserved.

<b>4.11.1</b>	<b>Introduction</b>	274
4.11.1.1	Stress Transfer Modes	274
4.11.1.2	Static and Quasistatic Stress Triggering	274
4.11.1.3	Dynamic Stress Triggering	275
4.11.1.4	Triggered or Coincidental?	276
<b>4.11.2</b>	<b>Early Inferences on Dynamic Triggering and Preinstrumental Examples</b>	276
<b>4.11.3</b>	<b>Instrumental Evidence for Dynamic Triggering</b>	277
4.11.3.1	Widespread Dynamic Triggering in the Seismogenic Crust	278
4.11.3.2	Dynamic Triggering of Volcanic/Geothermal and Hydrologic Systems	282
4.11.3.3	Dynamic Triggering of Tectonic (Nonvolcanic) Tremor in the Transitional Domain	284
<b>4.11.4</b>	<b>Triggered Response Characteristics</b>	285
4.11.4.1	The Global Search for a Triggering Threshold	285
4.11.4.2	Aftershocks and Stress Triggering at Near-to-Intermediate Distance	287
4.11.4.3	Tectonic Setting and Source Radiation Patterns	288
4.11.4.4	Onsets, Delay Times, Durations, and Repeat Intervals	290
4.11.4.5	Triggering and Modulation by Solid Earth Tides	291
4.11.4.6	Earthquake Hazard Implications of Dynamic Triggering	291
<b>4.11.5</b>	<b>Proposed Models</b>	292
4.11.5.1	Triggering by Frictional Failure	292
4.11.5.1.1	Coulomb failure under dynamic stresses	292
4.11.5.1.2	Nonlinear friction	296
4.11.5.2	Triggering Through Excitation of Crustal Fluids	296
4.11.5.2.1	Hydrous fluid transport: changes in permeability and pore pressure	297
4.11.5.2.2	Magmatic fluids	297
<b>4.11.6</b>	<b>Challenges for the Future</b>	298
<b>4.11.7</b>	<b>Conclusions</b>	299
<b>Acknowledgments</b>		299
<b>References</b>		299

### Abbreviations

CFF	Coulomb failure function
ETAS	Statistical model for epidemic-type aftershock sequences

ETS	Episodic tremor and slip
-----	--------------------------

### Symbols

$\sigma_n^*$	Rock matrix stress component	$M_s$	Surface-wave magnitude
$c$	Constant in Omori's law (eqn [1])	$M_w$	Moment magnitude
$C$	Cohesive strength	$n(t)$	Number of earthquakes per unit time
$C_T$	Tensile strength	$p$	Constant in Omori's law (eqn [1])
$g$	Gravitational acceleration	$P$	Pore pressure
$G_i, R_i$	( $i = 1, 2, \dots$ ) Love and Rayleigh waves circling the globe $i$ times	$P(\gamma)$	Triggering potential as a function of incidence angle
$k$	Constant in Omori's law (eqn [1])	$R, R(t)$	Radius in Mohr's circle $1/2 (\sigma_1 - \sigma_3)$ : see Figure 8
$K_i$	Constant values for CFF; $i = 1, 2, 3, \dots$ (Figure 8(a))	$t$	Time
$L$	Semimajor axis of a dynamic stress orbit	$t_0$	Arrival time of dynamic stresses (seismic waves)
$M$	Local magnitude	$t_1$	Onset of triggered response
$M_0$	Seismic moment	$t_2$	Termination of dynamic stresses
		$V_p, V_s$	P- and S-wave phase velocities

$\Delta CFF$	Static change in CFF	$\theta_c$	Critical angle for failure on an optimally oriented fault
$\Delta t$	Delay time ( $t_1 - t_0$ )	$\theta(t)$	Angle between the least principal stress, $\sigma_3$ , and a fault plane
$\Delta$	Epicentral distance (km); Rayleigh wave dilatational stress	$\rho$	Density
$T_p$	Peak dynamic stress	$\sigma_1, \sigma_3$	Greatest and least principal stress components
$T$	Traction acting on a fault plane at angle in Mohr's circle diagram (Figure 9)	$\sigma_m$	Mean stress, $\frac{1}{2}(\sigma_1 + \sigma_3)$
$\beta$	Beta statistic	$\sigma_n$	Effective normal stress component ( $\sigma_n^* - P$ )
$\delta CFF(t)$	Dynamic change in CFF	$\sigma_z$	Vertical principal stress
$\epsilon_p$	Peak dynamic strain	$\tau_s, \tau_d$	Shear stress components: $\tau_s$ strike parallel; $\tau_d$ dip parallel
$\gamma$	Seismic-wave incidence angle with respect to fault strike	$ \delta CFF _m$	Absolute value of maximum $\delta CFF(t)$ (see Figure 8(b))
$\mu_d(t)$	Dynamic coefficient of friction		
$\mu_s$	Static coefficient of friction		

### 4.11.1 Introduction

One of the outstanding questions in earthquake seismology involves the nature of short-term processes that ultimately trigger slip on a given fault. The Earth's crust is pervasively laced with faults, and multiple lines of evidence indicate that the brittle crust is in some sense critically stressed and in a state of incipient failure nearly everywhere (Zoback and Zoback, 2002). Because long-wavelength stresses associated with the relative motion of major tectonic plates accumulate relatively slowly (rates of  $\sim 10^{-5}$  MPa year $^{-1}$  or less), regional stresses may remain incrementally below the frictional strength of faults (typically on the order of  $\sim 10$ –100 MPa) for periods of decades to centuries. Insight into the triggering question thus depends on understanding the influence of short-term, short-wavelength fluctuations in both the stress field and the fault strength, such that the local stress state temporarily exceeds the local failure threshold leading to slip nucleation and an earthquake.

Sources of short- to mid-term stress fluctuations in the crust are many. Those most likely to be significant at seismogenic depths include (1) other earthquakes in the crust (Das and Scholz, 1981; Freed, 2005; Harris, 1998; Steacy et al., 2005; Chapter 4.10), (2) magmatic intrusions (Hill et al., 2002; Manga and Brodsky, 2006; Savage and Clark, 1982), (3) anthropogenic activities such as reservoir filling, mining, and fluid injection or withdrawal (McGarr et al., 2002), (4) solid Earth tides (Cochran et al., 2004; Thomas et al., 2009, 2012), (5) seasonal meteorologic factors such as snow loading and groundwater recharge (Christiansen et al., 2005; Miller, 2008), and (6) long-term static and quasistatic stressing by ocean loading (Luttrell and Sandwell, 2010) and glacial rebound (Wu and Johnston, 2000). Local fluctuations in fault strength may result from changes in fluid pore pressure within a fault zone (Lockner and Beeler, 2002), the nonlinear response of fault zone friction to small perturbations in local stresses (Dieterich, 1979, Chapter 4.04, this volume; Johnson and Jia, 2005), and subcritical crack growth (Atkinson, 1984).

In this chapter, we are concerned with slip nucleation triggered either directly or indirectly by dynamic stress. Our principal focus will be on the evidence for dynamic stresses in the form of seismic waves triggering earthquakes in the seismogenic crust (the brittle domain) and tectonic tremor (nonvolcanic tremor) in the brittle–plastic transition at depths of

20–40 km along major plate-boundary faults. We include evidence for tidal triggering as a low-frequency, low-amplitude reference point for the spectral range of oscillatory stressing with the potential for dynamic triggering. Because many sites displaying remotely triggered seismicity are volcanic and geothermal areas, our scope includes the response of magmatic, hydrothermal, and hydrologic systems to dynamic stresses as potential sources for locally triggered seismicity. We conclude with a perspective on key challenges to be met in advancing understanding of dynamic triggering and its implications for active crustal processes. Also see Prejean and Hill (2009).

#### 4.11.1.1 Stress Transfer Modes

Earthquake–earthquake interactions in the form of mainshock–aftershock sequences have been recognized since the late 1800s and the emergence of seismology as a quantitative science (Omori, 1894). With the global expansion of high-quality seismic networks coupled with the capabilities for resolving detailed spatial–temporal variations in deformation patterns afforded by borehole strain meters, tiltmeters, and satellite geodesy (continuous GPS and InSAR technologies in particular), it has become increasingly clear that stress changes resulting from sufficiently large earthquakes are capable of triggering a detectable response including earthquake activity, aseismic slip, and changes in volcanic and hydrothermal/hydrologic systems over a surprisingly wide range of distances and timescales. As currently understood, earthquake interactions are generally placed under one of the three rather general stress transfer modes: (1) static, (2) quasistatic, or (3) dynamic.

#### 4.11.1.2 Static and Quasistatic Stress Triggering

Research on earthquake interactions associated with the change in the static stress field (static stress triggering) from just before an earthquake to shortly after the dynamic stresses from the seismic waves have decayed away began in the late 1960s and blossomed in the early 1990s with the growing availability of high-quality seismic and deformation data against which to test the patterns predicted by elastic dislocation models (Das and Scholz, 1981; Harris, 1998; Chapter 4.10, this volume; King and Cocco, 2001; Stein, 1999). Shortly thereafter, extensions of the dislocation models were developed to account for gradual stress changes

(quasistatic stress triggering) associated with viscous relaxation of the plastic lower crust and upper mantle in response to the sudden dislocation (an earthquake) across a fault in the overlying brittle crust (Pollitz and Sacks, 2002). Both the static and quasistress interaction modes appeal to the permanent stress change produced by the triggering earthquake or external loads including filling of reservoirs, ocean and glacier loading, (e.g., Harris, 1998; Hudnut et al., 1989; Kilb et al., 2002; Luttrell and Sandwell, 2010; Stein and Lisowski, 1983).

Because static stress changes resulting from an earthquake decay relatively rapidly with distance (as  $\sim \Delta^{-3}$ , where  $\Delta$  is distance from the epicenter), their triggering potential is generally regarded as limited to one or two source dimensions from a given earthquake. Viscoelastic relaxation following a large crustal earthquake is largely confined to the lower crust and asthenosphere such that quasistatic stress changes propagate as a two-

dimensional stress change. Quasistatic stress changes thus decay more slowly with distance (as  $\sim \Delta^{-2}$ ), their triggering potential thus extends to greater distances than static stress changes, and the relatively low viscoelastic propagation speeds result in delayed triggering (Pollitz and Sacks, 2002). These two interaction modes are the focus of King (Chapter 4.10, this volume).

#### 4.11.1.3 Dynamic Stress Triggering

The amplitudes of dynamic stresses propagating as seismic waves decrease relatively slowly with distance (as  $\sim \Delta^{-2}$  for body waves and  $\sim \Delta^{-3/2}$  for surface waves), and thus, their triggering potential extends from the near field (the aftershock zone) to much greater distances than either the static or the quasistatic stress changes as illustrated in Figure 1 (Kilb et al., 2000). Amplification by radiation directivity, which is not a factor in either static

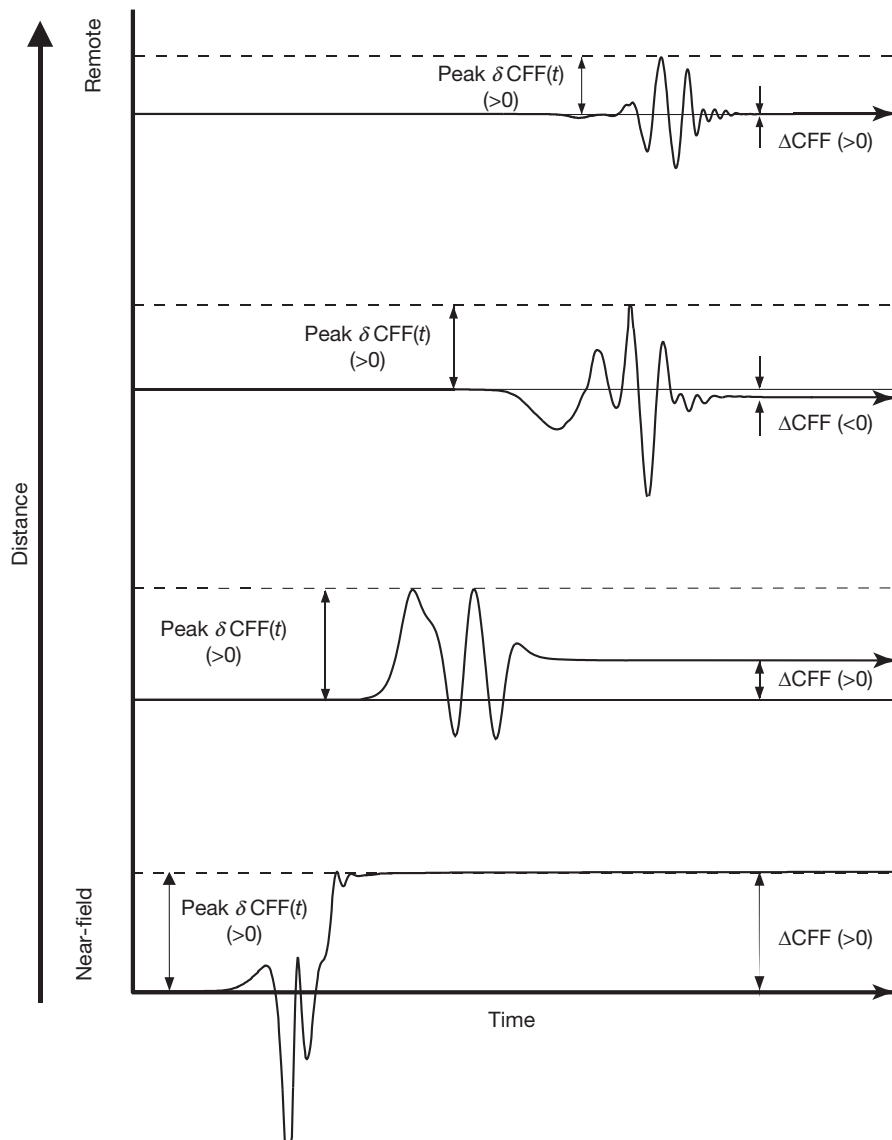


**Figure 1** Diagram from Kilb et al. (2000) illustrating differences between static and dynamic stresses with distance in terms of idealized time histories for peak changes in dynamic ( $\delta\text{CFF}(t)$ ) and static ( $\Delta\text{CFF}$ ) Coulomb stresses.  $\delta\text{CFF}(t)$  is the time-dependent version of  $\Delta\text{CFF}$  (eqn [1]). The double arrows show peak values for  $\delta\text{CFF}(t)$  and  $\Delta\text{CFF}$ . Adapted from Kilb D, Gomberg J, and Bodin P (2000) Triggering of earthquake aftershocks by dynamic stresses. *Nature* 408: 570–574, with permission.

or quasistatic stress changes, can further enhance the amplitudes of dynamic stresses in the case of mainshocks with asymmetric fault ruptures. Dynamic stresses are oscillatory, however, alternatively nudging the local stress field closer to and further from the local Coulomb failure stress over a range of frequencies leaving no permanent stress change. Indeed, it seems that Coulomb failure alone is not capable of explaining the full spectrum of observed dynamic triggering modes. In a number of cases, remotely triggered seismicity appears to be a secondary response to some more fundamental, aseismic process involving fluid activation or creep that was locally stimulated by the passing dynamic stresses. With periods of 12 and 24 h, the diurnal and semidiurnal tidal stresses induced in the solid Earth by the gravitational attraction of the sun and moon fall near the boundary between dynamic and quasistatic stresses (the inertial term is negligible), and they represent a lower bound on the frequency spectrum for dynamic triggering.

#### 4.11.1.4 Triggered or Coincidental?

Conceptually, dynamic triggering is based on the inference of a causal link between dynamic stresses, such as seismic waves from a distant earthquake (event 'a'), and the onset of a local response as those stresses propagate through a site (event 'b'). Credible evidence in support of such a causal link emerges with multiple, well-documented observations that event 'b' follows event 'a' within some 'reasonable' time interval,  $\Delta t$  (Figure 2). Statistical methods, if carefully formulated, can add backbone to malleable qualifiers such as 'reasonable' and 'sufficiently,' thereby enhancing objective credibility that the temporal sequences 'a' and then 'b' cannot be dismissed as chance coincidences between random, statistically independent processes. Credible physical models that link calculable stress changes (whether static, quasistatic, or dynamic) to failure processes in rock volumes at the site of a putative triggered response will certainly add weight to statistical evidence for causal links.

A number of tests for the statistical significance of dynamic triggering of earthquake sequences appear in the literature, the most common of which is the  $\beta$ -statistic of Mathews and Reasenberg (1988) and the ZMAP software package, which incorporates the  $\beta$ -statistic (Wiemer, 2001). Statistical tests provide permissive but not sufficient evidence for a causal link between passing dynamic stresses and the onset of a local activity. Estimating the likelihood that an isolated event is triggered poses a special challenge in this regard as does a suspected delayed response as the delay time increases. Some of the most compelling examples of dynamic triggering involve an abrupt increase in seismicity rate at multiple sites as in the case of the Landers earthquake (Figure 2) or the modulation of bursts of earthquakes or tectonic tremor in phase with specific components of passing surface waves (e.g., Hill et al., 2013; Rubinstein et al., 2007; West et al., 2005). There is little question of a causal link in such cases, although questions may remain over the physical processes involved.

#### 4.11.2 Early Inferences on Dynamic Triggering and Preinstrumental Examples

In an unpublished note dated 1955, Charles Richter wrote *The reverse effect – a major earthquake triggering a minor shock – is most*

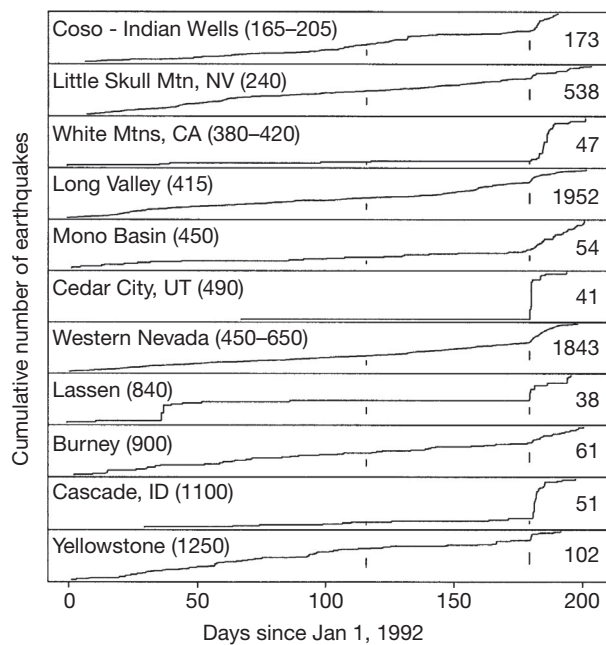


**Figure 2** Evidence for remote dynamic triggering by seismic waves from the  $M_w=7.4$  Landers, CA, earthquake on 28 June 1992 in a plot of cumulative number of locatable earthquakes at 11 sites in the western United States for 211 days beginning with 1 January 1992. Numbers in parentheses are distances in kilometers from the Landers epicenter. Numbers at the right indicate the total number of earthquakes in the respective areas for the entire time interval. The short vertical bars at day 114 mark the  $M_w=7.1$  Petrolia earthquake on 25 April 1992 and those at day 180 mark the  $M_w=7.4$  Landers earthquake. Reproduced from Hill DP, Reasenberg PA, Michael A, et al. (1993) Seismicity remotely triggered by the magnitude 7.3 Landers, California, earthquake. *Science* 260: 1617–1623, with permission.

probably [sic] within the immediate aftershock are [sic], but essentially by elastic wave propagation may set off action at a greater distance. If the distant effect is large enough, it may itself act as a trigger, so that there may be relay action, in which some of the later events are larger (Hough, personal communication). Many of the early published inferences on dynamic triggering were associated with investigations into acoustic emissions and high-frequency seismic noise (e.g., Armstrong and Stierman, 1989; Nicolaev and Troitskii, 1987 and references therein, Galperin et al., 1990), and concerns over the possibility that large, underground nuclear explosions might trigger a damaging earthquake (Emiliani et al., 1969). At the time, these studies were greeted within the scientific community by attitudes ranging from mild interest to strong skepticism. Skepticism prevailed largely because of questions regarding the statistical significance of isolated observations together with the lack of a compelling physical model. The fact that some of these studies were a part of efforts focused on even more controversial topics such as anomalous animal behavior induced by acoustic emissions as a means of earthquake prediction (e.g., Armstrong and Stierman, 1989) probably contributed to the skeptical reception within the mainstream scientific community.

In a retrospective effort to find anecdotal evidence of preinstrumental dynamic triggering, Hough (2001) and Hough et al. (2003) performed an extensive search through archive

newspapers and correspondence for felt reports of local earthquakes that may have been triggered at remote distances by the four  $M_w > 7$  New Madrid, Missouri, earthquakes of 1811–12 or the  $M_w > 7$  Charleston, South Carolina, earthquake in 1886. They uncovered evidence that two of the New Madrid  $M_w > 7$  events may have triggered locally felt earthquakes to distances of 1000 km or more.

Steebles and Stebbles (1996) and Meltzner and Wald (2003) investigated the distribution of aftershocks and possible triggered earthquakes for the great ( $M_w \sim 7.8$ ) San Francisco earthquake in 1906. They found evidence for nine earthquakes in the magnitude range  $M \sim 4$  to  $\sim 6$  within the first 48 h after the 1906 mainshock. The most distant, a  $M \sim 4$  earthquake in western Arizona at  $\sim 900$  km, occurred during the seismic waves from the 1906 mainshock and is a likely candidate for dynamic triggering.

Early investigations of dynamic triggering, however, are hampered by limited data. The situation began changing with the rapid expansion of continuously recorded, telemetered seismic networks around the globe through the 1980s and 1990s coupled with improvements in real-time processing and a growing number of broadband, high-dynamic-range digital installations. The latter set the stage for capturing a range of interesting seismic signals missed by earlier, short-period instrumentation.

#### 4.11.3 Instrumental Evidence for Dynamic Triggering

On 28 June 1992, the  $M_w = 7.3$  Landers earthquake ruptured a 70 km length of the Mojave Desert in southern California.

Over the next few hours, it became clear that seismicity rates had increased at a number of sites across western North America at distances ranging from 200 to as much as 1250 km (17 source dimensions, see Figure 2). This large number of independent occurrences provided the first compelling evidence that remote triggering by dynamic stresses is indeed a viable process in the Earth (Gomberg, 1996; Hill et al., 1993). The Landers mainshock resulted from a unilateral rupture propagating to the north-northwest along a series of north-northwest striking dextral fault segments. All of the recognized sites of dynamic triggering were north of the Landers epicenter (Figure 3(b)), suggesting that amplification enhanced by rupture directivity may influence the distribution of dynamic triggering – a suggestion supported by subsequent instances of dynamic triggering (Gomberg et al., 2001).

Seven years later, the  $M = 7.1$  Hector Mine earthquake on 16 October 1999 ruptured a 40 km length of the Mojave Desert along a series of faults located just 20 km east of the Landers rupture (Figure 3). In this case, fault rupture was bilateral but with the dominant rupture direction to the south-southeast. The most energetic triggered response to the dynamic stresses from the Hector Mine mainshock was in the Salton Trough south of the epicenter (Figure 3(a)), thus adding weight to the idea that rupture directivity and dynamic stress amplitudes are important factors in determining the distribution of dynamic triggering (Gomberg et al., 2001; Hough and Kanamori, 2002).

The  $M_w = 7.9$  Denali Fault earthquake on 3 November 2002, which was centered 65 km east of Denali National Park, Alaska, resulted from a complex rupture with maximum

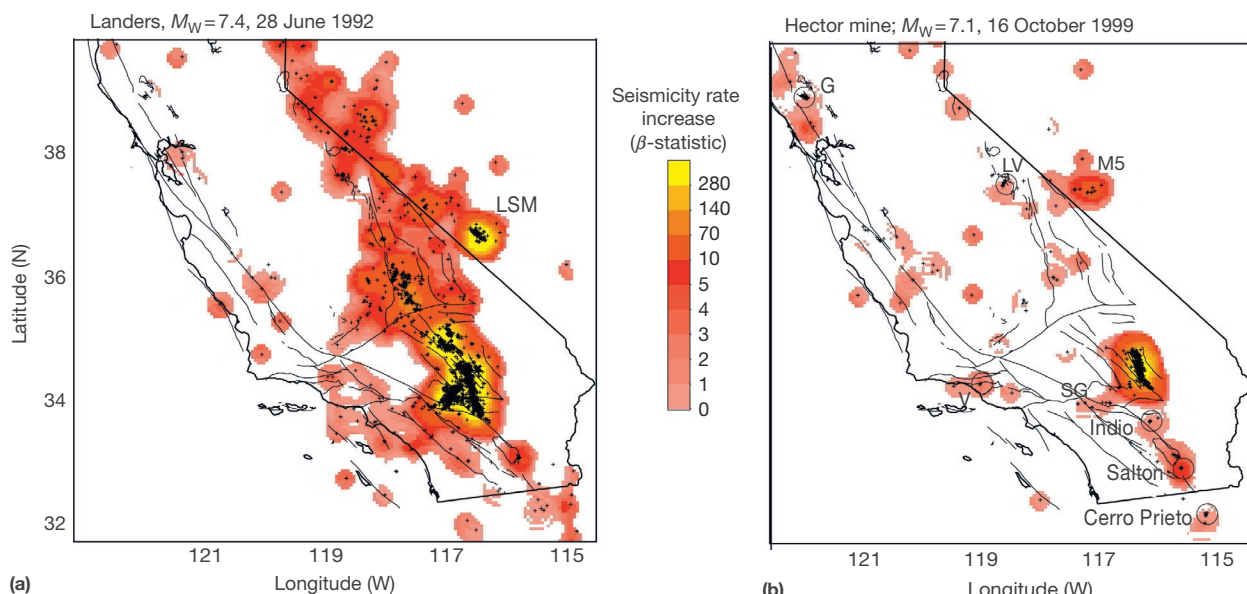


**Figure 3**  $\beta$ -statistic maps illustrating seismicity rate increases associated with the  $M_w = 7.4$  Landers earthquake on 28 June 1992 (a) and  $M_w = 7.1$  Hector Mine earthquake on 16 October 1999 (b). The plots show a spatially smoothed  $\beta$ -statistic over dimensions of 20 km for  $M \geq 2.0$  earthquakes from the Northern California Seismic Network (NCSN) and Southern California Seismic Network (SCSN) catalogs. The rate change was calculated for a 2-week period following the respective mainshocks with respect to the background period 1987 through mid-1992 (pre-Landers). Thin lines are major fault traces. Circles in (b) mark sites of activity triggered by the Hector Mine earthquake. M5 in (b) reflects aftershock activity to a  $M = 5.3$  earthquake that occurred  $\sim 2.5$  months prior to the Hector Mine earthquake. G, the Geysers geothermal area; LV, Long Valley Caldera; SG, San Gorgonio Pass; LSM, Little Skull Mountain. Modified from Gomberg J, Reasenberg PA, Bodin P, and Harris R (2001) Earthquakes triggering by seismic waves following the Landers and Hector Mine earthquakes. *Nature* 411: 462–465, with permission.

surface displacements reaching 8.8 m (Eberhart-Phillips et al., 2003; Rowe et al., 2004). The unilateral rupture produced pronounced directivity with peak amplification of dynamic stresses directed to the southeast through British Columbia and the western United States. With the exception of the Katmai volcanic cluster 740 km southwest of the epicenter, all recognized sites of dynamic triggering were located southeast of the epicenter in the sector of maximum directivity that spanned the areas responding to the Landers and Hector Mine earthquakes (Figure 4 in Hill and Prejean, 2007). In all cases, the onset of dynamic triggering developed as a seismicity rate increase during the passage of the Denali Love and Rayleigh waves (e.g., see Figure 4). In three cases, Mount Rainier, Long Valley Caldera, and Yellowstone, delayed earthquake swarms followed the initial surge in triggered seismicity by  $\Delta t \sim 2.5$  h, 23.5 h, and 8 days, respectively (Husen et al., 2004a,b; Prejean et al., 2004). Pankow et al. (2004) documented both rapid-onset triggering and delayed triggering along the Wasatch Front in central Utah following the Denali earthquake.

The rapidly accumulating literature on dynamic triggering in the 20 years since the Landers earthquake makes it clear that dynamic triggering at remote distances is a much more widespread and a much richer phenomenon than initially envisioned. In the following three sections, we highlight some general aspects of the triggered response to dynamic stresses from large, distant earthquakes as currently understood through (1) brittle failure in the seismogenic crust, (2) fluid activation in the hydrologic domain and volcanic/geothermal systems, and (3) shear failure as the source of tectonic (non-volcanic) tremor in the transition from brittle–plastic behavior along major plate-boundary faults.

#### 4.11.3.1 Widespread Dynamic Triggering in the Seismogenic Crust

Velasco et al. (2008) examined the records from 500 globally distributed broadband seismic stations for evidence of remote dynamic triggering by 15  $M > 7$  earthquakes occurring over the 18-year span from 1990 to 2007. They found that, out of the

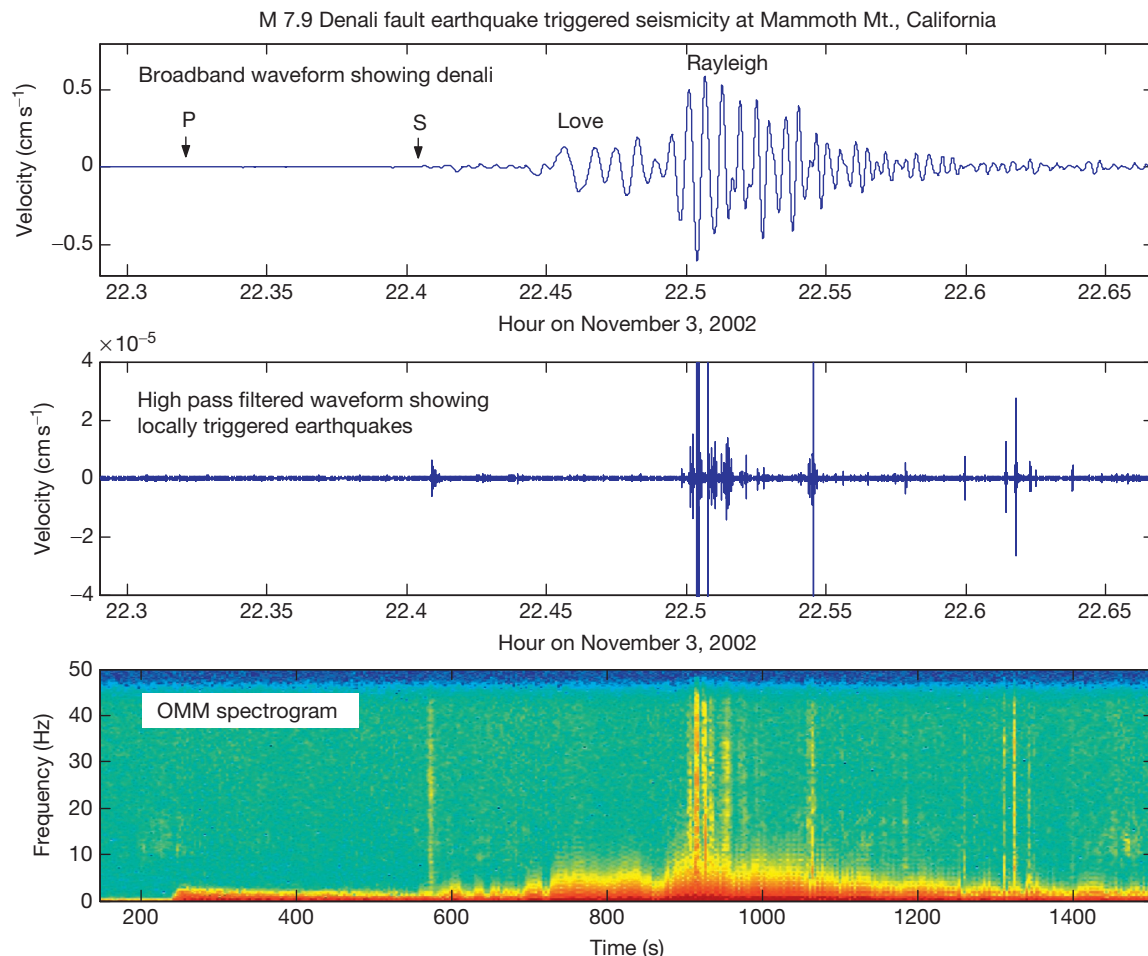


**Figure 4** Examples of triggered seismicity detected in the surface-wave coda from the Denali Fault earthquake at Mammoth Mountain. Top trace is the broadband seismogram from station OMM located 4 km SE of Mammoth Mountain. Middle and bottom panels show the high-pass-filtered version of the OMM seismogram and a spectrogram of the unfiltered seismogram. Modified from Prejean SG, Hill DP, Brodsky EE, et al. (2004) Remotely triggered seismicity on the United States west coast following the  $M_w = 7.9$  Denali Fault earthquake. *Bulletin of the Seismological Society of America* 94: S348–S359, courtesy of the Seismological Society of America.

15  $M > 7$  mainshocks studied, 12 were associated with significant increases in the detection of smaller earthquakes in the vicinity of the respective seismic stations all located at distances  $> 10^\circ$  ( $\sim 1110$  km) from the mainshock epicenters. Their analysis revealed that, on average, the local earthquake rate increased above background by 38% with the passage of the Love wave and 60% with the passage of the Rayleigh wave and that remote triggering occurred in all tectonic environments. Parsons and Velasco (2011) found no evidence for  $M > 5$  earthquakes triggered during the passage of surface waves at distances beyond two to three rupture lengths from any of the  $M > 7$  earthquakes having occurred in the previous 30 years. In a paper published just a year later, Pollitz et al. (2012) documented a fivefold increase in the global rate of  $M > 5.5$  earthquakes at distances  $< 1500$  km from the triggering mainshock during the first 6 days following the  $M_w = 8.6$  Indian Ocean earthquake on 11 April 2012. Only one of these  $M > 5.5$  events (a  $M = 5.5$  earthquake beneath the western Aleutian Islands) occurred during the passing seismic waves, however; the remainder were delayed by hours to several days. This underscores the rapid evolution of our perspective on dynamic triggering with time as new data become available (Tables 1 and 2; Figure 5).

Gonzalez-Huizar et al. (2012) found evidence that the 2011  $M_w = 9.0$  Tohoku-Oki earthquake triggered crustal seismicity in South Dakota (the United States), Russia, China, Ecuador, and Mexico. The latter involved the abrupt onset of an earthquake

swarm in a local spreading center in the Gulf of California that included a pair of  $M = 5.2$  earthquakes in same area as the  $M_w = 7.0$  earthquake triggered by the 2012  $M_w = 7.0$  Indian Ocean earthquake (Pollitz et al., 2012). Other examples from around the globe include the Netherlands (Camelbeeck et al., 1994), the Yammouneh fault along the Syria–Lebanon border (Mohamad et al., 2000), continental Greece (Brodsy et al., 2000), the Valley of Mexico (Singh et al., 1998), Taiwan (Wen et al., 1996), east-central China (Jiang et al., 2010; Wu et al., 2011), Japan (Miyazawa, 2011, 2012), geothermal areas in California (Brodsy, 2006; Brodsy and Prejean, 2005; Peng et al., 2011a,b), and Queensland, Australia (Gonzalez-Huizar and Velasco, 2011). The following examples are particularly noteworthy.

The epicenters of  $M_w = 6.5$  and  $6.4$  earthquakes in the South Iceland Seismic Zone on 17 and 21 June 2000, respectively, were separated by just 17 km in an east–west direction. The first and largest of these earthquakes triggered widespread seismicity on the Reykjanes Peninsula to distances of  $\sim 100$  km to the west and significant slip on at least three faults in the Reykjanes Peninsula, while the second, slightly smaller earthquake, although 17 km further west, triggered little response (Arnadottir et al., 2004; Daniel et al., 2008). The triggered seismicity included three  $M \sim 5$  earthquakes that followed the  $M_w = 6.5$  event by seconds to minutes. Arnadottir et al. (2004) concluded that these  $M \sim 5$  earthquakes were beyond the range for Coulomb failure due to static stress changes from the

**Table 1** Source earthquakes for cited instances of dynamic triggering

Earthquake	Magnitude	Date	Depth (km)	Slip	Representative references
New Madrid, MO, USA (4 $M > 7.5$ )	$M$ 7.5–7.7	1811–12	<15	SS	Hough (2001)
Charleston, NC, USA	$M$ 7.3	01 September 1886	<15	SS	Hough et al. (2003)
Kangra, India	$M_s$ 7.8	04 April 1905	<20	T	Hough et al. (2005)
San Francisco, CA, USA	$M$ 7.8	18 April 1906	<15	SS	Meltzner and Wald (2003)
Roer Valley, the Netherlands	$M_w$ 5.4	13 April 1992	<15	SS	Camelbeeck et al. (1994)
Landers, CA, USA	$M_w$ 7.4	28 June 1992	<15	SS	Hill et al. (1993)
Gulf of Aqaba	$M_w$ 7.3	22 November 1995	<15	SS	Mohamad et al. (2000)
Hector Mine, CA, USA	$M_w$ 7.1	16 November 1999	<15	SS	Gomberg et al. (2001)
Izmit, Turkey	$M_w$ 7.6	17 August 1999	15	SS	Brodsy et al. (2000)
Chi-Chi, Taiwan	$M_w$ 7.7	20 September 1999	5	T	Miyazawa et al. (2005)
Iceland	$M_w$ 6.5	17 June 2000	6	SS	Arnadottir et al. (2004)
Western Tottori, Japan	$M_w$ 6.7	06 November 2000	15	SS	Di Carli et al. (2008)
Bhuj, western India	$M_w$ 7.6	26 January 2001	10	T	Surve and Mohan (2012)
Kunlun, China	$M_w$ 7.8	14 November 2001	10	SS	Wu et al. (2011)
Denali Fault, AK	$M_w$ 7.9	11 March 2002	5	SS	Prejean et al. (2004)
Palermo, Italy	$M_w$ 6.0	09 June 2002	10	T	Walter et al. (2009)
Tonga	$M_w$ 7.6	08 September 2002	665	T	Tibi et al. (2003)
Tokachi–Oki, Japan	$M_w$ 8.3	25 September 2003	27	T	Miyazawa and Mori (2005)
SW Siberia, Russia	$M_w$ 7.3	27 September 2003	17	SS	Miyazawa and Mori (2005)
Sumatra, Indonesia	$M_w$ 9.1	26 December 2004	30	T	Lay et al. (2005)
Southern Greece	$M_w$ 6.8	09 June 2006	66	T	Cannata et al. (2010)
Yogyakarta, Indonesia	$M_w$ 6.3	26 June 2006	10	SS	Mori and Kano (2009)
Solomon Islands	$M_w$ 8.1	01 April 2007	10	T	Miyazawa et al. (2008)
Wenchuan, China	$M_w$ 7.9	12 May 2008	19	T	Miyazawa et al. (2008)
Halmahera, Indonesia	$M_w$ 6.6	11 September 2008	98	T	Lin (2012)
Kepulauan Talaud, Indonesia	$M_w$ 7.2	11 February 2009	20	T	Jousset and Rohmer (2012)
Maule, Chile	$M_w$ 8.8	27 February 2010	35	T	Zigone et al. (2012)
Tohoku–Oki, Japan	$M_w$ 9.0	11 March 2011	29	T	Gonzalez-Huizar et al. (2012)
Indian Ocean	$M_w$ 8.6	11 April 2012	20	SS	Pollitz et al. (2012)

Slip: SS, strike-slip; T, thrust or reverse.

**Table 2** Reported instances of remote dynamic triggering in the brittle domain

Site	Triggered $M_{max}$	Regime	Mainshock		References
			$M_{max}$	Distance (km)	
<i>North America</i>					
Mt. Wrangell, AK	<1	V	9.0	~11000	28
Katmai, AK	2.3	G, V	7.9	115–740	21, 43
South BC, Canada	N/A	C	7.9	1800–2200	9
Mt. Rainier, WA	<1	V	7.9	3108	23
Geysers, CA	<3	E, G, V	6.5–7.9	202–3120	7, 23, 17
Coso, CA	3.2	E, G, V	<7.9	165–3660	23
Long Valley, CA	3.4	E, G, V	7.4–7.9	414–3454	8, 23
Mammoth Mountain, CA	$M < 2$	E, G, V	7.2–7.9	420–3454	2, 16
Lassen Peak, CA	2.8	E, V	7.4	840	10
Burney, CA	2.8	E	7.4	900	10
Salton Sea area, CA	4.7	E, V, G	7.1	120–150	14
Central and south CA	5?	E, C	5.8–6.1	70–120	13
California	–	E, C	2.1–5.5	>3000	41
Offshore S. CA	2.5	E	7.9	4003	23
W. Nevada	~4	E, G	7.4	450–650	1
W. Arizona (1906)	~4	E	7.8	900	29, 30
Little Skull Mountain, NV	5.6	E	7.4	240	1
Yellowstone, WY	3.0	E, G, V	7.4–7.9	1250–3100	15
South Dakota	<3	I	9.0	8603	33
Wasatch Front, UT	3.2	E, G	7.4–7.9	3000–3500	22
Cascade, ID	1.7	E, G	7.4	1100	9
The eastern United States (1811–12)	~5	C	$M > 7$	~1000	12
<i>South and Central America</i>					
Cerro Prieto, Mexico	4.1	E, V, G	7.1	260	6
Valley of Mexico	~4	E, G, V	7.6–8.0	303–588	24
Gulf of CA, Mexico	5.2	E	9.0	~11000	33
Ecuador	–	E/C	9.0	~14000	33
<i>Asia</i>					
Aso, Japan	~2	E, V	7.1–7.7	900–2213	18
Japan	≤5	V, C	9.0	1350	37, 39
Hakone caldera, Japan	4.8	V	9.0	450	40
Iwo Jima, Japan	<2	IA, G, V	7.1–8.0	1228–2002	26
Taiwan region	>4	?	6.5–7.1	138–2959	27
Nankai Trough, Japan	N/A	S	7.3–8.1	900–4000	19
Tonga Trench	5.9–7.7	S	7.1–7.6	260–290	25
Central China	–	E	7.8–9.0	1497–19140	33, 34, 35, 42
Queensland, Australia	–	C	7.5–8.4	15000	36
<i>Europe</i>					
SISZ, Iceland	~5	E, G	6.5	80–100	2
Roer Valley, Holland	3.7	E	5.4	40	4
Greece	>3.5	E	7.4	400–1000	3
Turkey	>2.8–3.0	E	7.6	20–80	5
Paris Basin, France	<1		7.2	12000	38
Syria–Lebanon border	3.7	C	7.3	500	20
Russia	–	C	9.0	2971	33
<i>Global studies</i>					
Global waveforms	<1	–	>7	>10°	31
Global catalogs	>5.5	–	8.6		32

Tectonic regimes: E, extensional, transtensional; C, convergent, transpressional; I, intraplate; G, geothermal; V, volcanic; IA, island arc; S, subcrustal subduction zone; SISZ, South Iceland Seismic Zone.

References: 1. Anderson et al. (1994); 2. Arnadottir et al. (2004); 3. Brodsky et al. (2000); 4. Camelbeeck et al. (1994); 5. Durand et al. (2013); 6. Glowacka et al. (2002); 7. Gomberg (1996); 8. Gomberg et al. (2001); 9. Gomberg et al. (2004); 10. Hill et al. (1993); 11. Hill et al. (1995); 12. Hough (2001); 13. Hough (2005); 14. Hough and Kanamori (2002); 15. Husen et al. (2004a,b); 16. Husker and Brodsky (2004); 17. Johnston et al. (2004b); 18. Miyazawa et al. (2005); 19. Miyazawa and Mori (2005); 20. Mohamad et al. (2000); 21. Moran et al. (2004); 22. Pankow et al. (2004); 23. Prejean et al. (2004); 24. Singh et al. (1998); 25. Tibi et al. (2003); 26. Ukawa et al. (2002); 27. Wen et al. (1996); 28. West et al. (2005); 29. Steeples and Steeples (1996); 30. Meltzner and Wald (2003); 31. Velasco et al. (2008); 32. Pollitz et al. (2012); 33. Gonzalez-Huizar et al. (2012); 34. Jiang et al. (2010); 35. Wu et al. (2011); 36. Gonzales-Huizar and Velasco (2011); 37. Miyazawa (2011); 38. Jousset and Rohmer (2012); 39. Hirose et al. (2011); 40. Yukutake et al. (2011); 41. Van der Elst and Brodsky (2010); 42. Wu et al. (2012). Power et al. (2001).

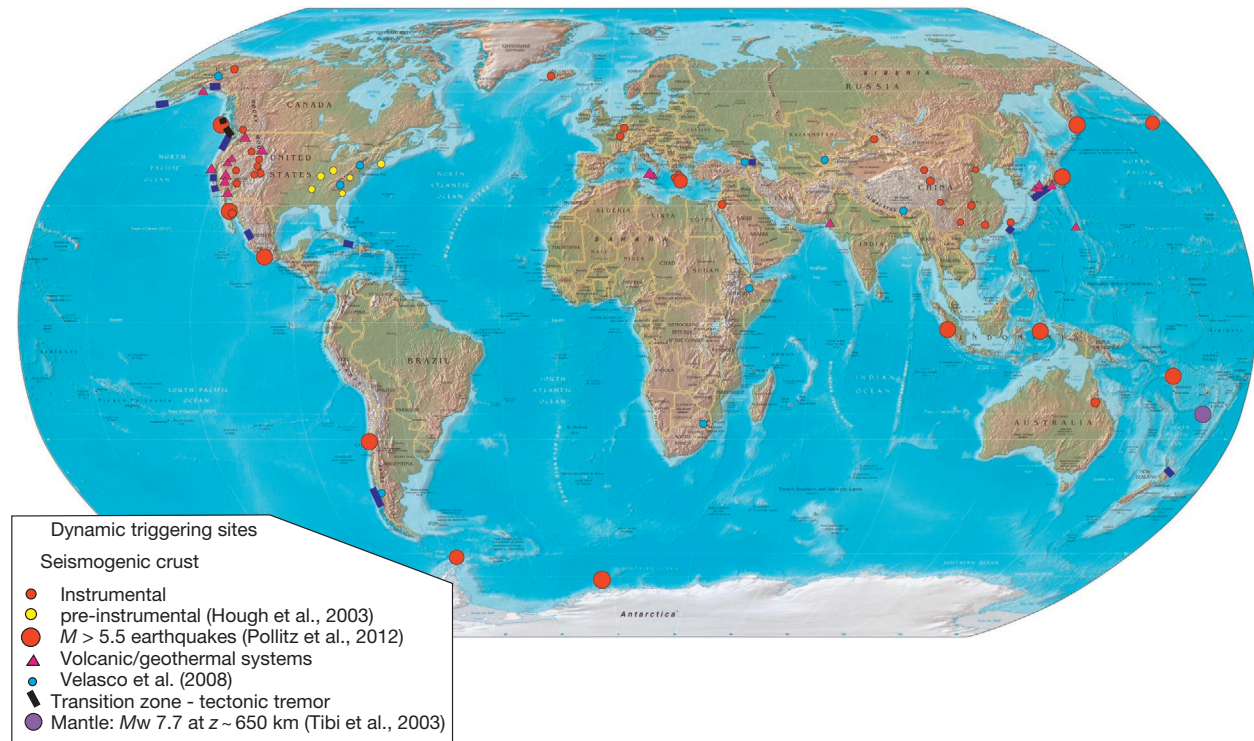


**Figure 5** Map indicating the distribution of published instances of dynamically triggered earthquakes referred to in this chapter. Triggered seismicity in the brittle crust indicated by red circles for instrumentally recorded sites and orange circles for inferred, preinstrumental sites (Hough et al., 2003). Red triangles indicate volcanic/geothermal sites showing a triggered response. Large red circles indicate the  $M > 5.5$  events that occurred in the first 6 days after the 2012  $M_w = 8.6$  Indian Ocean earthquake (Pollitz et al., 2012). Black bars indicate documented sites of triggered tectonic tremor. Blue circles indicate instrument clusters that showed an increase in seismicity rate following 12 out of 15  $M > 7$  earthquakes between 1990 and 2008 (Velasco et al., 2008). Large purple circle indicates the 650 km deep  $M_w = 7.7$  earthquake triggered by the 202  $M_w = 7.6$  earthquake beneath the Tonga subduction zone (Tibi et al., 2003).

$M_w = 6.5$  mainshock and thus that they were likely triggered by dynamic stresses. Their analysis of continuous GPS geodetic data spanning the Reykjanes Peninsula indicates that the geometric moment for the second of the triggered  $M \sim 5$  earthquakes ( $\Delta \sim 78$  km) was an order of magnitude larger than its seismic moment and that the Coulomb stress change from this largely aseismic, slow earthquake was sufficient to trigger the third and most distant  $M \sim 5$  event some 4 min later through quasistatic stress transfer.

A compelling example in support of dynamic triggering being confined to crustal volumes in a near-critical stress state comes from data recorded during a salt cavern collapse at the eastern edge of the Paris Basin, Lorraine, France (Jousset and Rohmer, 2012). The cavern was created by a salt-mining process that involves injecting freshwater into sedimentary salt layer through boreholes in one area and extracting brine from another some distance away. The cavern grew as the salt was extracted, with the process monitored by tracking ground deformation and seismicity. In this case, the mine operator decided to proceed to controlled cavern collapse. Jousset and Rohmer (2012) examined the local earthquake catalog for signs of dynamic triggering by  $M > 7$  earthquakes in the year before the planned collapse and found none. As the dimensions of the cavern approached a critical state, however, seismic

waves from the 2009  $M_w = 7.2$  Kepulauan Talaud earthquake (Indonesia) triggered the onset of a seismicity sequence that culminated in cavern collapse 3 days later. In their analysis of the sequence, Jousset and Rohmer (2012) concluded that Rayleigh wave dynamic stresses of 1–2 kPa from the  $M_w = 7.2$  earthquake were the dominant triggering agent.

Not all instances of remotely triggered brittle failure are confined to the brittle crust. Peng and Walter (2013) found that the 2010  $M_w = 8.8$  Maule, Chile, earthquake triggered ice quakes in the glacier near the Howard Nunataks and Ellsworth Mountains, Antarctica. Based on the nearby broadband station HOWD, they concluded that the triggered activity coincided with dilatational stresses associated with both  $P$ -waves and Rayleigh waves. At the other extreme, a  $M_w = 7.6$  earthquake on 19 August 2002 at a depth of  $\sim 665$  km beneath the Tonga subduction zone was followed by  $M_b = 5.9$  and  $M_w = 7.7$  earthquakes in the same depth range with delays of 2.2 and 7.4 min, respectively (Tibi et al., 2003). The latter two earthquakes occurred in a previously aseismic volume located  $\sim 290$  km southwest of the initial  $M_w = 7.6$  event. Tibi et al. (2003) found that the static Coulomb stress change at this distance from the initial  $M_w = 7.6$  earthquake is small and concluded that these earthquakes were most likely dynamically triggered by the body waves from the  $M_w = 7.6$  earthquake.

#### 4.11.3.2 Dynamic Triggering of Volcanic/Geothermal and Hydrologic Systems

Recognition that volcanic and geothermal areas appear to be particularly susceptible to dynamic triggering of local earthquake activity by seismic waves from distant earthquakes heightened interest in the broader topic of earthquake–volcano interactions (Delle Donne et al., 2010; Hill et al., 2002; Linde and Sacks, 1998; Manga and Brodsky, 2006). It has long been recognized that shallow hydrologic systems respond to seismic waves from large earthquakes (Chapter 4.12, this volume; Manga and Wang, 2007; Richter, 1958; Vohis, 1967; Wang and Manga, 2009). In the case of earthquake–volcano interactions, static or quasistatic stress transfer can work in both directions with the stress change associated with a magmatic intrusion or eruption triggering slip on a nearby fault or vice versa (e.g., Chesley et al., 2012; Nostro et al., 1998; Walter, 2007). Our focus here, however, remains on dynamic triggering.

Many of the areas responding to the 1992  $M_w=7.3$  Landers earthquake, the 1999  $M_w=7.1$  Hector Mine, and the 2002  $M_w=7.1$  Denali Fault earthquakes were volcanic or geothermal including Long Valley and Yellowstone Calderas. The response of Yellowstone Caldera to the Denali Fault earthquake in particular included pronounced transient changes in the hydrothermal and geyser/hot-spring systems (Husen et al., 2004b; Pankow et al., 2004). The response of Long Valley Caldera to the Landers, Hector Mine, and Denali Fault earthquakes was dominated by a largely aseismic deformation transient with the deformation moment significantly greater than the cumulative seismic moment of the triggered seismicity (Figure 6).

The Geysers geothermal field in the northern California Coast Ranges seems particularly susceptible to dynamic triggering. It responded with increased seismicity rates to dynamic stresses from eight regional earthquakes with magnitudes  $M=6.6\text{--}7.7$  at distances  $\Delta=212\text{--}2500$  km between 1988 and 1994 (Gomberg and Davis, 1996; Stark and Davis, 1995) and the 1999 Hector Mine earthquake (Gomberg et al., 2001), and the 2005  $M_w=7.2$  Mendocino earthquake (Brodsky, 2006) and to the teleseismic waves from the 2002 Denali Fault earthquake located 3120 km to the northwest (Prejean et al., 2004).

Surve and Mohan (2012) documented increased earthquake swarm activity in the Western Ghats geothermal area in the Deccan volcanic province of India following the 2001  $M_w=7.6$  Bhuj earthquake, which was located in western India 500 km to the northwest. The onset of swarm activity began  $\sim 2.5$  h after the Bhuj earthquake and continued with three bursts in activity over the next 2 months. In contrast, Sanchez and McNutt (2004) see intermediate-term declines in seismicity beneath Mt Warnell and Mt Veniaminof volcanoes in Alaska following the 2002  $M_w=7.9$  Denali Fault earthquake.

Harrington and Brodsky (2006) found that, except for volcanic systems on Kyushu, there was surprisingly little evidence for dynamic triggering in Japan by distant earthquakes. Miyazawa et al. (2005) described evidence for multiple increases in isolated tremor and microearthquakes at Aso volcano in central Kyushu following large, distant earthquakes

including the  $M_w=7.7$  Chi-Chi, Taiwan, earthquake on 20 September 1999. In 2011, however, the 11 March  $M_w=9.0$  Tohoku-Oki earthquake triggered widespread seismicity across Japan, much of which was located in volcanic or geothermal areas (Hirose et al., 2011; Miyazawa, 2011). A seismicity increase in Hakone caldera at an epicentral distance of 450 km from the Tohoku-Oki epicenter coincided with the passing surface waves with peak dynamic stresses of 0.6 MPa – an order of magnitude larger than the estimated  $\sim 0.04$  MPa static stress change at the caldera associated with the Tohoku-Oki mainshock (Yukutake et al., 2011, 2013).

The island of Iwo Jima in the Volcano Islands group situated between the Marianas and Izu island arcs some 1250 km south of Tokyo represents the resurgent dome of a large submarine caldera. Ukawa et al. (2002) examined Iwo Jima seismograms for  $21 M>7$  earthquakes located within 3000 km of the island and found four instances when local seismicity increased during the passage of the surface waves from the distant earthquakes. Iwo Jima seismograms showed a similar triggered response to the surface waves from the great  $M_w=9.1$  Sumatra–Andaman Islands earthquake on 26 December 2004 and those from the 2011  $M_w=9.0$  Tohoku-Oki earthquake (Ukawa, personal communication). In contrast, Okubo and Wolfe (2008) cited evidence for a significant decrease in the rate of 30 km deep long-period (LP) earthquakes beneath Mauna Loa volcano, Hawaii, a quiescence apparently triggered by dynamic stresses from the 2004  $M_w=9.1$  Sumatra earthquake.

Volcanic unrest at Mount Etna on Sicily responded to dynamic stresses from the 8 January 2006  $M_w=6.8$  earthquake in southern Greece and the 12 May 2008  $M_w=7.9$  earthquake in eastern Sichuan, China (Cannata et al., 2010). The latter was followed by an abrupt decrease in the frequency content of ongoing seismic activity within the volcano and the onset of an explosive eruption 27 h later. An unusual cluster of three eruptions followed a  $M_w=5.9$  earthquake on 6 September 2002 centered  $\sim 50$  km north of Palermo. The largest Mount Etna eruption in 55 years occurred on 28 October 2002 followed by a submarine degassing event near Panarea Island on 3 November 2002 and the largest effusive eruption of Stromboli in 17 years on 28 December 2002 all located within 150 km of the Palermo earthquake (Walter et al., 2009). The 2–4-month delay between the earthquake and the eruptions, however, leaves a causal link open to question.

The value of a well-monitored volcano with multi-parameter instrumentation is underscored by the eruption of Shinmoedake volcano in Japan, which followed the 11 March 2011  $M_w=9.0$  Tohoku-Oki earthquake by just 2 days. In this case, Yamazaki et al. (2011) concluded that the eruption was probably not triggered based on data from a nearby borehole strain meter showing no evidence for aseismic deformation nor a pressure increase in the magma chamber. Similarly, Mori and Kano (2009) concluded that evidence was at best ambiguous for a causal link between the  $M_w=6.3$  Yogyakarta earthquake at a distance of 250 km from the damaging and widely publicized Lusi mud volcano eruption that began 3 days later at a drill site in Sidoarjo, Indonesia. Indeed, Davies et al. (2010) provided compelling evidence that the Lusi eruption was the result of drilling operations at the drill site.

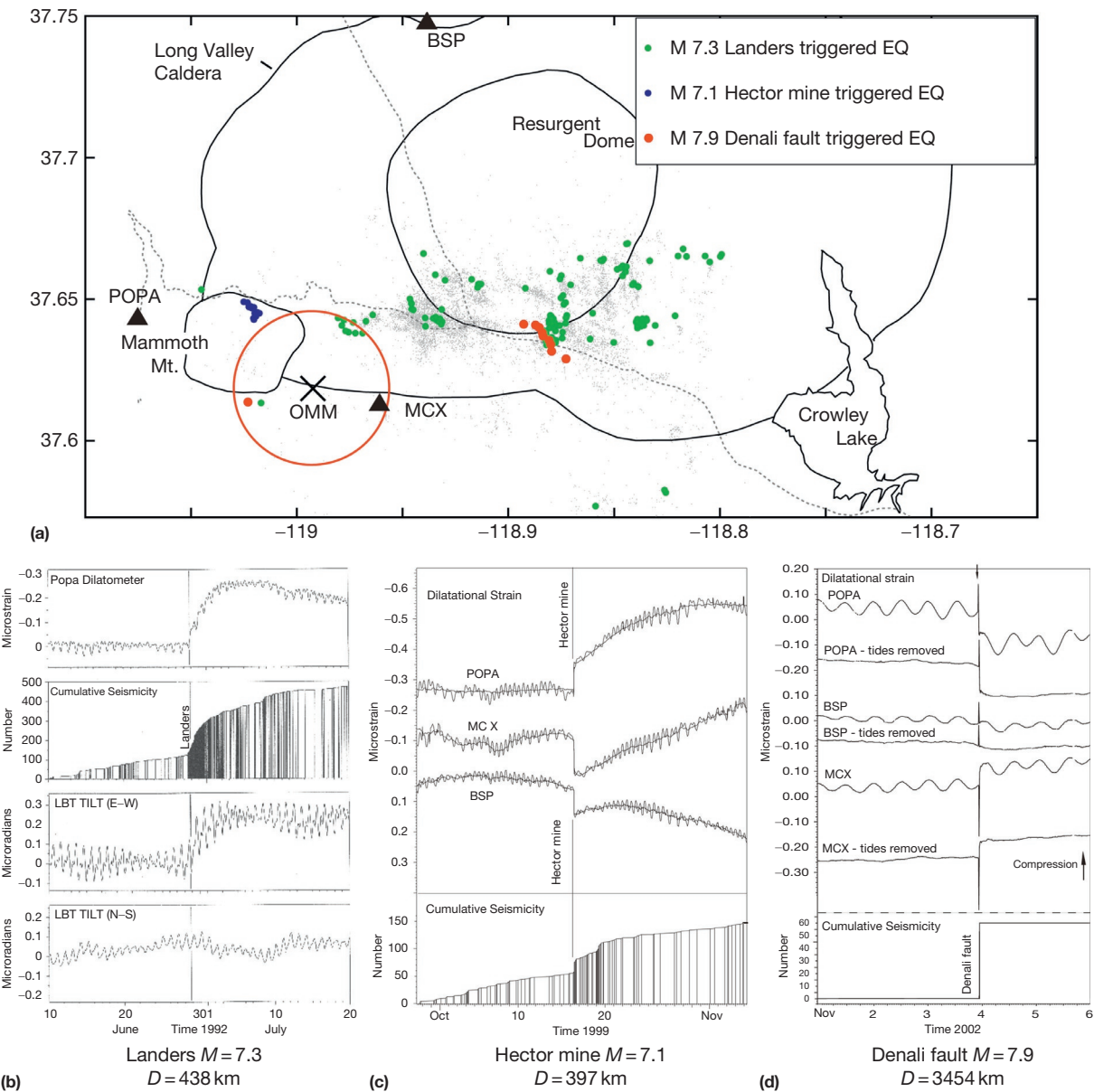


**Figure 6** (a) Map of triggered seismicity beneath Long Valley Caldera and Mammoth Mountain for the Landers (green), Hector Mine (blue), and Denali Fault earthquakes (red). Gray dots show seismicity for 1997–98. The red circle centered on station OMM indicates area within which the Denali Fault-triggered earthquakes must be located based on S-P times. The single red dot is the epicenter for those earthquakes large enough for a multistation location. Modified from Prejean SG, Hill DP, Brodsky EE, et al. (2004) Remotely triggered seismicity on the United States west coast following the Mw 7.9 Denali Fault earthquake. *Bulletin of the Seismological Society of America* 94: S348–S359, courtesy of the Seismological Society of America. (b) Deformation transient triggered by the Landers earthquake as recorded on the POPA borehole dilatometer (top) and the long base tiltmeter (LBT). The bottom two panels show E-W and N-S tilt components, respectively. Cumulative number of earthquakes plotted in second panel. Adapted from Johnston MJS, Hill DP, Linde AT, Langbein J, and Bilham R (1995) Transient deformation during triggered seismicity from the 28 June 1992 Mw = 7.3 Landers earthquake at long valley volcanic caldera, California. *Bulletin of the Seismological Society of America* 85: 787–795, courtesy of the Seismological Society of America. (c) Deformation transient triggered by the Hector Mine earthquake as recorded on borehole dilatometers POPA, MCX, and BSP. Cumulative number of earthquakes plotted in bottom panel. Reproduced from Johnston MJS, Hill DP, and Pitt AM (2000) Strain transient recorded in the Long Valley Caldera during triggered seismicity from the October 16, 1999 M7.1 Hector Mine, California, earthquake. *EOS, Transactions of the American Geophysical Union* 81: WP1384. (d) Deformation transient triggered by the Denali Fault earthquake as recorded on borehole dilatometers POPA, MCX, and BSP. Strain records for each dilatometer are shown with solid Earth tides (top) and with tides filtered out (bottom). Cumulative number of earthquakes plotted in bottom panel. Adapted from Johnston MJS, Prejean SG, and Hill DP (2004a) Triggered deformation and seismic activity under Mammoth Mountain in long valley caldera by the 3 November 2002 Mw 7.9 Denali fault earthquake. *Bulletin of the Seismological Society of America* 94: S360–S369, courtesy of Seismological Society of America.

#### 4.11.3.3 Dynamic Triggering of Tectonic (Nonvolcanic) Tremor in the Transitional Domain

Following the discovery of tectonic (nonvolcanic) tremor in Japan (Obara, 2002) and recognition of its relation to episodic slow slip on the Nankai and Cascadia subduction zone faults (Julian, 2002; Rogers and Dragert, 2003), the combination of episodic tremor and slip (ETS) in the transitional domain downdip of the seismogenic section of major plate-boundary faults is now recognized as an important component in the earthquake cycle for major, plate-boundary earthquakes (Beroza and Ide, 2011; Rubinstein et al., 2010; Chapter 4.17). Using cross correlation methods to obtain precise hypocentral locations of low-frequency earthquakes (LFEs) and recognizing their close association with slow slip events in Japan, Shelly et al. (2006) proposed that tectonic tremor results from sequences of LFEs with dominant energy in the 1–10 Hz frequency band, each of which represents an increment of shear failure along the megathrust fault plane at depths of 20–30 km.

Obara (2002) first recognized that levels of tremor activity beneath Japan can be modulated by dynamic stresses associated with seismic waves from both local and teleseismic earthquakes. Miyazawa and Mori (2005) applied a  $\beta$ -statistic analysis to tremor in the Nankai subduction zone and found a rate increase coincident with the Rayleigh waves from the  $M_w=8.1$  Tokachi-Oki earthquake on 25 September 2003, some 1000 km to the northwest. They found a similar response from a  $M_w=7.3$  earthquake in Siberia 40 h later (27 September). Subsequent studies by Miyazawa and Mori (2006), Miyazawa and Brodsky (2008), and Miyazawa et al. (2008) found triggered tremor in Nankai coincident with surface waves from the 2004  $M_w=9.1$  Sumatra-Andaman Islands earthquake, the 2007  $M_w=8.1$  Solomon Islands earthquake, and the 2008  $M_w=7.9$  Wenchuan earthquake. As documented by Rubinstein et al. (2007), Rubinstein et al. (2009), Gomberg (2010), and Chao et al. (2013), surface waves from  $M_w>7$  earthquakes at teleseismic distances commonly trigger tremor on the Cascadia subduction zone off coastal Washington and Oregon. Tremor and ETS events on both subduction zones occur on low-angle megathrust fault planes dipping at 10°–15° at depths of 30–40 km.

Triggered tremor has subsequently been identified on a growing number of subduction zone megathrust fault planes with low-angle dips (10°–15°) at depths of 30–50 km. This includes subduction zones off the west coasts of Mexico, southern Chile, and the east coast of New Zealand (Chao et al., 2013; Fry et al., 2011; Gonzalez-Huizar et al., 2012; Peng et al., 2013; Rubinstein et al., 2010; Zigone et al., 2012). Fry et al. (2011) identified tectonic tremor on the subduction zone beneath the east (Hikurangi) coast of the North Island, New Zealand. Ambient tectonic tremor and instances of triggered tremor have also been identified on several plate-boundary transform faults including the Parkfield section of the San Andreas Fault in central California (Guillhem et al., 2010; Hill et al., 2013; Peng et al., 2009, 2010a,b; Shelly et al., 2011) and some of its branches in northern and southern California (Chao et al., 2012; Gomberg et al., 2008; Wang et al., 2013; Yang and Peng, 2013); the Queen Charlotte Fault on Queen Charlotte Island, Canada; the Oriente fault in

southern Cuba; and the Enriquillo-Plantain Garden fault in Haiti (Aiken et al., 2013a; Gonzales-Huizar et al., 2012; Peng et al., 2013). Triggered tremor has also been identified beneath the Central Range in Taiwan, although it is still not clear whether tremor occurred on a low-angle detachment fault at depths of 15–25 km (Chao et al., 2011; Peng and Chao, 2008) or high-angle thrust faults (Tang et al., 2010, 2013). Wech et al. (2012) identified tectonic tremor at depths of 25–45 km along the deep extension of the transpressional Alpine Fault along the west coast of the South Island of New Zealand, but as of yet anyway, it has no instances of triggered tremor (Table 3).

In most cases, triggered tremor on major subduction zone and transform faults begins with the arrival of the fundamental Love wave with periods ranging from 20 to 200+s and often continues well into the Rayleigh wave coda, in many cases with tremor amplitudes apparently modulated by the Rayleigh wave. Triggered tremor generally occurs in the same source volume that produces background tremor and ETS events, but it is usually somewhat more energetic than the background tremor (Peng et al., 2008; Rubinstein et al., 2007). The Nankai subduction zone represents an exception with most tremor activity commencing with the arrival of the Rayleigh wave. For surface waves arriving with near strike-parallel incidence on the megathrust fault plane (e.g., waves from the 2004  $M_w=9.1$  Sumatra and the 2011  $M_w=9.0$  Tohoku-Oki earthquakes on both Cascadia and Nankai, the 2003  $M_w=8.1$  Tokachi-Oki earthquake on Nankai, and the  $M_w=7.9$  2002 Denali Fault earthquake on Cascadia), Love waves should have a much higher potential for triggering reverse slip than Rayleigh waves. This is consistent with the Cascadia observations (Hill, 2012a) and the inference by Rubinstein et al. (2007) that Cascadia tremor results from small increments of reverse slip on the fault plane. Miyazawa and Brodsky (2008) and Miyazawa et al. (2008) suggested that in Nankai, the Rayleigh wave dilatational stress may have an important role in modulating tectonic tremor beneath southwestern Japan by modulating fracture-zone permeability and pumping fluids through vertical fractures in combination with a relatively high friction coefficient along the megathrust interface (also see Hill, 2012a). More recently, however, Enescu et al. (2012) reported clear evidence of Love wave triggered tremor in the Nankai subduction zone following the 2001  $M_w=7.9$  Kunlun earthquake and the 2012  $M_w=8.6$  Indian Ocean earthquake, both with near strike-parallel incidence.

Surface waves with near strike-parallel incidence ( $\gamma=0$ ) on vertical strike-slip faults also commonly show tremor modulation in phase with the Rayleigh wave following initial, energetic tremor bursts triggered by the Love wave. In this case as well, Rayleigh wave potential for triggering strike-parallel slip is minimal for strike-parallel incidence on vertical faults (see Figure 7(a)). Both observations suggest a possible role for the Rayleigh wave dilatational stress, which, although small, is the largest Rayleigh wave stress component for strike-parallel incidence on vertical faults.

Sufficiently energetic body waves are also capable of triggering tremor. Ghosh et al. (2009) found evidence for tremor on the Parkfield section of the San Andreas Fault triggered by the body-wave phases PKP, PP, SKP, and SKS from the  $M_w=9.1$  Sumatra earthquake. Hill et al. (2013) showed that the 100 s period S- and SS-waves from the  $M_w=9.0$  Tohoku-Oki earthquake also triggered tremor on the Parkfield

**Table 3** Reported instances of dynamic triggering of tectonic tremor

Site	Number of responses	Distance (km)	Triggering phase	Back azimuth (degrees)	Triggering stress (kPa)	References
<i>Subduction zones</i>						
Nankai	6	1033–5100	L, R	Various	~10–20	1–5, 9
Cascadia	5	2309–12 400	L, R	134–311	~10	6–9, 10
S. Alaska, Aleutian	1	4232–5407	L, R	267–276	~10	9
Mexico	1	6751	S, L, R, O	–	5.7	11
Costa Rica	1	12 736	L	320.5	6	9
Southern Chile	1	15 067	R		1–10	17
New Zealand	2	9100–9259	R	S-N; 334	9–10	12, 9
<i>Transform faults</i>						
San Andreas	17		S, L, R, O	Various	0.7–10	9, 13, 14, 18, 19, 20
S. California	1	8606	L, R	307	9	9
Queen Charlotte	3–5		L, R	S-P	7	15
Oriente, Cuba	4	6203–12 479	L, R	80, 302, 328	5–10	10, 16
Garni, Armenia	1	7950	R	55	24	10
<i>Other</i>						
Central Taiwan	T	2652	S, L, R	46	~40	9, 10

Phases: L, Love; R, Rayleigh; S, S-wave; P, P-wave; O, others.

Back azimuth: S-P, strike parallel; S-N, strike normal.

References: 1. Obara (2003); 2. Miyazawa and Mori (2005); 3. Miyazawa and Mori (2006); 4. Miyazawa and Brodsky (2008); 5. Miyazawa et al. (2008); 6. Rubinstein et al. (2007); 7. Rubenstein et al. (2009); 8. Gomberg (2010); 9. Chao et al. (2013); 10. Gonzales-Huizar et al. (2012); 11. Zigone et al. (2012); 12. Fry et al. (2011); 13. Hill et al. (2013); 14. Peng et al. (2010a); 15. Aiken et al. (2013a); 16. Peng et al. (2013); 17. Peng et al. (2012); 18. Guilhem et al. (2010); 19. Shelly et al. (2011); 20. Guilhem and Nadeau (2012).

section of the San Andreas Fault. Zigone et al. (2012) documented triggering by S, ScS, and SS and both Love and Rayleigh waves on the Guerrero segment of the subducting plate beneath the southwest coast of Mexico by the 2010  $M_w=8.8$  Maule earthquake. Miyazawa (2012) described evidence that the P-wave from the Tohoku-Oki earthquake may have triggered tremor bursts and brittle-failure earthquakes in volcanic and geothermal areas as it propagated to the southwest across Shikoku and the Nankai subduction zone.

Episodes of tectonic tremor are commonly triggered by telesismic seismic waves with periods from ~20 to ~200 s and peak dynamic stresses on the order of ~10 kPa with individual tremor bursts modulated by stresses as small as ~1 kPa. Tidal stresses in the solid Earth with periods of 12 and 24 h also modulate tremor activity on both megathrust and transform plate-boundary faults (Hawthorne and Rubin, 2010; Lambert et al., 2009; Nakata et al., 2008; Shelly et al., 2007; Thomas et al., 2009, 2012). The tidal stresses are comparable with the minimum surface-wave stresses that trigger tremor, consistent with tremor-generating sections of the faults being extremely weak with near-lithostatic pore pressures. In the case of tidal-modulated tremor along the Parkfield sections of the San Andreas Fault, for example, the strike-parallel shear stress is ~0.1 kPa consistent with an effective fault-normal stress of between 1 and 10 kPa and a near-lithostatic pore pressure (Thomas et al., 2009, 2012).

#### 4.11.4 Triggered Response Characteristics

Many of the response characteristics of tectonic tremor are covered in the previous section. Here, we focus primarily on

the varied response characteristics of triggered earthquakes in the brittle domain.

##### 4.11.4.1 The Global Search for a Triggering Threshold

Since the early evidence of dynamic triggering emerged, the seismological community has examined waveform characteristics from large remote events responsible for dynamic earthquake triggering for evidence of a triggering threshold. Threshold parameters explored include dependence on peak dynamic strain or stress, frequency, duration, and particle motion of the responsible seismic waves. Evidence for a clear threshold has yet to emerge; indeed, it seems that thresholds are likely site- and time-dependent.

Seismic-wave amplitudes responsible for dynamic triggering are variously reported as peak ground velocity; peak dynamic stress,  $T_p$ ; or peak dynamic strain,  $\epsilon_p$  (e.g., see note 20 in Hill et al., 1993). Although peak dynamic stresses at depth will in general differ from those based on seismograms recorded on the Earth's surface, they can be estimated given a reasonable model for the physical properties of the underlying crust (Gomberg, 1996). In computations of stress amplitudes at depth, for example, the tendency for surface-wave displacement amplitudes and strains to decrease with depth will be offset by one degree or another by the tendency of elastic moduli to increase with depth. Furthermore, surface-wave stresses show considerable variation over depths less than a wavelength (e.g., ~70 km for 20 s waves) depending on fault orientation, incidence angle, and velocity structure (see Figure 7).

As more studies of dynamic triggering have been conducted over the past decade, estimates of the minimum peak dynamic

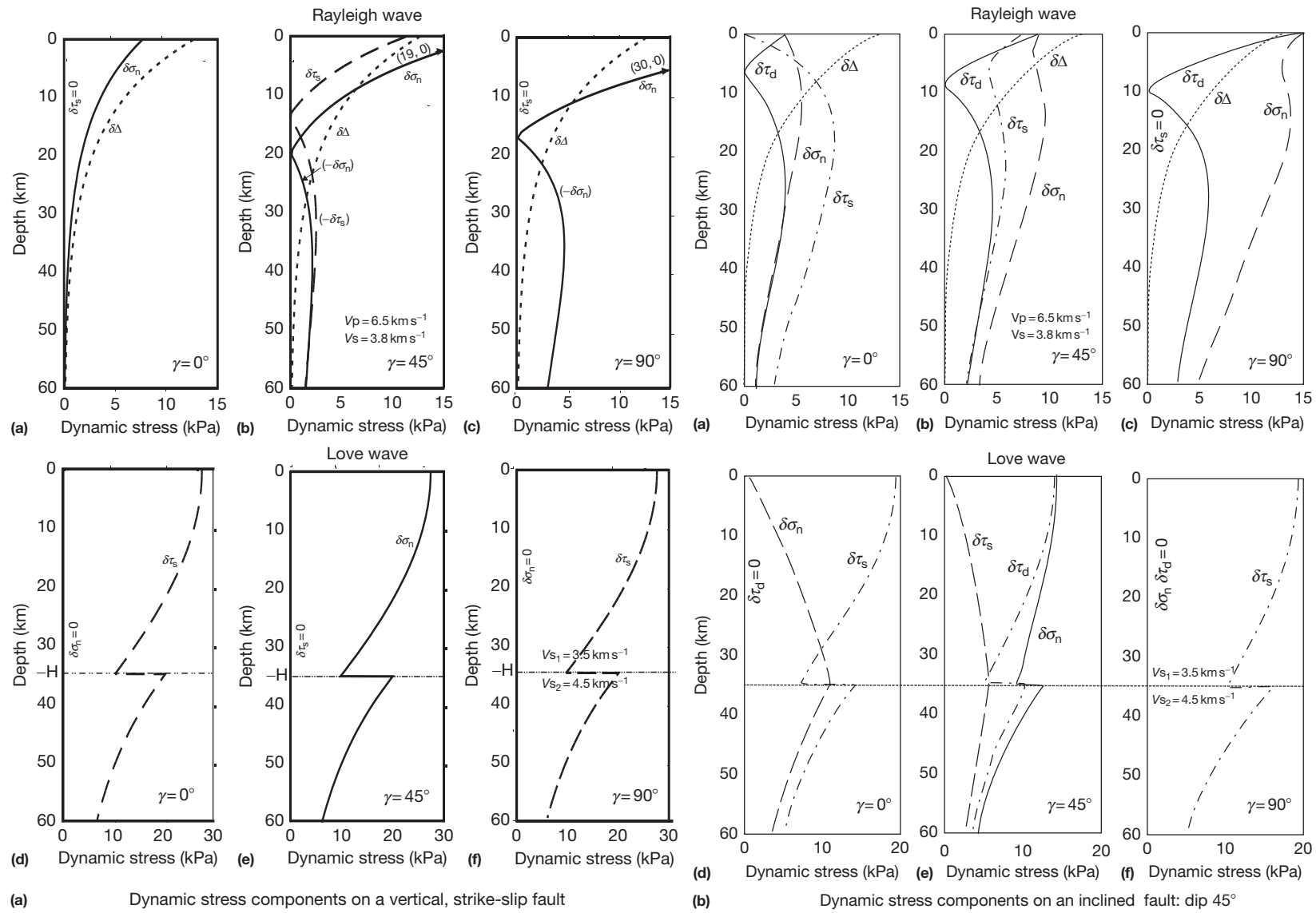


**Figure 7** Peak values of surface-wave stress components as a function of depth for surface waves with period 20 s and displacement amplitudes of 1 cm incident on (a) a vertical fault and (b) inclined fault dipping 45°. Incidence angles are  $\gamma=0^\circ$  (strike parallel),  $45^\circ$  (oblique), and  $90^\circ$  (strike normal). Stress components resolved on the fault planes are  $\delta\sigma_n$ , fault-normal stress;  $\delta\tau_d$  and  $\delta\tau_s$ , dip-parallel and strike-parallel stresses, respectively; and  $\delta\Delta$ , the Rayleigh wave dilatational stress.  $V_p$  and  $V_s$  are the P- and S-wave velocities for the Rayleigh wave half-space model.  $V_{s1}$  and  $V_{s2}$  are S-wave velocities for the top layer and underlying half-space model for Love waves.

strain necessary to trigger earthquakes have been decreasing. Peak dynamic strain associated with specific remotely triggered earthquakes has been reported to be as small as  $3 \times 10^{-7}$  ( $\sim 10$  kPa) at the Coso volcanic field 3660 km from the 2002  $M_w=7.9$  Denali Fault earthquake (Prejean et al., 2004). A recent study based on statistical analyses of earthquake catalogs suggests that dynamic earthquake triggering may result from peak dynamic strains as small as  $3 \times 10^{-9}$  or peak stresses of  $\sim 0.1$  kPa (van der Elst and Brodsky, 2010). At the upper end, peak dynamic stresses can easily exceed 4 MPa within the transitional region to the aftershock zone and near field of a large earthquake (Kilb et al., 2002). Van der Elst and Brodsky (2010) suggested that a simple amplitude threshold may exist for specific areas in California and Japan based on their finding that the number of triggered earthquakes is linearly proportional to peak dynamic strain from large remote earthquakes.

The large range in peak dynamic stresses (or strains) that have resulted in remote triggering together with variations in intrinsic site characteristics indicate that the triggering process does not depend on a simple minimum amplitude threshold for dynamic stresses to be effective in all locales. Laboratory work by Savage and Morone (2008) suggests that variations in fault properties affect the potential for earthquake triggering. Thus, although most instances of dynamic triggering involve dynamic strains,  $\varepsilon_p \sim 10^{-6}$ , or dynamic stresses,  $T_p \sim 30$  kPa (Gomberg and Johnson, 2005), this is neither a necessary nor a sufficient threshold for dynamic triggering (most areas with  $T_p \sim 30$  kPa are not triggered and some areas with  $T_p < 1$  kPa are triggered). In the case of the propagating front of triggered crustal earthquakes that moved across Japan with the P- and surface-wave velocities, Miyazawa (2011) concluded that the triggering P-wave strains of  $\sim 10^{-7}$ – $10^{-8}$  (stresses  $\sim 0.3$  to  $\sim 3$  kPa) were an order of magnitude smaller than the surface-wave strains of  $\sim 10^{-6}$  (stress  $\sim 30$  kPa) from the 2011 Tohoku-Oki earthquake required for dynamic triggering.

The frequency of seismic waves may also be a factor in dynamic triggering thresholds in some environments. Specifically, dynamic stresses with periods of 20–30 s or longer commonly appear to be more effective at inducing a triggered response than those at higher frequencies. Brodsky and Prejean (2005) found that in a volcanic and geothermal environment, the Long Valley Caldera area lower-frequency seismic waves are more likely to trigger seismicity than higher-frequency seismic waves, as lower frequencies are more effective in stimulating fluid flow and fracture unclogging processes in hydrothermal systems (Brodsky et al., 2003). This is consistent with Parsons and Velasco (2009), who concluded that the lack of dynamic triggering at near-to-intermediate distances from underground nuclear explosions reflects minimal surface-wave amplitudes at periods  $\geq 20$  s generated by explosions. In contrast, Wu et al. (2012) showed that in a stable continental interior environment near Beijing, China, a triggering threshold for the area does not depend on frequency of shaking. Gomberg and Johnson (2005) also cited evidence for a frequency-independent threshold. Thus, it seems that a frequency threshold may only exist for specific sites, fault zone properties (Savage and Morone, 2008), or physical triggering mechanisms.

#### 4.11.4.2 Aftershocks and Stress Triggering at Near-to-Intermediate Distance

Stress triggering at near and intermediate distances from a large earthquake is tied to the long-standing question of aftershock generation (Gomberg et al., 2003; Kilb et al., 2002; Nur and Booker, 1972; Marsan, 2003). The most intense aftershock activity generally occurs within a source dimension of the mainshock rupture (the near field), where static and dynamic stresses have comparable amplitudes and minimal temporal separation (Figure 1). Distal portions of an aftershock zone, however, commonly extend one to two source dimensions beyond the rupture zone in the range where static and dynamic stresses begin to assume separate identities. Efforts to distinguish between static stress triggering and dynamic stress triggering in aftershock zones have sought evidence in spatial distribution of aftershocks with respect to stress shadows predicted by static stress transfer models (e.g., Felzer and Brodsky, 2005; Kilb et al., 2002; Chapter 4.10, this volume; Richards-Dinger et al., 2010; Toda et al., 2012; Voisin et al., 2004) as well as for the influence of rupture directivity (Gomberg et al., 2003) and the variation in peak dynamic stress amplitudes with distance (Felzer and Brodsky, 2006). For example, Pollitz and Johnston (2006) pointed to the relative absence of aftershocks following slow earthquakes along the central section of the San Andreas Fault compared with typical earthquakes of similar location and seismic moment as evidence for the importance of dynamic stresses in aftershock production. Di Carli et al. (2008) found that the largest aftershock ( $M_s=5.5$ ) at a distance of 20 km from the 2000  $M=6.7$  western Tottori (Japan) mainshock epicenter was located in the stress shadow of the mainshock and thus that it was dynamically triggered. Similarly, Meng et al. (2013b) found clear evidence that seismic waves from the 2010  $M_w=7.2$  El Mayor-Cucapah earthquake produced dynamic triggering in the Salton Sea area in southern California, which lies within the static stress shadow of the El Mayor-Cucapah mainshock. Based on such studies, it seems that dynamic stresses are important in aftershock generation at all distances, particularly for short times (hours) following the mainshock.

The 2011  $M_w=9.0$  Tohoku-Oki earthquake triggered seismicity throughout much of Japan, most of which was concentrated in the aftershock zone. Toda et al. (2011) cited evidence that static triggering of aftershocks in central Japan extended to distances of  $\sim 425$  km from the Tohoku-Oki epicenter, and as Miyazawa (2011, 2012) documented, the propagation of triggered seismicity across southwestern Japan coincident with both the P-wave and surface waves. The surface wave-triggered activity extended  $\sim 1400$  km southwest of the Tohoku-Oki epicenter with little evidence of propagation to the northeast suggesting the influence of rupture directivity and, therefore, dynamic stress.

This is currently a rapidly evolving research topic with the relative merits of static versus dynamic aftershock triggering the subject of energetic exchanges between advocates of one or the other viewpoint (Harris and Day, 1993; Harris et al., 2002; Stein, 1999; Voisin et al., 2004). Accumulating evidence suggests that dynamic triggering does indeed have a role in aftershock generation and in complex rupture processes in

which major earthquakes consist of multiple, large subevents (e.g., [Aagaard et al., 2004](#); [Antonioli et al., 2002](#); [Rybicki et al., 1985](#); [Voisin et al., 2000](#)). Accumulating results also provide clear evidence for reduced seismicity in the static stress shadow quadrants of mainshocks ([Meng et al., 2013a](#); [Toda et al., 2012](#)). Together, these results indicate that both static triggering and dynamic triggering contribute near-field aftershock generation.

#### **4.11.4.3 Tectonic Setting and Source Radiation Patterns**

The tectonic setting and stress regime have a first-order effect on the style of earthquake activity in any given area. Accumulating evidence indicates that these environmental factors also have an influence on patterns of remotely triggered seismicity. Although remote dynamic triggering occurs in all tectonic environments ([Gonzalez-Huizar et al., 2012](#); [Velasco et al., 2008](#)), extensional or transtensional tectonic regimes, geothermal areas and areas of Quaternary to Recent volcanism, and the tremor-producing transition zones on major plate-boundary faults appear to be particularly susceptible. Dynamic triggering commonly coincides with areas of elevated background seismicity consistent with these areas being in a near-critical stress state.

Seismic-wave radiation patterns from a triggering main-shock can influence the spatial pattern of sites likely to respond to dynamic triggering. Love waves generally have a higher triggering potential than Rayleigh waves ([Hill, 2012a,b](#)). For a given moment and source depth, the four-lobe Love wave radiation pattern for strike-slip faults is more energetic than the corresponding pattern for Rayleigh waves. Peaks in the Love wave radiation pattern are in strike-parallel and strike-normal directions, while peaks in the Rayleigh wave pattern are rotated 45° with respect to the Love wave pattern. As a result, some of the most common and most compelling displays of remote dynamic triggering are associated with  $M > 6.5$  earthquakes on strike-slip faults with unilateral rupture and pronounced strike-parallel directivity as exemplified by the  $M_w = 7.4$  Landers,  $M_w = 7.9$  Denali Fault, and the  $M_w = 8.9$  Indian Ocean earthquakes.

In contrast, the two-lobe Rayleigh wave radiation pattern for dip-slip faults is more energetic than the corresponding four-lobe Love wave pattern for a given moment and source depth. Peaks in the two-lobe Rayleigh wave radiation pattern are in the slip direction and normal to fault strike (see Figure 11.19 in [Dahlen and Tromp, 1998](#)). Moment matters, of course, and the energetic Love and Rayleigh waves produced by megathrust earthquakes on subduction zones both contribute to widespread dynamic triggering as underscored by the 2004  $M_w = 9.1$  Sumatra-Andaman earthquake ([Lay et al., 2005](#)), the 2010  $M_w = 8.8$  Maule earthquake, and the 2011  $M_w = 9.0$  Tohoku-Oki earthquake. The lack of published descriptions of remote dynamic triggering attributable to large normal fault earthquakes may be largely a matter of sampling. Few  $M > 6.5$  normal earthquakes have occurred in well-instrumented continental environments in the last 25 years. In any case, and in spite of triggering-potential expatiations based on theoretical seismic wave radiation patterns, there is no substitute for using observed seismic waveforms recorded on broadband seismic stations (if available) to evaluate the

triggering potential of seismic waves incident on a nearby fault of known orientation.

The predominate remote response triggered by the Landers, Hector Mine, and Denali Fault strike-slip earthquakes was in the direction of maximum rupture directivity and in areas of transtensional tectonics characterized by elevated background seismicity ([Hill and Prejean, 2007](#)). This was underscored, for example, by the absence of a triggered response along the creeping section of the San Andreas Fault through central California and Parkfield that, although a persistent source of small earthquakes and in the peak directivity direction for the Landers rupture, is a transpressional stress regime ([Spudich et al., 1995](#)). In all three cases, many of the triggered sites were areas of geothermal activity and/or Quaternary volcanism.

In contrast, [Jiang et al. \(2010\)](#) found that the 2008  $M_w = 7.9$  Wenchuan earthquake in southern China triggered seismicity increases in the vicinity of widely scattered, historically active faults north of the epicenter (in the general direction of rupture propagation). The triggered seismicity occurred in both transtensional and transpressional tectonic regimes and mostly in areas not associated with geothermal or volcanic activity.

Extensional and transtensional stress regimes have three closely related properties that might enhance their susceptibility to dynamic triggering: (1) The least principal stress is subhorizontal. Extension cracks, which form in planes normal to the least principal stress, that are vertical. This facilitates the upward migration of crustal fluids from warmer, higher-pressure conditions at depth toward the surface through vertically oriented cracks. Volcanic and geothermal areas tend to be concentrated in extensional regimes. (2) As illustrated in [Figure 8\(a\)](#), faults in an extensional regime are intrinsically weaker than those in compressional regimes given a uniform coefficient of friction and Andersonian faulting ([Sibson, 1982](#)). [Hough and Kanamori \(2002\)](#), for example, suggested that elevated pore pressures and temperatures associated with geothermal areas should enhance this difference (illustrated by the dashed Mohr's circle in [Figure 8\(a\)](#)). (3) Normal faults are more susceptible to triggering by surface waves than reverse faults in the upper crust (e.g.,  $z < 10$  km for 20 s waves), although this difference diminishes with increasing depth ([Hill, 2012a](#)).

Subduction-related volcanic centers are located on convergent plate boundaries. Locally, however, they commonly coincide with a zone of crustal extension and transtensional deformation associated with upward flexure of the overriding plate. This is the case for the Katmai volcanic field in Alaska ([Moran, 2003](#)), for example, and most of the Cascade volcanoes in the Pacific Northwest states. Mt. Rainier in Washington is exceptional with its setting in a transpressional stress regime. Even here, however, focal mechanisms for earthquakes occurring within the edifice of the volcano or shallow crust immediately below the volcano show a combination of strike-slip and normal faulting ([Moran et al., 2000](#); [Shelly et al., 2013](#)).

Examples of evidence for remote triggering in compressional/transpressional regimes include the Bowen Basin in the stable Australian craton ([Gonzalez-Huizar and Velasco, 2011](#)), the Ohio River Valley area, and Atlantic coast states following the 1811–12 New Madrid, Missouri, earthquakes and the Charleston, South Carolina, earthquake in 1887 ([Hough, 2001](#); [Hough et al., 2003](#)). Another involves evidence for apparent seismicity increases at distances of 70–200 km

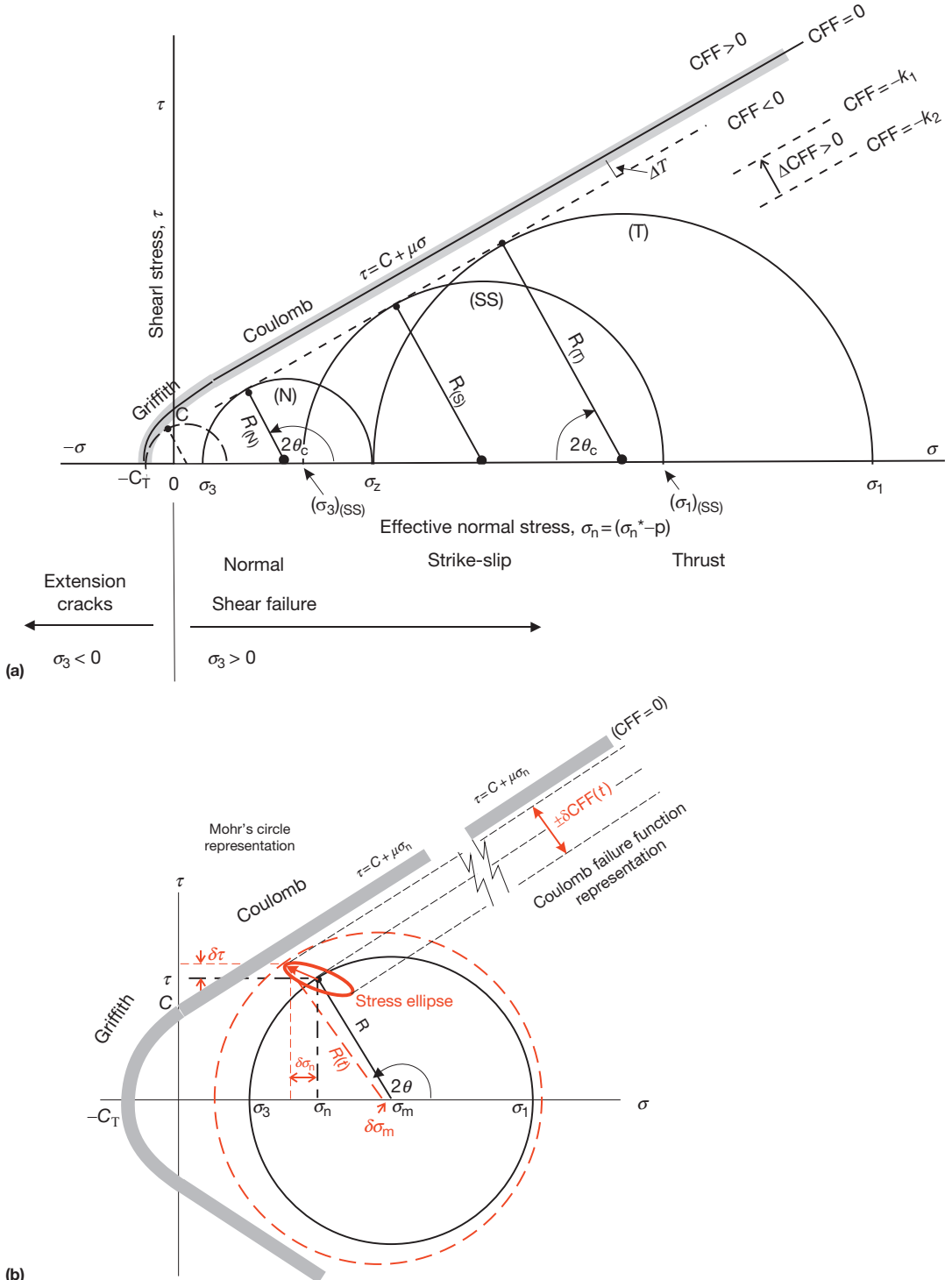


**Figure 8** (a) Mohr's diagram comparing maximum stress levels for extensional (normal faulting,  $N$ ) and compressional (thrust faulting,  $T$ ) regimes in a pervasively faulted crust with a common (e.g., hydrostatic) pore pressure and with frictional strength limited by the Coulomb failure criteria.  $\tau$  and  $\sigma$  are the shear stress and effective normal stress components, respectively, acting on a fault plane at an angle,  $\theta$ , with respect to the least principal stress,  $\sigma_3$ . The coefficient of static friction is  $\mu \sim 0.6$  with the gray band representing scatter in data.  $C$  and  $C_t$  are the cohesive and tensile strengths, respectively. The effective normal stress  $\sigma = (\sigma_n^* - P)$ , or the rock matrix normal stress  $\sigma_n^*$  reduced by the pore pressure,  $P$ . The vertical (lithostatic) stress,  $\sigma_z$ , is the greatest principal stress,  $\sigma_1$ , and least principal stress,  $\sigma_3$ , for the extensional (normal faulting) and compressional (thrust faulting) regimes. The radius,  $R$ , is half the stress difference, or  $R = \frac{1}{2}(\sigma_1 - \sigma_3)$ . Failure occurs when the Mohr's circles for optimally oriented faults ( $\theta = \theta_c$ ) first touch the Coulomb failure envelope ( $CFF = 0$ ). The strike-slip stress (SS) regime is intermediate between the thrust (T) and normal (N) regimes. The small dashed circle illustrates the case for superhydrostatic pore pressure in an extensional regime. Hydrofracturing results along vertically oriented cracks in the extensional regime if the pore pressure exceeds the least principal stress such that  $\sigma_3 \leq 0$ .

(b) A dynamic stress orbit (red ellipse) in the  $\sigma-\tau$  coordinate space of a two-dimensional Mohr's circle and the Coulomb–Griffith failure criteria. Black lines define the background stress state,  $R(t < t_0)$ , for a fault at an angle,  $\theta(t < t_0)$ , with respect to the least principal stress,  $\sigma_3$ .  $\sigma_m = \frac{1}{2}(\sigma_1 - \sigma_3)$  is the two-dimensional mean stress. The red lines represent a snapshot in time of the stress state perturbed by dynamic stresses. The dynamic stress orbit is traced by the point  $R$  on the circumference of the circle through one stressing cycle. The dynamic Coulomb failure function  $\delta CFF(t)$  corresponds to the projection of the stress orbit onto a normal to the Coulomb failure envelope,  $\tau = C + \mu\sigma_n$ .

triggered by dynamic stresses associated with supercritical SmS waves from 15 moderate earthquakes ( $M \sim 5$ ) in coastal California (Hough, 2005). In this case, several areas of slightly elevated  $\beta$ -statistic values were located within the transpressional Coast Ranges. Hough et al. (2005) also suggested that SmS waves may have triggered a  $M > 7$  earthquake a few minutes after the  $M_w = 7.8$  earthquake in 1905 in the compressional Kangra region of India.

This raises a question regarding the meaning of the crust being in a state of incipient failure nearly everywhere (Zoback and Zoback, 2002). Within the context of Figure 8(a), a weak, extensional crust offers no particular advantage over a strong compressional crust if incipient failure means that, on average, the stress level everywhere hovers below the failure strength by some common increment,  $\Delta T$  (this corresponds to a stress state defined by a line parallel with but incrementally below the Coulomb failure curve, CFF=0 in Figure 8(a)). A weak crust would be more susceptible to dynamic triggering, however, if average stress levels were some large fraction of the failure stress (represented by a line with a smaller slope than that for CFF=0 in Figure 8(a)). Currently available data seem ambiguous on this point. Any diminished propensity for triggering in stable intraplate regions due to a stronger crust may be at least partially offset, however, by the fact that seismic wave amplitudes generally decay more rapidly with distance in tectonically active regimes than in stable intraplate regions because of the higher intrinsic attenuation and the presence of velocity inversions in the lower crust and upper mantle that partially channel both body-wave energy and normal-mode (surface-wave) energy within depth intervals below the brittle crust (Bakun and McGarr, 2002).

#### 4.11.4.4 Onsets, Delay Times, Durations, and Repeat Intervals

Rapid-onset triggering commonly coincides with the arrival of the large-amplitude Love or Rayleigh waves. Less commonly, it coincides with the S-wave arrivals (Hill et al., 2013; Prejean et al., 2004; Shelly et al., 2011; Zigone et al., 2012) and occasionally with P-wave arrivals (Ghosh et al., 2009; Miyazawa, 2012).

Reported delay times,  $\Delta t$ , between the arrival of the dynamic waves and the apparent onset of locally triggered seismicity vary from minutes to weeks or more. Delay times for the well-recorded instances of dynamic triggering from the Landers, Hector Mine, and Denali Fault earthquakes ranged from tens of seconds to between 24 and 33 h. The triggered response of the Western Ghats geothermal area in India to the 2001  $M_w = 7.6$  Bhuj earthquake was delayed by 2.5 h (Surve and Mohan, 2012). Delay times reported for suspected dynamically triggered earthquakes in the Taiwan region approach 15 days (Beresnev and Wen, 1995; Wen et al., 1996) and, in the Valley of Mexico,  $\sim 30$  days (Singh et al., 1998). The longer the delay time, of course, the more tenuous the case for a causal link between the dynamic stresses and a local seismicity rate increase. Establishing a causal link between passing dynamic stresses and an isolated event or the onset of sequence with longer delay times requires independent, multiparameter data indicating the ‘triggered’ seismicity is a secondary response to some aseismic process (e.g., aseismic slip or pressure change in

the case of volcanic systems) triggered by passing dynamic waves and/or a well-tested physical model that accounts for the delay between the arrival of dynamic stresses and the local onset of brittle failure.

Durand et al. (2010, 2013) described a pattern of rapid-onset and delayed triggering in the near-to-intermediate field following the 1999  $M_w = 7.6$  Izmit earthquake that they attribute to dynamic triggering and static triggering, respectively. The rapid-onset triggering was limited to strike-slip faults subparallel with the westward extension of the North Anatolian Fault in the eastern Marmara Sea west of the Izmit rupture and within a static stress shadow of the Izmit rupture. Here, the seismicity increased abruptly with passing of the seismic waves from the Izmit earthquake and abruptly died away. In contrast, seismicity in extensional areas to the north and south began more slowly and continued at elevated rates for months to years, which they attribute to static pressure changes and fluid flow.

Reported delay times based on recordings from standard, short-period seismic networks may overestimate actual delay times because local earthquakes are typically masked by the large-amplitude surface waves from large earthquakes. The development of broadband, high-dynamic-range instrumentation and digital processing has greatly enhanced our ability to recognize the early onset of local earthquake activity within coda waves from large, distant earthquakes through effective filtering. Prejean et al. (2004) found this to be the case in their search for dynamic triggering along the west coast of the United States following the  $M_w = 7.9$  Denali Fault earthquake in 2002 (see Figure 4). Applying a  $\beta$ -statistic test to the Pacific Northwest and California earthquake catalogs produced no clear evidence for dynamic triggering. By applying a high-pass filter to seismograms from broadband and strong motion instruments, however, they discovered a plethora of small earthquakes embedded in the strong surface waves from the Denali earthquake at four sites in Washington and California from Mount Rainier ( $\Delta \sim 3108$  km) south to the Coso volcanic field in southern California ( $\Delta \sim 3660$  km). Small delay times were the rule for most instances of dynamic triggering from the Denali Fault earthquake.

This underscores two points: (1) Rapid-onset dynamic triggering with small delay times ( $\Delta t \sim 0$ ) with respect to peak dynamic stresses is probably considerably more common than generally realized, and (2) our ability to detect dynamic triggering remains extremely uneven depending critically on the distribution of dense, high-quality seismic networks that include broadband, high-dynamic-range digital instruments.

Durations of dynamically triggered seismicity sequences range from a few minutes to several weeks. Short-lived episodes of triggered seismicity often appear as a rapid-fire sequence of overlapping, brittle-failure earthquakes (spasmodic bursts) within the surface-wave train. Longer-lived episodes more commonly evolve as earthquake swarms or foreshock–aftershock sequences with a temporal decay well described by a modified Omori’s law of the form

$$n(t) = k/(t+c)^p \quad [1]$$

where  $n(t)$  is the number of earthquakes per unit time  $t$  and  $k$ ,  $c$ , and  $p$  are parameters (Kisslinger and Jones, 1991). Pankow et al. (2004), for example, use this relation to estimate

durations of ~25 days for the seismicity triggered in central Utah by the 2002 Denali Fault earthquake. [Hainzl and Ogata \(2005\)](#) described a promising application of the epidemic-type aftershock sequence (ETAS) model that can be used to recognize the modulating role pore pressure diffusion in swarm-like triggered sequences. Generally speaking, longer durations tend to be associated with more energetic episodes of triggered seismicity. Indeed, [Brodsky \(2006\)](#) argued that the duration of most triggered sequences can in principle be predicted from the cumulative seismic moment of events triggered during the passage of seismic waves (dynamic stressing).

Many sites with documented remote triggering have responded more than once to the dynamic waves from distant earthquakes. Notable examples include the tremor-generating transition zones on the Nankai and Cascadia subduction megathrust faults, the Parkfield section of the San Andreas Fault, and the Central Range in Taiwan, which seem to respond to most  $M > 7.5$  earthquakes. Other commonly repeating sites are in volcanic/geothermal areas including the Geysers geothermal field in northern California; the Coso volcanic field in southeastern California; the Katmai volcanic field in Alaska; Iwo Jima and Aso volcano in Japan; and the Fangshorn pluton in China. [Peng et al. \(2011a,b\)](#) described a special case of repeated triggering in which successive passes of surface waves circling the Earth ( $G_1$ ,  $G_2$ , and  $G_3$  and  $R_1$  and  $R_2$ ) from the 2010  $M_w = 8.8$  Chile earthquake triggered successive bursts of seismicity in the Coso geothermal field with delays of roughly 80, 160, and 240 min. Similar cases of tremor and microearthquakes triggered by multiple surface waves from the Chile mainshock were documented by [Jay et al. \(2012\)](#) and [Zigone et al. \(2012\)](#).

Repeating sites raise the question of recharge times. Each instance of remotely triggered seismicity releases locally stored energy, thus moving the responding site incrementally away from the near-critical state that existed just prior to the arrival of the dynamic stresses. The time required for the site to return to a near-critical state (the recharge time) will depend on a host of factors including (1) the energy released during the most recent episode of seismic activity whether remotely triggered or not and (2) the background rate of active processes feeding energy into the local crustal volume ([Harrington and Brodsky, 2006](#); [Miyazawa et al., 2005](#)). As an example of (1), Rabaul caldera (Papua New Guinea) responded to a  $M7$  earthquake at a distance of 180 km with a pronounced earthquake swarm but produced no detectable activity in response to a second  $M7$  earthquake 2 months later at a distance of only 60 km ([Mori et al., 1989](#)). [Wu et al. \(2012\)](#) showed a similar need for recharge time for dynamic triggering in the Fangshorn pluton region near Beijing China. Recharge times for the Geysers geothermal area appear to be short – a matter of months or less ([Gomberg and Davis, 1996](#)). They are apparently much longer (but ill-constrained) for Long Valley Caldera where none of the triggered sites are strictly repetitive ([Brodsky and Prejean, 2005](#)). The short recharge times for triggered tectonic tremor on plate-boundary megathrust and transform faults are consistent with small stress drops, persistent background tremor, and exceptionally low fault strength ( $\mu \leq 0.2$ ) such that the tremor-generating transition zone is in a perpetual state of incipient failure. Recharge times and their spatial-temporal fluctuations complicate efforts to establish triggering thresholds for

dynamic stresses (e.g., [Gomberg, 1996](#); [Gomberg and Johnson, 2005](#)). At the same time, they offer important clues to the processes behind dynamic triggering at any given site.

#### 4.11.4.5 Triggering and Modulation by Solid Earth Tides

One of the long-standing puzzles in seismology has been why the periodic stressing of the Earth's crust by solid Earth tides appears to have little or no influence on temporal patterns of earthquake occurrence – particularly given evidence that broad sections of the crust are in a state of incipient failure. Exceptions appeared to be limited to (1) shallow earthquake swarm activity in volcanic and geothermal areas ([Klein, 1976](#); [Tolstoy et al., 2002](#); [Wilcock, 2001](#)) and (2) modulation of tectonic tremor in the transition zones along major plate-boundary faults ([Ide, 2010](#); [Rubinstein et al., 2008](#); [Thomas et al., 2009, 2012](#)). [Tanaka et al. \(2004\)](#) and [Cochran et al. \(2004\)](#), however, presented convincing evidence that the solid Earth tides in combination with ocean loading tides do indeed modulate the occurrence of crustal thrust earthquakes in convergent margins around the Pacific basin at the 10–20% level. The key to the latter apparently lies in correlating well-constrained focal mechanisms from a massive number of earthquakes (tens of thousands) with the phase of the tidal cycle that augment the local tectonic stress directions. These results are consistent with inferences based on laboratory measurements that cyclical stressing at the 1–4 kPa level should modulate ~1% of the background seismicity ([Beeler and Lockner, 2003](#); [Lockner and Beeler, 1999](#)). While strictly speaking, solid Earth tides represent a quasistatic process (the inertial component in the equations of motion are negligible for solid Earth tides), they suggest a lower bound of 0.1–1 kPa as a low-frequency triggering threshold based on the strike-parallel, shear stress component of the tides capable of modulating tectonic tremor on the San Andreas Fault ([Thomas et al., 2012](#)).

#### 4.11.4.6 Earthquake Hazard Implications of Dynamic Triggering

Most earthquakes triggered during passing seismic waves from large earthquakes are small to moderate ( $\leq M_w = 5.0\text{--}5.5$ , e.g., [Anderson et al., 1994](#); [Lei et al., 2011](#); [Parsons and Velasco, 2011](#)). [Parsons et al. \(2012\)](#) suggested that stress changes from surface waves of large, distant earthquakes are too short and spatially limited to trigger a damaging earthquake based on modeling stress changes from the seismic wave field on a fault. They based their modeling on 20–60 s surface waves recorded in Utah from the 2002  $M_w = 7.9$  Denali earthquake. Love waves from the  $M_w = 9.1$  Tohoku earthquake recorded along the San Andreas Fault in California, however, had a period of 200 s ([Hill et al., 2013](#)). Longer periods imply coherent stresses over longer times and greater areas and thus the possibility of larger earthquakes triggered during dynamic stressing.

Accumulating evidence, however, indicates that larger, potentially damaging earthquakes are more likely to occur as a result of delayed triggering. This was underscored by the dramatic fivefold increase in the global rate of  $M_w = 5.5\text{--}7.0$  earthquakes in the 6 days following the 2012  $M_w = 8.6$  Indian Ocean earthquake ([Pollitz et al., 2012](#)). Also, [Gonzalez-Huizar et al. \(2012\)](#) found that delayed dynamically triggered

earthquakes are larger than events triggered during the surface waves, and Lin (2012) suggested that surface waves from the 2008  $M_w=6.6$  earthquake in Indonesia may have triggered a  $M=6.9$  earthquake in Hokkaido, Japan. More recently, it has been seen that the rate of  $M>5.5$  crustal earthquakes is significantly increased in the days following all large subduction thrust earthquakes ( $>M8.6$ ) since 1960 by examining historical earthquake catalogs and moment tensors.

Although many questions remain over the significance of delayed triggering and the processes linking the triggering stress to the nucleation of the delayed earthquake, there can be little doubt that delayed triggering is real. The challenge lies in obtaining high-resolution, broadband data capable of resolving aseismic processes linking an applied dynamic stress to the nucleation of a triggered event, thereby precluding random coincidence (e.g., Tape et al., 2013). In any case, the chance that a local, damaging earthquake will be triggered by a major earthquake elsewhere on the globe, while finite, remains quite small.

#### 4.11.5 Proposed Models

The rapidly accumulating evidence for widespread dynamic triggering has spawned a host of physical models to explain how relatively low-amplitude oscillatory seismic waves can trigger earthquakes at distances of 100s to 1000s of km. Here, we describe the more widely cited of these models and the conditions and locations under which each is viable.

Although most instances of instantaneous remote dynamic triggering coincide with surface waves from large earthquakes, a minority coincide with energetic body-wave arrivals (Ghosh et al., 2009; Hill et al., 2013; Miyazawa, 2012; Shelly et al., 2011; Zigone et al., 2012). Because dynamic stresses associated with both surface- and body-wave stresses are calculable as a function of depth, they provide a means of quantitatively evaluating the stress components acting on the source structure (most commonly a fault) hosting triggered activity. The same is true for tidal stresses responsible for modulating levels of crustal seismicity or tremor activity in the transitions zone (Thomas et al., 2009, 2012).

##### 4.11.5.1 Triggering by Frictional Failure

This class of models involves direct triggering with either static or dynamic stresses providing the stress increment necessary to exceed the frictional strength of faults, thus leading to unstable slip and local earthquakes. This concept is commonly expressed in terms of a change in the Coulomb failure function, or

$$\Delta CFF = \Delta\tau - \mu_s \Delta\sigma_n \quad [2]$$

where

$$CFF = |\tau| - \mu_s \sigma_n - C \quad [3]$$

is the Coulomb failure function,  $\tau$  and  $\sigma_n$  are the shear and normal stress components acting on the fault, respectively,  $\mu_s$  is the static coefficient of friction, and  $C$  is the cohesive strength (e.g., Cocco and Rice, 2002; Harris, 1998; Kilb et al., 2002; Openheimer et al., 1988).  $CFF=0$  corresponds to Byerlee's law for frictional failure (Byerlee, 1980), and a positive change

in  $CFF$ , or  $\Delta CFF > 0$ , indicates that the stress state has moved incrementally toward  $CFF=0$  and Coulomb failure.

Under a generalized Coulomb failure model, shear failure on a fault is imitated when the shear stress,  $\tau$ , acting on a fault plane exceeds the combined cohesive strength,  $C$ , and frictional strength ( $\mu_s \sigma_n$ ) of the fault, or

$$\tau = \pm [C + \mu_s \sigma_n] \quad [4]$$

such that the Coulomb failure function (eqn [3])  $CFF \geq 0$ . In the  $\sigma-\tau$  space of a Mohr's diagram (Figure 8), the constants  $CFF=K_\nu$  form a family of straight lines of with slope,  $\mu_s$  with  $CFF=0$  representing Byerlee's law for frictional failure. Slip evolution following the onset of shear failure may be governed by one of the several nonlinear laws such as the Dieterich-Ruina rate-state friction law (Dieterich, 1979, Chapter 4.04, this volume).

Frictional models are commonly discussed within the context of a steady loading rate (far-field plate motion or the steady extension of a spring in the case of a slider block model) and a 'clock change.' A 'clock advance,' for example, results if a small dynamic perturbation in the applied stress triggers a slip event that would not have otherwise occurred until the failure threshold was reached under the steady, far-field loading rate (e.g., Gomberg et al., 1997, 2005; Perfettini et al., 2003). One consequence of a clock advance in this context is that the time to the next slip event under far-field loading is inversely proportional to the far-field loading rate. Frictional models involve fluids only indirectly through the effect of pore pressure on the effective normal stress (or equivalently, an effective coefficient of friction) on fault planes. For dynamic stresses with periods of minutes or less, the rock matrix will behave as an undrained poroelastic medium with fluid transport having a negligible influence on pore pressure fluctuations (Cocco and Rice, 2002). Frictional models for dynamic triggering will be limited to areas where the stress state on preexisting crustal faults hovers below the Coulomb failure stress by less than the peak dynamic stress amplitude.

##### 4.11.5.1.1 Coulomb failure under dynamic stresses

By analogy with eqn [2], the dynamic Coulomb failure function is

$$\delta CFF(t) = |\delta\tau(t)| - \mu_s \delta\sigma_n(t) \quad [5]$$

(Kilb et al., 2000). In the stable domain ( $CFF < 0$ ), a positive  $\delta CFF(t)$  indicates that the stress state has moved incrementally toward failure. Under the Coulomb failure model for dynamic triggering (Figure 9), the traction  $T[R(t), \theta(t)]$  on a fault at angle  $\theta$  with respect to the least principal stress,  $\sigma_3$ , of the initial stress state,  $T(t_0)$ , begins an oscillatory trajectory as the seismic waves arrive at time  $t_0$ . A triggered earthquake results if the trajectory of the stress orbit enters the Coulomb failure zone  $CFF \sim 0$  (gray band in Figure 9).

One can estimate an in situ triggering potential,  $0 \leq P(\gamma) \leq 1$ , for seismic surface waves as a function of incidence angle,  $\gamma$ , on a fault of known orientation based on the shape and orientation of the stress orbit for given wave type with respect to the Coulomb failure envelope with a friction coefficient appropriate for the target fault (Hill, 2012a,b).  $P(\gamma)$  represents the maximum positive value of  $\delta CFF$  normalized by the largest semimajor axis,  $L$ , for the stress orbits spanning the entire

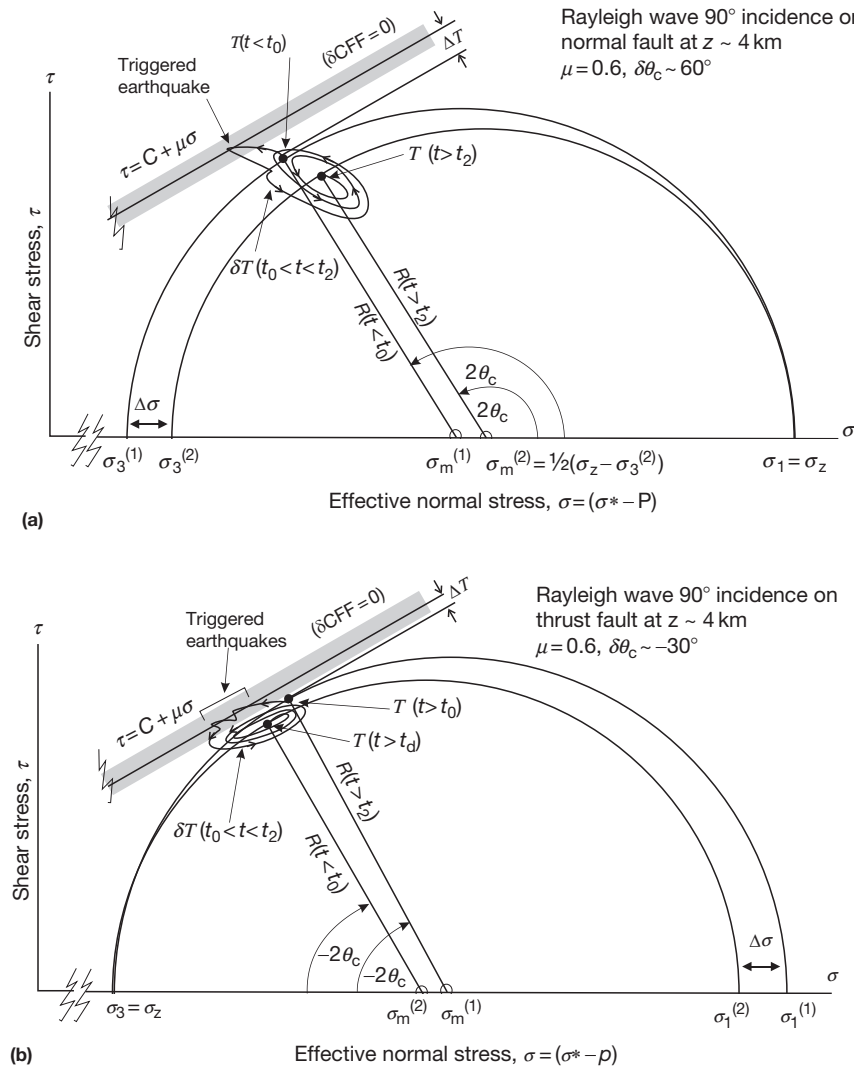


**Figure 9** Schematic illustration comparing the dynamic triggering under the Coulomb failure model for (a) extensional and (b) compressional regimes. The point  $T(t < t_0)$  represents a stable stress state slightly below the failure threshold on a fault at an angle  $\theta(t < t_0)$  with respect to the local least principal stress direction,  $\sigma_3$ , which is horizontal in extensional regimes (a) and vertical in compressional regimes (b). Note that the vertical stress (lithostatic load),  $\sigma_z$ , corresponds to  $\sigma_1$  in (a) and  $\sigma_3$  in (b). At  $t = t_0$ , dynamic stresses from a distant earthquake arrive producing an oscillatory perturbation  $\delta T(t_0 < t < t_2)$  in both the orientation and the magnitude of the local stress field. Slip occurs whenever  $\delta T(t_0 < t < t_2)$  intersects the Coulomb failure zone,  $CFF \sim 0$  (gray band) confining  $T(R(t), \theta(t))$  excursions to within or below this zone ( $CFF \geq 0$ ). The dynamic stresses die away at time  $t_2$ , and the stress state on the fault settles to  $T(t > t_2)$  reflecting the stress drop associated with the triggered seismicity. The lithostatic load,  $\sigma_z$ , corresponds to the greatest and least principal stresses in extensional and compressional regimes, respectively.

range of incidence angles,  $-90^\circ \leq \gamma \leq 90^\circ$ , or  $P(\gamma) = |\delta CFF|_{m/L}$  (see Figure 10 in Hill, 2012b). In the case of Love waves incident on a vertical fault, the stress orbits are rectilinear and of the same length for all incidence angles. They rotate in  $\delta\sigma - \delta\tau$  space from 0 to  $2\pi$  as the incidence angle varies from 0 to  $\pi$ . Thus,  $P(\gamma)$  varies from 0 to 1 as the orbit rotates from a parallel to perpendicular orientation with respect to the slope of the Coulomb failure envelope (Figures 8 and 10 in Hill, 2012a). Note that (1)  $P(\gamma)$  is a 'floating' potential in the sense that the absolute ambient stress acting on a given fault and thus its proximity to

criticality are generally not known and (2) its value depends on the assumed friction coefficient,  $\mu_s$  (the slope of the Coulomb failure envelope). Results for surface waves indicate that for most configurations, Love waves have a higher triggering potential than Rayleigh waves with comparable surface displacement amplitudes but that details depend critically on fault type (e.g., normal, reverse, and strike-slip), orientation, depth, friction coefficient, and the wave incidence angle,  $\gamma$ .

Figure 10 illustrates the sensitivity of triggering potentials to incidence angle,  $\gamma$ , and friction coefficient,  $\mu$ , on vertical

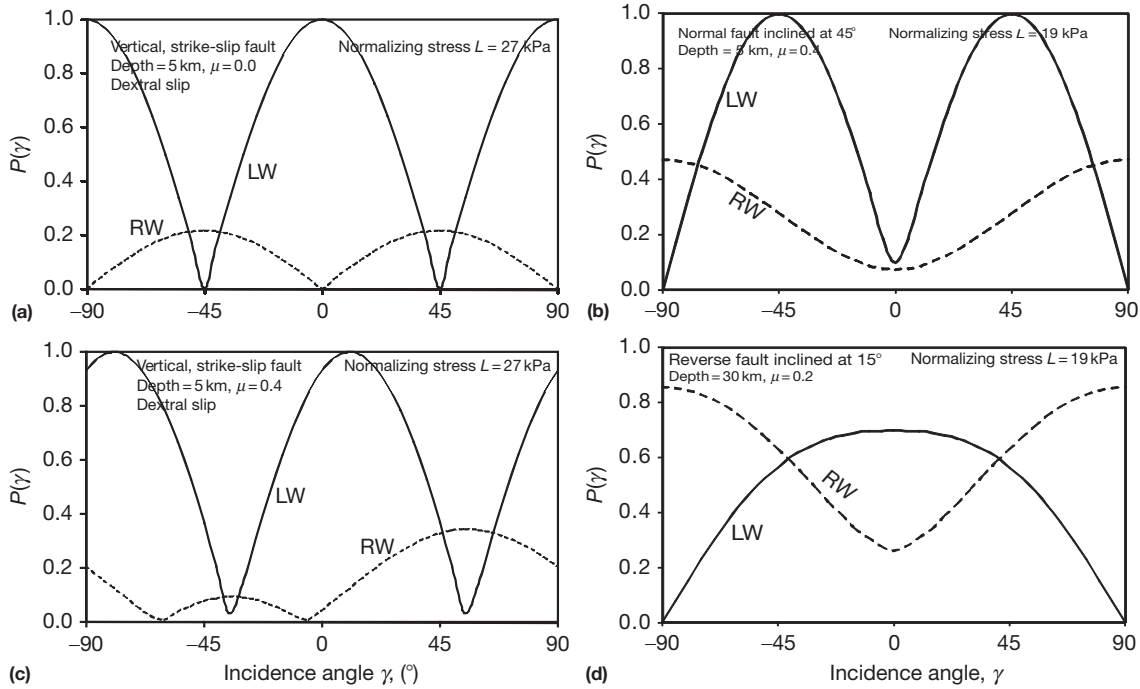


**Figure 10** Variations in triggering potentials as a function of incidence angle,  $\gamma$ , for Love and Rayleigh waves incident on a vertical right-lateral, strike-slip fault at 5 km depth with friction coefficients (a)  $\mu=0$  and (b)  $\mu=0.4$  and inclined faults (c) with normal slip on a fault dipping  $45^\circ$  at a depth of 5 km and (d) reverse slip on a fault dipping  $15^\circ$  at 30 km with dip of  $15^\circ$ . The friction coefficients are  $\mu=0.4$  and 0.2 for (c) and (d), respectively. Multiplying the triggering potential  $P(\gamma)$  by the normalizing stress,  $L$ , gives amplitudes of the strike-parallel (a) or dip-parallel (b) shear stress components acting on the respective fault planes for 20 s Love and Rayleigh waves with comparable displacement amplitudes,  $A=0.01 \text{ m}$ , at the Earth's surface.

strike-slip faults (Figure 10(a) and 10(b)) and dip-slip faults at two depths both inclined at  $45^\circ$  (Figure 10(c) and 10(d)). Note in the case of vertical strike-slip faults (left panels) the following:

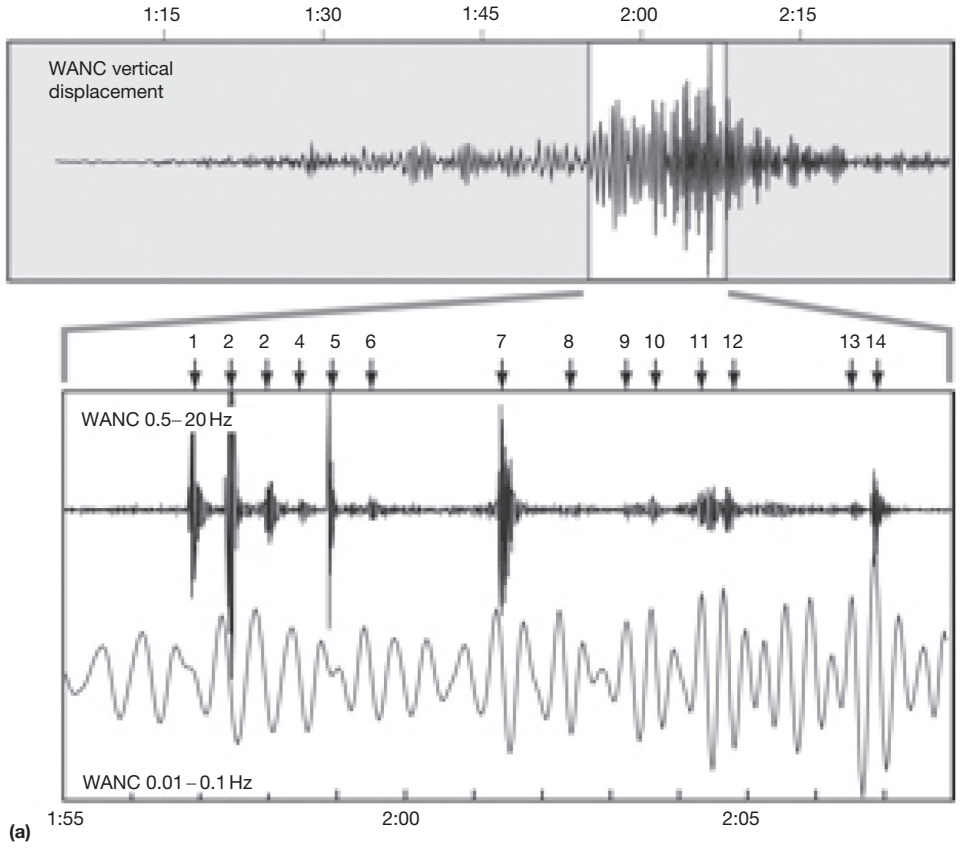
- Love and Rayleigh wave potentials are anticorrelated with Love wave potentials dominating except near peaks in Rayleigh wave potentials.
- For a frictionless fault (Figure 10(a)), the potential curves are symmetric about  $\gamma=0$  (strike-parallel incidence) with Love wave potentials peaking at  $0^\circ$  and  $\pm 90^\circ$  and Rayleigh wave potential peaking at  $\pm 45^\circ$ .
- For a finite friction ( $\mu=0.4$  in this case), the peaks and troughs are shifted to the right for dextral slip and by an equal amount to the left for sinistral slip (not illustrated). The amount of shift varies with the friction coefficient.

Note in the case of the inclined, dip-slip faults the following:

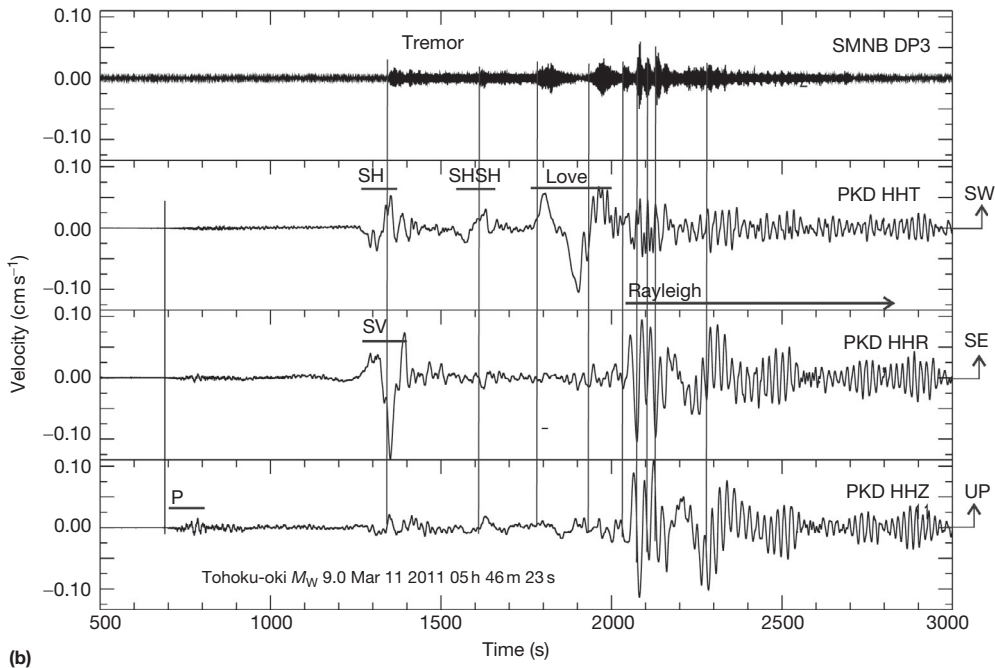
- At 5 km depth and  $\mu=0.4$ , the Love wave potential peaks at  $\pm 45^\circ$ , while the Rayleigh wave potential for normal faults peaks at  $\pm 90^\circ$ . The Love wave potential dominates except in the vicinity of  $\pm 90^\circ$ . Both approach null values at  $0^\circ$ .
- At 30 km depth (tremor-generating depths) and  $\mu=0.2$ , Love and Rayleigh wave potentials are anticorrelated with comparable peak amplitudes. The Love wave peaks at  $0^\circ$  and the Rayleigh wave potential for reverse faults peaks at  $\pm 90^\circ$ .

The complex variations in triggering potentials with fault orientation, incidence angle, depth, and fault friction for the examples in Figures 7 and 10 emphasize the importance of having some constraints on these parameters when attempting to understand what role the various surface-wave stress components play in a given incidence of triggered seismicity.

As illustrated in Figure 9, the stress drop associated with the triggered earthquake alters the stress state (its orientation,  $\theta$ , and the stress difference,  $R(t_2) < R(t_0)$ ) in the vicinity of the fault such that the traction on the fault settles to a new value,  $T$  ( $t > t_2$ ), after the seismic waves have passed. In the case of small stress drops and weak fault, bursts of triggered earthquakes may occur in phase with several cycles of the passing surface waves. In Figure 11(a), for example, small earthquakes triggered at Mt. Wrangell, Alaska, occur in phase with peaks in the horizontal extensional stresses during the Rayleigh wave train from the  $M_w=9.1$  Sumatra-Andaman Islands earthquake on 26 December 2004 (West et al., 2005). In Figure 11(b), tremor bursts on the Parkfield section of the San Andreas Fault occur in phase with the SH, SHSH, Love, and Rayleigh waves from the  $M_w=9.0$  Tohoku-Oki earthquake on 11 March 2011 (Hill et al., 2013). Multiple earthquakes may occur during a single dynamic stress cycle if (1) the initial triggered earthquake produces its own aftershock sequence, (2) the stress cycle triggers earthquakes on multiple nearby faults, or, (3) for the case of reverse slip on low-angle faults as illustrated in Figure 9(b), the semimajor axis of the stress orbit is subparallel with the



(a)



(b)

**Figure 11** Examples illustrating the phase-lock between triggering teleseismic waves and triggered seismicity for (a) Mt. Wrangle, Alaska, seismicity triggered by the 2004  $M_w = 9.1$  Sumatra–Andaman earthquake. (Top) Short-period vertical displacement seismogram at the summit station WANC. Time in hours. (Bottom) Expanded view of highlighted section top panel showing triggered seismicity band-passed at 0.5–20 Hz and the Rayleigh wave coda band-passed at 0.01–0.1 Hz. Reproduced from West M, Sanchez JJ, and McNutt SR (2005) Periodically triggered seismicity at Mount Wrangell, Alaska, after the Sumatra earthquake. *Science* 308: 1144–1146, with permission. (b) Tectonic tremor on the Parkfield section of the San Andreas Fault triggered by the 2011  $M_w = 9.0$  Tohoku-Oki earthquake. (Top) Tremor recorded by short-period station SMNB. (Bottom) Three traces are teleseismic waveforms recorded on the broadband station PKD. Reproduced from Hill DP, Peng Z, Shelly DR, and Aiken C (2013) S-wave triggering of tremor beneath the Parkfield, CA, section of the San Andreas Fault by the 2011 Tohoku-Oki Japan earthquake: Observations and theory. *Bulletin of the Seismological Society of America* 103: 1541–1550. <http://dx.doi.org/10.1785/0120120114>, courtesy of the Bulletin of the Seismological Society of America.

Coulomb failure envelope such that a single cycle of the orbit intersects the failure envelope several times.

In principle, the Coulomb failure model should be viable in any region where faults are critically stressed and favorably oriented with respect to the polarity of the dynamic stresses from a distant earthquake. If most of the seismogenic crust is pervasively fractured and critically stressed as suggested by Zoback and Zoback (2002), earthquakes triggered by this process have an equal likelihood of occurring nearly everywhere. If this were the dominant triggering mechanism, one would expect that, given some minimum dynamic stress level, the distribution of observed triggered seismicity would correlate directly with the density of seismic networks and the sensitivity of earthquake detection techniques. As Rivera and Kanamori (2002) argued, however, the heterogeneity of both the stress field and the frictional strength seems to be an essential property of the crust. In a similar vein, Lapusta and Rice (2003) argued for heterogeneous strength along a given fault such that earthquake nucleation is confined to weak spots, while the average fault strength remains well above the Coulomb failure threshold.

#### **4.11.5.1.2 Nonlinear friction**

Extensive laboratory experiments on rock friction reveal that frictional failure involves a much richer range of (nonlinear) behaviors than predicted by the simple first-order model involving a constant static  $\mu_s$  and dynamic  $\mu_d$  coefficients of friction with  $\mu_s > \mu_d$ .

The Dieterich–Ruina rate-state friction laws (Dieterich, 1979, Chapter 4.04, this volume) have been widely used in studies of both static triggering and dynamic triggering. These rate-state laws, in which static friction retains a memory of sliding history along the fault surface and dynamic friction depends on the sliding velocity and an evolving state parameter, predict a range of behaviors depending on temporal variations in the applied stress and the parameter for a particular constitutive regime (Dieterich, 1979; Scholz, 1998). They include the possibility of delayed triggering (Parsons, 2005) and an Omori-like decay of triggered seismicity after shaking has stopped (Gomberg et al., 2005; Parsons, 2005). In the unstable, velocity-weakening regime, rate-state friction appears to be most effective under conditions of low effective normal stress (high pore pressure and weak faults) together with high-frequency vibrations (Gomberg et al., 2003; Perfettini et al., 2003; Scholz, 1998). Under rate-state friction in a conditionally stable (velocity-strengthening) regime, dynamic stresses can temporarily convert stable sliding (steady fault creep) to a stick-slip mode. The result is ‘new seismicity’ in the sense that the earthquakes generated during the stick-slip mode would not have occurred in the absence of dynamic triggering (Gomberg et al., 1997).

Subcritical crack growth or stress corrosion has long been known in material science to make cracks unstable (Anderson and Grew, 1977; Atkinson, 1984; Gomberg et al., 2001). When a crack experiences a change in its environment, such as a sudden increase in loading in the presence of particularly high temperatures and fluids, it may grow due to weakening at the crack tip by chemical corrosion. The crack may then rupture catastrophically. Thus, a sudden increase in loading or oscillatory loading (dynamic stressing) may shorten the

time to earthquake failure. The equations governing subcritical crack growth are mathematically identical to those governing failure by rate-state friction (Kanamori and Brodsky, 2004), and thus, as Brodsky and Prejean (2005) pointed out, subcritical crack growth requires near-lithostatic pore pressures to be effective as a dynamic triggering process.

Daub et al. (2011) used both laboratory and field data to develop a brittle–ductile friction model that mimics tectonic tremor in the transition zones of major plate-boundary faults. They found that tremor-like signals result if 40–70% of the contact asperities on a fault interface are brittle (the remainder being ductile). They suggest that at tremor-generating depths of  $\sim 25$  km, the brittle elements likely consist of feldspar, which remains brittle at temperatures of  $\sim 600$  °C under low effective normal stresses consisted with a weak fault.

The response of granular media to imposed dynamic stresses offer insight on another possible mode of nonlinear frictional failure. Laboratory experiments imposing acoustic vibrations on granular media under low normal stress ( $\sim 7$  kPa) suggest that seismic waves incident on a weak fault with a core composed of fault gouge (the granular medium) with peak amplitudes comparable to the normal stress can result in an abrupt decrease in the modulus of the fault gouge and catastrophic slip in the form of an earthquake (Johnson and Jia, 2005; Johnson et al., 2008, 2012; van der Elst et al., 2012).

Because each of the nonlinear models (rate-state friction, granular media, and subcritical crack growth) mentioned earlier apparently requires near-lithostatic pore pressures to be effective in dynamic triggering (Brodsky and Prejean, 2005), it seems unlikely that they offer a universal explanation for dynamic triggering. Any of the three, however, may be important in volumes where pore pressures approach the lithostatic limit. All have pressure-sensitive failure thresholds such that the Coulomb failure model provides a useful criterion for the initiation of catastrophic slip. Nonlinear friction will take over once accelerated slip is under way governing subsequent behavior including sustained episodes of triggered earthquakes or tremor apparently modulated by the coda of teleseismic waves (see Figure 11).

#### **4.11.5.2 Triggering Through Excitation of Crustal Fluids**

Crustal fluids play a critical role in a wide range of tectonic and magmatic processes (see Chapter 4.12, this volume), including dynamic triggering. Large earthquakes have long been recognized as capable of disturbing hydrologic regimes at distances of thousands of kilometers beginning with the  $M_w=9.2$  1964 Alaska earthquake (Roeloffs, 1996; Vohis, 1967), and fluids have long been known to play a role in earthquake rupture (e.g., Nur and Booker, 1972). These observations have inspired a class of physical models in which dynamic strains from the distant earthquake trigger local seismicity through fluid transport and pore pressure changes. This process may modify the Coulomb failure function (Section 4.11.5.1.1) such that the effective normal stress is decreased sufficiently to trigger failure (Beeler et al., 2000; Cocco and Rice, 2002) or that quasistatic (aseismic) strains associated with local, fluid-driven deformation are sufficient to trigger earthquakes. Fluids are active agents in geothermal

and volcanic areas, which appear to be particularly susceptible to dynamic triggering, and a number of explanations for triggered seismicity involving the movement of fluids have been proposed in the literature (e.g., Brodsky et al., 1998; Hill et al., 1995; Johnston et al., 1995; Linde et al., 1994; Manga and Brodsky, 2006; Moran et al., 2004). The hydrologic response to earthquakes includes changes in stream and spring discharge, groundwater properties (geochemistry, temperature, and turbidity), water-level fluctuations in wells, mud volcanoes, and soil liquefaction (Chapter 4.12, this volume; Wang and Manga, 2009). Wang and Manga (2009) showed that aside from liquefaction, which is limited to the near field, most hydrologic phenomena in the intermediate and far field are dynamically triggered. They suggest that changes in permeability resulting from oscillatory deformation and fluid flow associated with dynamic stresses play an important role in the triggering process.

In geothermal and volcanic areas, the simple linear version of 'clock advance' may be compromised because, in addition to steady loading from far-field tectonic stresses, the advection of magmatic fluids and heat from lower crustal or upper mantle source supplies local energy into a recently triggered volume of the brittle crust. As is evident from the behavior of the Long Valley Caldera volcanic–geothermal system over the past 25 years, these processes may operate episodically over time-scales ranging from weeks to years (Hill, 2008). Long Valley Caldera responded with remote triggering multiple times during periods of active unrest and deformation in the 1990s. Since 2000, however, unrest has been minimal and the caldera has failed to respond with dynamic triggering by any of the four  $M \sim 9$  earthquakes since 2000.

The susceptibility to dynamic triggering does not correlate with unrest in all volcanic systems, however. Japan with its many active volcanoes, for example, appears to be relatively insensitive to dynamic triggering (Harrington and Brodsky, 2006). With the exception of the Katmai volcanic cluster, Alaskan volcanoes show a similar insensitivity to dynamic triggering. The reason for this is not yet clear, although the compressional tectonic environment common to both areas may be a factor.

#### **4.11.5.2.1 Hydrous fluid transport: changes in permeability and pore pressure**

In this class of models for earthquake triggering, the dynamic strains from a distant earthquake modify crustal permeability by disrupting clogged fractures and hydraulic fracturing, thus leading to a redistribution of pore pressure (Elkhouri et al., 2011; Wang and Manga, 2010). These models should be viable in any area where isolated pockets of high-pressure fluids develop. Brodsky et al. (2003), for example, proposed that coseismic water-level changes observed in wells at Grants Pass in southern Oregon might result from dynamic stresses from the 1994  $M = 7.2$  Petrolia, CA, and the 1999  $M = 7.4$  Oaxaca, Mexico, earthquakes at  $\sim 300$ ,  $\sim 3850$  km, respectively, opening permeable fractures clogged by accumulating detritus over time.

The pore pressure redistribution mechanism may be particularly relevant in active geothermal areas, such as the Geysers and Coso geothermal fields, as fractures are sealed and high-pressure compartments form over relatively short timescales as

minerals are precipitated from hot brines. The mechanism may also be important in the crust above a magma body in which hydrous magmatic fluids may reach near-lithostatic pressures in the low-permeability plastic zone between the roof of the magma body and the brittle crust, where hydrothermal fluids circulate under hydrostatic conditions. This is the hydraulic surge model proposed by Fournier (1999) in which dynamic stresses from a large distant earthquake may rupture this impermeable zone, permitting high-pressure fluids to surge into the overlying brittle crust. This mechanism may explain both earthquakes triggered during and after the wave train of the large distant earthquake has passed as pore fluids move by diffusion through the crust.

Hough and Kanamori (2002) looked for evidence of fluid movement in the failure process of earthquakes triggered in the Salton Sea by the 1999 Hector Mine earthquake by examining earthquake source parameters. They found that the triggered earthquakes had essentially normal to slightly low stress drops and spectral contents typical of brittle shear failure with no resemblance to the long-period (LP) earthquakes or tremor-like sequences often seen in volcanic areas (Chouet, 1992; Julian, 1994).

#### **4.11.5.2.2 Magmatic fluids**

Growing evidence indicates that dynamic stresses are capable of perturbing the state of crustal or upper mantle magma bodies triggering internal pressure changes and, in some cases, eruptions (Hill et al., 2002; Linde and Sacks, 1998; Manga and Brodsky, 2006; Marzocchi, 2002). Under these models, triggered seismicity is a secondary result of locally triggered deformation associated with the change in state of a nearby magma body or intrusion from a critically pressurized magma body. Because these models predict distinctive patterns of ground deformation associated with triggered seismicity, continuous, high-resolution deformation monitoring networks are key to testing their validity.

Bubble excitation by dynamic stressing may explain some earthquake–magmatic interactions. Bubbles play a central role in the source mechanisms for LP and very LP volcanic earthquakes (Chouet, 1992) and in eruption dynamics (Mangan and Sisson, 2000). Two highly idealized physical models widely mentioned as possible explanations for remotely triggered seismicity appeal to changes in bubble pressurization in a two-phase fluid. In the rectified diffusion model, volatiles in a saturated fluid are selectively pumped into bubbles during the dilatational phase of each strain cycle as the wave train of the distant earthquake passes (Brodsky et al., 1998; Sturtevant et al., 1996). In the idealized advective overpressure model, a bubble adhering to the walls of a magma body is shaken loose by the dynamic stresses from the remote earthquake. Under the assumptions of rigid walls and an incompressible magma, the bubble maintains the same size as it buoyantly rises a distance,  $h$ . By the gas law, the product of bubble volume and pressure is constant in an isothermal system. Thus, the pressure in the magma chamber increases by  $\rho gh$ , where  $\rho$  is magma density and  $g$  is the acceleration of gravity (Linde et al., 1994; Sahagian and Prousevitch, 1992). In both models, increasing pressure in the bubbles is transmitted to the surrounding interstitial fluid, thereby increasing pore pressure and triggering earthquakes. These models could apply to either hydrous fluids or

magma. Both, however, have been criticized on the basis that they depend on restrictive assumptions that are unrealistic under natural conditions in the Earth (Bagdasarov, 1994; Brodsky et al., 1998; Ichihara and Brodsky, 2006; Pyle and Pyle, 1995).

Bubble nucleation stimulated by dynamic stressing in a supersaturated magma is yet another fluid activation model (Manga and Brodsky, 2006). Under proper conditions, small pressure changes associated with dynamic stresses in a crystallizing magma that is close to critical supersaturation should be capable of triggering a significant excess in bubble nucleation leading to a marked pressure increase and deformation with local seismicity as a secondary response. Numerical modeling by Shimomura et al. (2006) and Chouet et al. (2006) indicates that when subject to a small externally imposed pressure drop, a densely packed matrix of tiny bubbles in a magma-filled crack can lead to rapid diffusion-driven bubble growth and volumetric expansion of the crack. These models have yet to be evaluated for their response to realistic dynamic stresses, but they keep open the possibility that bubbles may have an important role in the triggered response of magmatic systems to dynamic stresses.

Bubble excitation in a critically pressurized magma body may be sufficient to trigger an intrusion into the surround crust accompanied by seismicity in response to deformation associated with the intrusion. Dilatational strain meters at Mammoth Mountain recorded deformation transients coincident with the seismicity triggering in the Long Valley Caldera area following the Landers, Hector Mine, and Denali Fault earthquakes (Figure 6). Based on these data, Johnston et al. (2000) and Johnston et al. (2004a) proposed that, in the case of Mammoth Mountain and Long Valley, the dynamic waves from distant earthquakes trigger magmatic intrusions into the shallow crust. These intrusions, which may involve a massive hydrofracture by aqueous magmatic fluids or magma itself, then trigger earthquakes by changing the static stress field or locally increasing the pore pressure as fluids are exsolved. Thus, the local seismicity is a secondary response to the initiating ground motion.

Dynamic waves from a large distant earthquake may disrupt the stability of a partially crystallized magma body releasing accumulated deviatoric stress supported by the interconnected crystal structure (Hill et al., 1995). As in the magmatic intrusion model, the local seismicity triggered by a relaxing magma body is responding to a local, quasistatic strain source rather than the initiating dynamic stresses. The recharge time for this model is presumably rather long depending on both the crystallization rate in cooling magma body and the far-field strain rate.

Yet another possible response of a magma body to dynamic stresses suggests that passing seismic waves may dislodge dense crystals from the ceiling and walls of a magma chamber. As these crystals then sink due to gravity, they may stimulate convection in the magma chamber. Bubbles would presumably nucleate and grow in the ascending volatile-rich magma, thereby increasing pressure in the magma body and deforming the overlying crust (Hill et al., 2002). Manga and Brodsky (2006) showed that this process may be capable of creating sufficient overpressure to trigger a volcanic eruption on the timescale of days. It is likely the process could trigger earthquakes on a similar timescale.

#### 4.11.6 Challenges for the Future

Because the *in situ* perturbing dynamic stresses are calculable, the study of remotely triggered seismicity gives us a unique window into the earthquake nucleation process. Although this rapidly advancing field has great potential for illuminating the earthquake initiation process, many fundamental issues remain regarding the detection, temporal and spatial distribution, and physical processes behind dynamically triggered seismicity. Some of these issues include the following:

- *Uniform detection of triggered seismicity.* Automated earthquake detection algorithms are ineffective at identifying small triggered events recorded by a single, low-dynamic-range station. Reliable identification and location of triggered seismicity buried in the surface-wave coda from a large earthquake require a network of broadband, high-dynamic-range seismic stations. Spectrograms (Peng et al., 2011a,b) together with visual scanning of high-pass-filtered data from such arrays greatly facilitate the identification of early triggered activity (see Figure 4; Prejean et al., 2004). This capability is unevenly distributed across the globe in existing seismic networks.
- *Statistical and physical significance of delayed triggering.* As the delay time between passing seismic waves and the onset of a suspected triggered response increases, it becomes increasingly difficult to establish statistical significance and a credible causal link between the two. Isolated earthquakes suspected of being triggered pose a particular problem in this regard regardless of delay times. Multiparameter monitoring networks capable of continuously tracking local changes in deformation, the hydrologic system, and other aseismic phenomena can provide important clues to aseismic processes that might link the perturbing dynamic stresses to a delayed or isolated seismic response – particularly when coupled with plausible physical models.
- *Distinguishing triggered earthquakes from aftershocks to triggered earthquakes.* The problem of distinguishing between static triggering and dynamic triggering of aftershocks to major earthquakes in the near-to-intermediate fields applies to remotely triggered earthquake swarms as well. In particular, deciding which earthquakes in a triggered swarm are directly triggered by teleseismic dynamic stresses and which earthquakes are aftershocks to the triggered earthquakes remains a challenge (Ziv, 2006). One promising approach to this problem involves the ETAS model described by Hainzl and Ogata (2005) to distinguish earthquakes driven by external forcing (such as fluid transport) from those resulting from an Omori-type aftershock sequence. High-resolution imaging of spatial-temporal patterns of swarm evolution can also provide evidence for fluid forcing, particularly when the seismicity front propagates as  $(r/\sqrt{t})$  characteristic of fluid diffusion (Shapiro et al., 1997).
- *Quantitative physical models for the triggering process.* To determine the physical processes responsible for a remotely triggered earthquake, we need thorough knowledge of the triggering wave field in space and time together with precise hypocentral locations for the triggered seismicity and associated focal mechanisms. The more information available

on the physical environment under which triggering occurs, the better (e.g., fault orientations, frictional properties of faults, stress field, rock type, temperature, and the hydrologic regime). Strain transients have preceded or accompany episodes of triggered seismicity in volcanic regimes monitored by continuous, high-resolution strain data. Strain data are key in testing models that involve fluid activation and transport and whether triggered seismicity is a secondary response to a more fundamental aseismic process. High-frequency water well data will also be helpful in testing models that involve crustal fluid flow and pore pressure changes (Roeloffs, 1996), as these data can help determine how the crust responds hydrologically to large distant earthquakes.

#### 4.11.7 Conclusions

Evidence in support of remote dynamic triggering as a common phenomenon is compelling. Remaining key questions include the following: what conditions favor dynamic triggering, and what physical processes do dynamic stresses induce in given crustal volumes that trigger local earthquakes and, at least in some cases, local aseismic deformation? To a large degree, emerging answers will come into focus as we obtain more complete sampling of the triggered response to future large earthquakes in terms of both spatial distribution and variations in response characteristics over a wide spectrum of timescales afforded by more widely distributed broadband seismic and continuous deformation instrumentation.

Based on the still uneven sampling available through mid-2013, it appears as though the seismogenic crust in tectonically active extensional regimes (such as the Basin and Range province in the western United States with strain rates of  $\sim 10^{-8}$  year $^{-1}$ ) is more susceptible to dynamic triggering than stable cratonic regimes (such as the eastern United States with strain rates generally  $< 10^{-9}$  year $^{-1}$ ). Higher tectonic strain rates mean shorter recovery (recharge) times between episodes of strain release (whether dynamically triggered or not). In volcanic and geothermal areas, recovery times may be further shortened by episodic advection of magmatic fluids into the crust from the lower crust or upper mantle that serve as local stress sources. Shorter recovery times mean that, at any given time, more areas are likely to be hovering in a near-critical state and thus susceptible to triggering by small dynamic stresses than in areas with low strain rates and extended recovery times. Elevated strain rates alone, however, are not sufficient. The seismogenic crust along the transpressional section of the San Andreas Fault through the California Coast Ranges with its high strain rate ( $\sim 5 \times 10^{-7}$  year $^{-1}$ ) and frequent seismicity appears not to be particularly susceptible to dynamic triggering (Spudich et al., 1995), while the transition zone in the lower crust beneath the Parkfield section of the San Andreas Fault responds frequently with triggered tectonic tremor (Peng et al., 2009).

The transition zones at depths of 15–30 km along major plate-boundary megathrust and transform faults are particularly susceptible to frequent repeated dynamic triggering of tectonic tremor by seismic waves from large earthquakes and to modulation by tidal stresses. The triggered tremor occurs in

the same volume as background tremor and ETS on mega-thrust faults. In both cases, the tremor appears to be composed of closely spaced sequences of low-frequency, shear-failure earthquakes on extremely weak fault surfaces under near-lithostatic pore pressure and low effective friction coefficients  $< 0.1$ .

Models proposed to explain dynamic triggering fall into two broad categories: (1) frictional models and direct triggering of local seismicity and (2) models that appeal to the excitation of local crustal fluids or aseismic creep with seismicity developing as an indirect (and possibly delayed) response. For dynamic triggering under the frictional models, the stress state in the crust must differ from the Coulomb failure stress by less than the peak amplitudes of the dynamic stresses (typically  $< 10$  kPa for remote triggering). These models are generally consistent with the rapid onset of triggered seismicity during the dynamic stresses followed by an Omori-like decay depending on the parameters for the specific friction law (e.g., rate-state and granular media).

Fluid excitation models involve fluid transport or a phase change driven by the triggered release of locally stored gravitational or chemical potential energy. These fluid-based models, whether hydrous or magmatic, together with models based on aseismic creep, involve some degree of crustal deformation through, for example, intrusion, pressure changes in the case of bubble excitation, advection in a magma body, or poroelasticity in the case of fluid diffusion. Triggered seismicity for many of these models can be a secondary response to quasi-static stresses generated by local deformation. These models admit the possibility of delayed onsets of triggered seismicity and increasing or sustained activity rates for extended periods following the passage of the dynamic stresses. In general, fluid-based models are likely to be more applicable in extensional stress regimes that host geothermal and volcanic systems than in stable regimes. Indeed, it is likely that frictional and fluid-driven processes both have some role in most instances of dynamic triggering.

Although currently available data are not yet adequate to clearly distinguish between the many competing models for the triggering process, the three-dimensional dynamic stress fields for seismic waves from large earthquakes or solid Earth tides, which can be calculated with reasonable accuracy, offer useful tools for investigating the state of stress in the crust and what it means to be in a near-critical state and providing insight on the earthquake nucleation process.

#### Acknowledgments

We are grateful to Tom Parsons and Zhigang Peng for constructive reviews of this manuscript and to Hiroo Kanamori for his guidance and patience as volume editor.

#### References

- Aagaard BT, Anderson G, and Hudnut KW (2004) Dynamic rupture modeling of the transition from thrust to strike-slip motion in the 2002 Denali Fault earthquake, Alaska. *Bulletin of the Seismological Society of America* 94: S190–S201.

- Aiken C, Peng Z, and Chao K (2013a) Tremors along the Queen Charlotte Margin triggered by large teleseismic earthquakes. *Geophysical Research Letters* 40(5): 829–834. <http://dx.doi.org/10.1002/grl.50220>.
- Anderson JG, Brune JN, Louie JN, et al. (1994) Seismicity in the western Great Basin apparently triggered by the Landers, California, earthquake 28 June 1992. *Bulletin of the Seismological Society of America* 84: 863–891.
- Anderson OL and Grew PC (1977) Stress corrosion theory of crack propagation with applications to geophysics. *Reviews of Geophysics* 15: 77–104.
- Antonioli A, Cocco M, Das S, and Henery C (2002) Dynamic stress triggering during the great 25 March 1998 Antarctic Plate earthquake. *Bulletin of the Seismological Society of America* 92: 896–903.
- Armstrong BH and Stierman DJ (1989) Acoustic emissions from foreshocks and secular strain changes prior to earthquakes. In: Reginald Hardy Jr. (ed.) *Acoustic Emission/Microseismic Activity in Geologic Structures and Materials*, vol. 17, pp. 309–326. Pennsylvania State University, State College PA: Trans Tech Publications.
- Arnadottir T, Geirsson H, and Einarrson P (2004) Coseismic stress changes and crustal deformation on the Reykjanes Peninsula due to triggered earthquakes on 17 June 2000. *Journal of Geophysical Research* 109. <http://dx.doi.org/10.1029/2004JB003130>.
- Atkinson BK (1984) Subcritical crack growth in geological materials. *Journal of Geophysical Research* 89: 4077–4114.
- Bagdassarov N (1994) Pressure and volume changes in magmatic systems due to the vertical displacement of compressible materials. *Journal of Volcanology and Geothermal Research* 63: 95–100.
- Bakun WH and McGarr A (2002) Differences in attenuation among stable continental regions. *Geophysical Research Letters* 29: 36:1–36:4.
- Beeler NM, Simpson RW, Hickman SH, and Lockner DA (2000) Pore fluid pressure, apparent friction and Coulomb failure. *Journal of Geophysical Research* 105(B11): 25533–25542.
- Beeler NM and Lockner DA (2003) Why earthquakes correlate weakly with the solid Earth tides: Effects of periodic stress on the rate and probability of earthquake occurrence. *Journal of Geophysical Research* 108. <http://dx.doi.org/10.1029/2001JB001518>.
- Beresnev IA and Wen K-L (1995) Remotely triggered seismicity inferred from Taiwan regional catalog. *Geophysical Research Letters* 22: 3155–3158.
- Beroza GC and Ide S (2011) Slow earthquakes and nonvolcanic tremor. *Annual Review of Earth and Planetary Sciences* 39: 271–296.
- Brodsky EE (2006) Long-range triggered earthquakes that continue after the wave train passes. *Geophysical Research Letters* 33. <http://dx.doi.org/10.1029/2006GL026605>.
- Brodsky EE, Karakostas V, and Kanamori H (2000) A new observation of dynamically triggered regional seismicity: Earthquakes in Greece following the August, 1999, Izmit, Turkey earthquake. *Geophysical Research Letters* 27: 2741–2744.
- Brodsky EE and Prejean SG (2005) New constraints on mechanisms of remotely triggered seismicity at Long Valley Caldera. *Journal of Geophysical Research* 110. <http://dx.doi.org/10.1029/2004JB003211>.
- Brodsky EE, Roeloffs E, Woodcock D, Gall I, and Manga M (2003) A mechanism for sustained groundwater pressure changes induced by distant earthquakes. *Journal of Geophysical Research* 108. <http://dx.doi.org/10.1029/2002JB002321>.
- Brodsky E, Sturtevant B, and Kanamori H (1998) Earthquakes, volcanoes, and rectified diffusion. *Journal of Geophysical Research* 103: 23827–23838.
- Byerlee JD (1980) Friction of rocks. *Pure and Applied Geophysics* 116: 615–626.
- Camelbeek T, van Eck T, Pelzing R, et al. (1994) The 1992 Roermond earthquake, the Netherlands, and its aftershocks. *Geologie en Mijnbouw* 73: 181–197.
- Cannata A, Di Grazia G, Montalto P, Aliotta M, Patane D, and Boschi E (2010) Response of Mount Etna to dynamic stresses from distant earthquakes. *Journal of Geophysical Research* 115: B12304. <http://dx.doi.org/10.1029/2010JB007487>.
- Chao K, Peng Z, Fabian A, and Ojha L (2012) Comparisons of triggered tremor in California. *Bulletin of the Seismological Society of America* 102(2): 900–908.
- Chao K, Peng Z, Gonzalez-Huizar H, et al. (2013) Global search of triggered tremor following the 2011 Mw9.0 Tohoku-Oki earthquake. *Bulletin of the Seismological Society of America* 103(2b). <http://dx.doi.org/10.1785/0130120171>.
- Chao K, Peng Z, Wu C, Tang C-C, and Lin C-H (2011) Remote triggering of non-volcanic tremor around Taiwan. *Geophysical Journal International* 188: 301–324.
- Chesley C, LaFemina PC, Puskas C, and Kobayashi D (2012) The 1707 Mw8.7 Hoei earthquake triggered the largest historical eruption of Mt. Fuji. *Geophysical Research Letters* 39: L224309.
- Chouet B (1992) A seismic model for the source of long-period events and harmonic tremor. In: Gasparini P, Scarpa R, and Aki K (eds.) *Volcanic Seismology*, pp. 133–156. Berlin: Springer-Verlag.
- Chouet B, Dawson P, and Nakano M (2006) Dynamics of diffusive bubble growth and pressure recovery in a bubbly rhyolitic melt embedded in an elastic solid. *Journal of Geophysical Research* 111: B07310. <http://dx.doi.org/10.1029/2005JB004174>.
- Christiansen L, Hurwitz S, Saar MO, Ingebritsen SE, and Hsieh P (2005) Seasonal seismicity at western United States volcanic centers. *Earth and Planetary Science Letters* 240: 307–321.
- Cocco M and Rice JR (2002) Pore pressure and poroelasticity effects in Coulomb stress analysis of earthquake interactions. *Journal of Geophysical Research* 107. <http://dx.doi.org/10.1029/2002JB002319>.
- Cochran ES, Vidale JE, and Tanaka S (2004) Earth tides can trigger shallow thrust fault earthquakes. *Science* 306: 1164–1166.
- Daniel D, Marsan D, and Bouchon M (2008) Earthquake triggering in southern Iceland following the June 2000 M<sub>s</sub> 6.6 doublet. *Journal of Geophysical Research* 113: B05310. <http://dx.doi.org/10.1029/2007JB005107>.
- Das S and Scholz C (1981) Off-fault aftershock clusters caused by shear stress increase? *Journal of Geophysical Research* 71: 1669–1675.
- Daub EG, Shelly DR, Guyer RA, and Johnson PA (2011) Brittle and ductile friction and the physics of tectonic tremor. *Geophysical Research Letters* 38: L10301. <http://dx.doi.org/10.1029/2010GL046866>.
- Delle Donne D, Harris AJL, Ripepe M, and Wright R (2010) Earthquake-induced thermal anomalies at active volcanoes. *Geology* 38: 771–774.
- Di Carli S, Voisin C, Cotton F, and Semmane F (2008) The 2000 western Tottori (Japan) earthquake: Triggering of the largest aftershock and constraints on the slip-weakening distance. *Journal of Geophysical Research* 113: B05307. <http://dx.doi.org/10.1029/2007JB004951>.
- Dieterich JH (1979) Modeling of rock friction 1. Experimental results and constitutive equations. *Journal of Geophysical Research* 84: 2161–2168.
- Durand V, Bouchon M, Karabulut H, Marsan D, and Schmittbuhl J (2013) Link between Coulomb stress changes and seismic activation in the eastern Marmara sea after the 1999, Izmit (Turkey), earthquake. *Journal of Geophysical Research: Solid Earth* 118: 681–688.
- Durand V, Bouchon M, Karabulut H, et al. (2010) Seismic interaction and delayed triggering along the north Anatolian Fault. *Geophysical Research Letters* 37: L18310. <http://dx.doi.org/10.1029/2010GL044688>.
- Eberhart-Phillips D, Haussler PJ, Freymueller JT, et al. (2003) The 2002 Denali fault earthquake, Alaska: A large magnitude, slip-partitioned event. *Nature* 300: 1113–1118.
- Elkhouri JE, Niemeijer A, Brodsky E, and Marone C (2011) Laboratory observations of permeability enhancement by fluid pressure oscillations of an in situ fractured rock. *Journal of Geophysical Research* 116: B02311. <http://dx.doi.org/10.1029/2010JB007759>.
- Emiliani C, Harrison CGA, and Swanson M (1969) Underground nuclear explosions and the control of earthquakes. *Science* 165: 1255–1256.
- Enescu B, Chao K, Peng Z, et al. (2012) Love wave triggering of non-volcanic tremor in the Nankai region, southwest Japan: Observations and physical interpretation. In: *Abstract S33B-2550 presented at 2012 Fall Meeting, 3–7 December, AGU, San Francisco, CA*.
- Felzer KR and Brodsky EE (2005) Testing the stress shadow hypothesis. *Journal of Geophysical Research* 110. <http://dx.doi.org/10.1029/2004JB003277>.
- Felzer KR and Brodsky EE (2006) Evidence for dynamic aftershock triggering from earthquake densities. *Nature* 441: 735–738.
- Fournier RO (1999) Hydrothermal processes related to movement of fluid from plastic to brittle rock in the magmatic-epithermal environment. *Economic Geology* 94: 1193–1211.
- Freed AM (2005) Earthquake triggering by static, dynamic, and postseismic stress transfer. *Annual Review of Earth and Planetary Sciences* 33: 335–367.
- Fry B, Chao K, Bannister S, and Peng Z (2011) Deep tremor beneath the Hikurangi margin in New Zealand triggered by the 2010 M<sub>w</sub> 8.8 Chile earthquake. *Geophysical Research Letters* 38: L15306.
- Galperin EI, Petersen NV, Slinikov AV, and Vinnik LP (1990) On the properties of short-period seismic noise. *Physics of the Earth and Planetary Interiors* 63: 163–171.
- Ghosh A, Vidale JE, Peng Z, Creager KC, and Houston H (2009) Complex nonvolcanic tremor near Parkfield, California, triggered by the great 2004 Sumatra earthquake. *Journal of Geophysical Research* 114. <http://dx.doi.org/10.1029/2008JB006062>.
- Glowacka E, Nava AF, Cossio DD, Wong V, and Farfan F (2002) Fault slip, seismicity, and deformation in the Mexicali Valley, Baja California, Mexico, after the M 7.1 Hector Mine earthquake. *Bulletin of the Seismological Society of America* 92: 1290–1299.
- Gomberg J (1996) Stress/strain changes and triggered seismicity following the Mw 7.3 Landers, California, earthquake. *Journal of Geophysical Research* 101: 751–764.
- Gomberg J (2010) Lessons from (triggered) tremor. *Journal of Geophysical Research* 115: B10302. <http://dx.doi.org/10.1029/2009JB007011>.
- Gomberg J, Blanpied ML, and Beeler NM (1997) Transient triggering of near and distant earthquakes. *Bulletin of the Seismological Society of America* 87: 294–309.

- Gomberg J, Bodin P, Larson K, and Dragert H (2004) Earthquakes nucleated by transient deformations caused by the  $M=7.9$  Denali, Alaska, earthquake. *Nature* 427: 621–624.
- Gomberg J, Bodin P, and Reasenberg PA (2003) Observing earthquakes triggered in the near field by dynamic deformations. *Bulletin of the Seismological Society of America* 93: 118–138.
- Gomberg J and Davis S (1996) Stress/strain changes and triggered seismicity at the Geysers, California. *Journal of Geophysical Research* 101: 733–749.
- Gomberg J and Johnson P (2005) Dynamic triggering of earthquakes. *Nature* 437: 830.
- Gomberg J, Reasenberg PA, Bodin P, and Harris R (2001) Earthquakes triggering by seismic waves following the Landers and Hector mine earthquakes. *Nature* 411: 462–465.
- Gomberg J, Reasenberg PA, Cocco M, and Belardinelli ME (2005) A frictional population model of seismicity rate change. *Journal of Geophysical Research* 110. <http://dx.doi.org/10.1029/2004JB003404>.
- Gomberg J, Rubinstein JL, Peng Z, Crager KC, Vidale JE, and Bodin P (2008) Widespread triggering of nonvolcanic tremor in California. *Science* 319: 173.
- Gomberg J and Sherrill B (2014) Crustal earthquake triggering by modern great earthquakes on subduction zone thrusts. *Journal of Geophysical Research: Solid Earth* 119.2: 1235–1250.
- Gonzalez-Huizar H and Velasco AA (2011) Dynamic triggering: Stress modeling and a case study. *Journal of Geophysical Research* 116. <http://dx.doi.org/10.1029/2009JB007000>.
- Gonzalez-Huizar H, Velasco AA, Peng Z, and Castro RR (2012) Remote triggered seismicity caused by the 2011,  $M_{9.0}$  Tohoku-Oki, Japan, earthquake. *Geophysical Research Letters* 39: L10302.
- Guillhem A, Peng Z, and Nadeau RM (2010) High-frequency identification of non-volcanic tremor triggered by regional earthquakes. *Geophysical Research Letters* 37. <http://dx.doi.org/10.1020/2010GL044660>.
- Guillhem A and Nadeau RM (2012) Episodic tremor and deep slow slip events in central California. *Earth and Planetary Science Letters* 357: 1–10.
- Hainzl S and Ogata Y (2005) Detecting fluid signals in seismicity data through statistical earthquake modeling. *Journal of Geophysical Research* 110. <http://dx.doi.org/10.1029/2004JB003247>.
- Harrington RM and Brodsky EE (2006) The absence of remotely triggered seismicity in Japan. *Bulletin of the Seismological Society of America* 96: 871–878.
- Harris RA (1998) Introduction to a special section: Stress triggers, stress shadows, and implications for seismic hazards. *Journal of Geophysical Research* 103: 24347–24358.
- Harris RA and Day SM (1993) Dynamics of fault interaction: Parallel strike-slip faults. *Journal of Geophysical Research* 98: 4461–4472.
- Harris RA, Dolan JF, Hartlib R, and Day SM (2002) The 1999 Izmit, Turkey, earthquake: A 3-D dynamic stress transfer model of interearthquake triggering. *Bulletin of the Seismological Society of America* 92: 245–255.
- Hawthorne JC and Rubin AM (2010) Tidal modulation of slow slip in Canada. *Journal of Geophysical Research* 115: B09406.
- Hill DP (2008) Unrest in Long Valley Caldera, California: 1978–2004. In: De Natale G, Troise C, and Kilburn CRJ (eds.) *Mechanisms of Activity and Unrest at Large Calderas*, pp. 1–24. London: Geological Society. Publication No. 269.
- Hill DP (2012a) Dynamic stresses Coulomb failure, and remote triggering – Corrected. *Bulletin of the Seismological Society of America* 102. <http://dx.doi.org/10.1785/0120120085>.
- Hill DP (2012b) Surface-wave potential for triggering tectonic (nonvolcanic) tremor – Corrected. *Bulletin of the Seismological Society of America* 102. <http://dx.doi.org/10.1785/0120120086>.
- Hill DP, Johnston MJS, Langbein JO, and Bilham R (1995) Response of Long Valley Caldera to the  $M_w=7.3$  Landers, California, earthquake. *Journal of Geophysical Research* 100: 12985–13005.
- Hill DP, Peng Z, Shelly DR, and Aiken C (2013) S-wave triggering of tremor beneath the Parkfield, CA, section of the San Andreas Fault by the 2011 Tohoku-Oki Japan earthquake: Observations and theory. *Bulletin of the Seismological Society of America* 103. <http://dx.doi.org/10.1785/0120120114>.
- Hill DP, Pollitz F, and Newhall C (2002) Earthquake-volcano interactions. *Physics Today* 55: 41–47.
- Hill DP and Prejean SG (2007) Dynamic triggering. In: Kanamori H (ed.) *Treatise on Geophysics. Earthquake Seismology*, vol. 4, pp. 257–291. Amsterdam: Elsevier.
- Hill DP, Reasenberg PA, Michael A, et al. (1993) Seismicity remotely triggered by the magnitude 7.3 Landers, California, earthquake. *Science* 260: 1617–1623.
- Hirose F, Miyaoka K, Hayashimoto N, Yamazaki T, and Nakamura M (2011) Outline of the 2011 off the Pacific coast of Tohoku Earthquake ( $M_w 9.0$ ) – seismicity: Foreshocks, mainshock, aftershocks, and induced activity. *Earth, Planets and Space* 63: 513–518.
- Hough SE (2001) Triggered earthquakes and the 1811–1812 New Madrid, central United States, earthquake sequence. *Bulletin of the Seismological Society of America* 91: 1547–1581.
- Hough SE (2005) Remotely triggered earthquakes following moderate mainshocks (or why California is not falling into the ocean). *Seismological Research Letters* 76: 58–66.
- Hough SE, Billham R, Ambroseys N, and Feldl N (2005) Revisiting the 1897 Shillong and 1905 Kangra earthquakes in northern India: Site response, Moho reflections and a triggered earthquake. *Current Science* 88: 1632–1638.
- Hough SE and Kanamori H (2002) Source properties of earthquakes near the Salton Sea triggered by the 16 October 1999  $M_w 7.1$  Hector Mine, California, earthquake. *Bulletin of the Seismological Society of America* 92: 1281–1289.
- Hough SE, Seeber L, and Armbruster JG (2003) Intraplate triggered earthquakes: Observations and interpretation. *Bulletin of the Seismological Society of America* 93: 2212–2221.
- Hudnut KWL, Seeber L, and Pacheco J (1989) Cross-fault triggering in the November 1978 Superstition Hill earthquake sequence, southern California. *Geophysical Research Letters* 16: 199–202.
- Husen S, Taylor R, Smith RB, and Heasler H (2004a) Changes in geyser eruption behavior and remotely triggered seismicity in Yellowstone National Park produced by the 2002  $M 7.9$  Denali Fault earthquake, Alaska. *Geology* 32: 537–540.
- Husen S, Wiemer S, and Smith RB (2004b) Remotely triggered seismicity in the Yellowstone National Park region by the 2002  $M_w 7.9$  Denali Fault earthquake, Alaska. *Bulletin of the Seismological Society of America* 94: S317–S331.
- Husker AL and Brodsky EE (2004) Seismicity in Idaho and Montana triggered by the Denali Fault earthquake: A window into the geologic context for seismic triggering. *Bulletin of the Seismological Society of America* 94: S310–S316.
- Ichihara M and Brodsky EE (2006) A limitation on the effect of rectified diffusion in volcanic systems. *Geophysical Research Letters* 33. <http://dx.doi.org/10.1029/2005GL024733>.
- Ide S (2010) Striations, duration, migration and tidal response in deep tremor. *Nature* 466: 356–360.
- Jay JA, Pritchard ME, West ME, et al. (2012) Shallow seismicity, triggered seismicity, and ambient noise tomography at the long-dormant Uturuncu volcano. *Bulletin of Volcanology* 74: 817–837. <http://dx.doi.org/10.1007/s00445-011-0568-7>.
- Jiang T, Peng Z, Wang W, and Chen Q-F (2010) Remotely triggered seismicity in continental China following the 2008  $M_w 7.9$  Wenchuan earthquake. *Bulletin of the Seismological Society of America* 100: 2574–2589.
- Johnson PA, Carpenter BM, Knuth M, et al. (2012) Nonlinear dynamical triggering of slow-slip on simulated earthquake faults. *Journal of Geophysical Research* 117: B04310. [http://dx.doi.org/10.1029/2011JB\\_008594](http://dx.doi.org/10.1029/2011JB_008594).
- Johnson PA and Jia X (2005) Nonlinear dynamic, granular media and dynamic earthquake triggering. *Nature* 437: 871–874.
- Johnson PA, Savage M, Knuth K, and Marone C (2008) Effects of acoustic waves on stick-slip in granular media and implications for earthquakes. *Nature* 451: 57–60.
- Johnston MJS, Hill DP, Linde AT, Langbein J, and Bilham R (1995) Transient deformation during triggered seismicity from the 28 June 1992  $M_w=7.3$  Landers earthquake at Long Valley volcanic caldera, California. *Bulletin of the Seismological Society of America* 85: 787–795.
- Johnston MJS, Hill DP, and Pitt AM (2000) Strain transient recorded in the Long Valley Caldera during triggered seismicity from the October 16, 1999  $M_w 7.1$  Hector Mine, California, earthquake. *EOS, Transactions of the American Geophysical Union* 81, WP1384.
- Johnston MJS, Prejean SG, and Hill DP (2004a) Triggered deformation and seismic activity under Mammoth Mountain in Long Valley caldera by the 3 November 2002  $M_w 7.9$  Denali Fault earthquake. *Bulletin of the Seismological Society of America* 94: S360–S369.
- Johnston MJS, Prejean S, and Hill DP (2004b) Triggered deformation and seismic activity in Long Valley Caldera by the November 3, 2002,  $M 7.9$  Denali Fault earthquake. *Bulletin of the Seismological Society of America* 94: S360–S369.
- Jousset P and Rohmer J (2012) Evidence for remotely triggered microearthquakes during salt cavern collapse. *Geophysical Journal International* 191: 207–223.
- Julian BR (1994) Volcanic tremor: Nonlinear excitation by fluid flow. *Journal of Geophysical Research* 99: 11859–11877.
- Julian BR (2002) Seismological detection of slab metamorphism. *Science* 296: 1625–1626.
- Kanamori H and Brodsky EE (2004) The physics of earthquakes. *Reports in Progress in Physics* 67: 1429–1496.
- Kilb D, Gomberg J, and Bodin P (2000) Triggering of earthquake aftershocks by dynamic stresses. *Nature* 408: 570–574.
- Kilb D, Gomberg J, and Bodin P (2002) Aftershock triggering by complete Coulomb stress changes. *Journal of Geophysical Research* 107. <http://dx.doi.org/10.1029/2001JB000202>.

- King GCP and Cocco M (2001) Fault interactions by elastic stress changes: New clues from earthquake sequences. *Advances in Geophysics* 44: 1–38.
- Kisslinger C and Jones LM (1991) Properties of aftershock sequences in southern California. *Journal of Geophysical Research* 96: 11947–11958.
- Klein FW (1976) Earthquake swarms and the semidiurnal solid earth tide. *Geophysical Journal of the Royal Astronomical Society* 54: 245–295.
- Lapusta N and Rice JR (2003) Nucleation and early seismic propagation of small and large events in a crustal earthquake model. *Journal of Geophysical Research* 108. <http://dx.doi.org/10.1029/2001JB000793>.
- Lay T, Kanamori H, Armon CJ, et al. (2005) The great Sumatra-Andaman earthquake of 26 December 2004. *Science* 308: 1127–1132.
- Lei X, Xie C, and Fu B (2011) Remotely triggered seismicity in Yunnan, southwestern China, following the 2004  $M_w$  9.3 Sumatra earthquake. *Journal of Geophysical Research* 116: B08303. <http://dx.doi.org/10.1029/2011JB008245>.
- Lin C-H (2012) Remote triggering of the  $M_w$  6.9 Hokkaido earthquake as a result of the  $M_w$  6.6 Indonesian Earthquake on September 11, 2008. *Terrestrial, Atmospheric and Oceanic Sciences* 23: 283–290.
- Linde AT and Sacks IS (1998) Triggering of volcanic eruptions. *Nature* 395: 888–890.
- Linde AT, Sacks IS, Johnston MJS, Hill DP, and Billham RG (1994) Increased pressure from rising bubbles as a mechanism for remotely triggered seismicity. *Nature* 371: 408–410.
- Lockner DA and Beeler NM (1999) Premonitory slip and tidal triggering of earthquakes. *Journal of Geophysical Research* 104: 20133–20151.
- Lockner DA and Beeler NM (2002) Rock failure and earthquakes. In: Lee WHK, Kanamori H, Jennings PC, and Kisslinger C (eds.) *International Handbook of Earthquake and Engineering Seismology Part A*, pp. 505–537. Amsterdam: Academic Press.
- Luttrell K and Sandwell D (2010) Ocean loading effects on stress at near shore boundary fault systems. *Journal of Geophysical Research* 115: B08411. <http://dx.doi.org/10.1029/2009JB006541>.
- Manga M and Brodsky EE (2006) Seismic triggering of eruptions in the far field: Volcanoes and geysers. *Annual Review of Earth and Planetary Sciences* 34: 263–291.
- Manga M and Wang C-Y (2007) Earthquake hydrology. In: Kanamori H (ed.) *Treatise on Geophysics. Earthquake Seismology*, vol. 4, pp. 293–320. Amsterdam: Elsevier.
- Mangan M and Sisson T (2000) Delayed, disequilibrium degassing in rhyolite magma: Decompression experiments and implications for explosive volcanism. *Earth and Planetary Science Letters* 183: 441–455.
- Marsan D (2003) Triggering of seismicity at short distances following California earthquakes. *Journal of Geophysical Research* 108. <http://dx.doi.org/10.1029/2002JB001946>.
- Marzocchi W (2002) Remote seismic influence on large explosive eruptions. *Journal of Geophysical Research* 107. <http://dx.doi.org/10.1029/2001JB000307>.
- Matthews MV and Reasenberg PA (1988) Statistical methods for investigating quiescence and other temporal seismicity patterns. *Pure and Applied Geophysics* 126: 357–372.
- McGarr A, Simpson D, and Seeber L (2002) Case histories of induced and triggered seismicity. In: Lee WHK, Kanamori H, Jennings PC, and Kisslinger C (eds.) *International Handbook of Earthquake and Engineering Seismology, Part A*, pp. 647–664. Amsterdam: Academic Press.
- Meltzner AJ and Wald DJ (2003) Aftershocks and triggered events of the great 1906 California earthquake. *Bulletin of the Seismological Society of America* 93: 2160–2186.
- Meng X, Peng Z, and Hardebeck J (2013a) Seismicity around Parkfield correlates with static shear stress changes following the 2003  $M_w$  6.5 San Simeon earthquake. *Journal of Geophysical Research* 118: 3576–3591. <http://dx.doi.org/10.1002/jgrb.50271>.
- Meng X, Peng Z, Withers K, Olsen K, Yu X, and Hong B (2013b) Systematic search of missing earthquakes near the Salton Sea geothermal field and San Jacinto fault around the 2010  $M_w$  7.2 El Mayor-Cucapah earthquake. (abs.) *Seismological Research Letters* 84(2): 391.
- Miller SA (2008) Note on rain-triggered earthquakes and their dependence on karst geology. *Geophysical Journal International* 173: 334–338.
- Miyazawa M (2011) Propagation of an earthquake triggering front from the 2011 Tohoku-oki earthquake. *Geophysical Research Letters* 38: L23307. <http://dx.doi.org/10.1029/2011GL049795>.
- Miyazawa M (2012) Detection of seismic events triggered by P-waves from the 2011 Tohoku-oki earthquake. *Earth, Planets and Space* 64: 1223–1229.
- Miyazawa M and Brodsky E (2008) Deep low-frequency tremor that correlates with passing surface waves. *Journal of Geophysical Research* 113. <http://dx.doi.org/10.1029/2006JB004890>.
- Miyazawa M, Brodsky E, and Mori J (2008) Learning from dynamic triggering of low-frequency tremor in subduction zones. *Earth, Planets and Space* 60: e17–e20.
- Miyazawa M and Mori J (2005) Detection of triggered deep low-frequency events from the 2003 Tohoku-oki earthquake. *Geophysical Research Letters* 32: L10307.
- Miyazawa M and Mori J (2006) Evidence suggesting fluid flow beneath Japan due to periodic seismic triggering from the 2004 Sumatra-Andaman earthquake. *Geophysical Research Letters* 33: L05303-L. <http://dx.doi.org/10.1029/2005GL025087>.
- Miyazawa M, Nakanishi I, Sudo Y, and Ohkura T (2005) Dynamic response of frequent tremors at Aso volcano to teleseismic waves from the 1999 Chi-Chi, Taiwan earthquake. *Journal of Volcanology and Geothermal Research* 147: 173–186.
- Mohamad R, Darkal AN, Seber D, Sandoval E, Gomez F, and Barazangi M (2000) Remote earthquake triggering along the Dead Sea Fault in Syria following the 1995 Gulf of Aqaba earthquake ( $M_s = 7.3$ ). *Seismological Research Letters* 71: 47–52.
- Moran SC (2003) Multiple seismogenic processes for high-frequency earthquakes at Katmai National Park, Alaska: Evidence from stress tensor inversions of fault plane solutions. *Bulletin of the Seismological Society of America* 93: 94–108.
- Moran SC, Power JA, Stihler SD, Sanchez JJ, and Caplin-Auerback J (2004) Earthquake triggering at Alaskan volcanoes following the 3 November 2002 Denali Fault earthquake. *Bulletin of the Seismological Society of America* 94: S300–S309.
- Moran SC, Zimbelman DR, and Malone SD (2000) A model for the magmatic-hydrothermal system at Mount Rainier, Washington, from seismic and geochemical observations. *Bulletin of Volcanology* 61: 425–436.
- Mori J and Kano Y (2009) Is the 2006 Yogyakarta earthquake related to the triggering of the Sidoarjo, Indonesia mud volcano? *Journal of Geography* 118: 492–498.
- Mori J, McGee C, Talai B, and Itikarai I (1989) A summary of precursors to volcanic eruptions in Papua New Guinea. In: Latter JH (ed.) *Volcanic Hazards Assessment and Monitoring*, pp. 260–291. Berlin: Springer-Verlag.
- Nakata R, Suda N, and Tsuruoka H (2008) Non-volcanic tremor resulting from the combined effect of Earth tides and slow slip events. *Nature Geoscience* 1: 676–678.
- Nicolae AV and Troitskii PA (1987) Lithospheric studies based on array analysis of P-waves and microseisms. *Tectonophysics* 140: 103–113.
- Nostro C, Stein RS, Cocco M, Belardinelli ME, and Marzocchi W (1998) Two-way coupling between Vesuvius eruptions and southern Apennine earthquakes, Italy, by elastic stress transfer. *Journal of Geophysical Research* 103(B10): 24487–24504.
- Nur A and Booker JR (1972) Aftershocks caused by pore fluid flow? *Science* 175: 885–887.
- Obara K (2002) Nonvolcanic deep tremor associated with subduction in southwest Japan. *Science* 296: 1679–1681.
- Obara K (2003) Time sequence of deep low-frequency tremors in the southwest Japan subduction zone: Triggering phenomena and periodic activity (in Japanese). *Journal of Geography (Japan)* 112: 837–849.
- Omori F (1894) On the aftershocks of earthquakes. *Journal of the College of Science, Imperial University of Tokyo* 7: 111–120.
- Oppenheimer DH, Reasenberg PA, and Simpson RW (1988) Fault plane solutions for the 1984 Morgan Hill, California, earthquake sequence: Evidence for the state of stress on the Calaveras fault. *Journal of Geophysical Research* 93: 9007–9026.
- Pankow KL, Arabasz WJ, Pechmann JC, and Nava SJ (2004) Triggered seismicity in Utah from the 3 November 2002 Denali fault earthquake. *Bulletin of the Seismological Society of America* 94: S332–S347.
- Parsons T (2005) A hypothesis for delayed dynamic earthquake triggering. *Geophysical Research Letters* 32: L04302. <http://dx.doi.org/10.1029/2004GL021811>.
- Parsons T, Kaven JO, Velasco AA, and Gonzalez-Huizar H (2012) Unraveling the apparent magnitude threshold of remote earthquake triggering using full wave-field surface wave simulations. *Geochemistry, Geophysics, Geosystems* 13: Q06016. <http://dx.doi.org/10.1029/2012GC004164>.
- Parsons T and Velasco AA (2009) On near-source earthquake triggering. *Journal of Geophysical Research* 114: B10307. <http://dx.doi.org/10.1029/2008JB006277>.
- Parsons T and Velasco AA (2011) Absence of remotely triggered large earthquakes beyond the mainshock region. *Nature Geoscience* 4: 312–316.
- Peng Z and Chao K (2008) Non-volcanic tremor beneath the Central Range in Taiwan triggered by the 2001  $M_w$  7.8 Kunlun earthquake. *Geophysical Journal International* 175: 825–829.
- Peng Z, Chao K, Wu C, Fry B, Enescu B, and Aiken C (2012) Global observations of triggered tectonic tremor. *Seismological Research Letters* 83(2): 417.
- Peng Z, Gonzalez-Huizar H, Chao K, Aiken C, Moreno B, and Armstrong G (2013) Tectonic tremor beneath Cuba triggered by the  $M_w$  8.8 Maule and  $M_w$  9.0 Tohoku-Oki earthquakes. *Bulletin of the Seismological Society of America* 103(1): 595–600.
- Peng Z, Hill DP, Shelly DR, and Aiken C (2010a) Remotely triggered microearthquakes and tremor in central California following the 2010  $M_w$  8.8 Chile earthquake. *Geophysical Research Letters* 37: L24314.

- Peng Z, Long LT, and Zhao P (2011a) The relevance of high-frequency analysis artifacts to remote triggering. *Seismological Research Letters* 82(5): 662–856. <http://dx.doi.org/10.1785/gssrl.82.5.656>.
- Peng Z, Vidale JE, Creager KC, Rubinsteine JL, Gomberg J, and Bodin P (2008) Strong tremor near Parkfield, CA, excited by the 2002 Denali fault earthquake. *Geophysical Research Letters* 35: L23305. <http://dx.doi.org/10.1029/2008GL036080>.
- Peng Z, Vidale JE, Wech AG, Nadeau RM, and Creager KC (2009) Remote triggering of tremor along the San Andreas fault in central California. *Journal of Geophysical Research* 114. <http://dx.doi.org/10.1029/2008JB006049>.
- Peng Z, Walter J, Aster R, Nyblade A, Wiens D, and Anandakrishnan S (2014) Antarctic icequakes triggered by the 2010 Maule earthquake in Chile. *Nature Geoscience* (in press).
- Peng Z, Wang W, Chen Q-F, and Jiang T (2010b) Remotely triggered seismicity in northeast China following the 2008 Mw 7.9 Wenchuan earthquake. *Earth, Planets and Space* 62: 893–898.
- Peng Z, Wu C, and Aiken C (2011b) Delayed triggering of microearthquakes by multiple surface waves circling the Earth. *Geophysical Research Letters* 38: L04306. <http://dx.doi.org/10.1029/2010GL046373>.
- Perfettini HJ, Schmittbuhl J, and Cochard A (2003) Shear and normal load perturbations on a two-dimensional continuous fault: 2. Dynamic triggering. *Journal of Geophysical Research* 108.
- Pollitz FF and Johnston MJS (2006) Direct test of static stress versus dynamic stress triggering of aftershocks. *Geophysical Research Letters* 33. <http://dx.doi.org/10.1029/2006GL026764>.
- Pollitz FF and Sacks IS (2002) Stress triggering of the 1999 Hector Mine earthquake by transient deformation following the 1992 Landers earthquake. *Bulletin Seismological Society of America* 92: 1487–1496.
- Pollitz FF, Stein RS, Sevilgen V, and Burgmann R (2012) The 11 April 2012 east Indian Ocean earthquake triggered large aftershocks worldwide. *Nature* 490: 250–253.
- Power JA, Moran SC, McNutt SR, Stihler SD, and Sanchez JJ (2001) Seismic response of the Katmai volcanoes to the 6 December 1999 magnitude 7.0 Karluk Lake earthquake, Alaska. *Bulletin of the Seismological Society of America* 91: 57–63.
- Prejean SG and Hill DP (2009) Earthquakes, dynamic triggering of. In: Meyers R (ed.) *Complexity in Earthquakes, Tsunamis, and Volcanoes, and Forecast*, pp. 2600–2621. Berlin: Springer.
- Prejean SG, Hill DP, Brodsky EE, et al. (2004) Remotely triggered seismicity on the United States west coast following the Mw 7.9 Denali fault earthquake. *Bulletin of the Seismological Society of America* 94: S348–S359.
- Pyle DM and Pyle DL (1995) Bubble migration and the initiation of volcanic eruptions. *Journal of Volcanology and Geothermal Research* 67: 227–232.
- Richards-Dinger K, Stein RS, and Toda S (2010) Decay of aftershock density with distance does not indicate triggering by dynamic stress. *Nature* 467: 583–588.
- Richter CF (1958) *Elementary Seismology*. San Francisco, CA: Freeman and Co, 768 p.
- Rivera L and Kanamori H (2002) Spatial heterogeneity of tectonic stress in the crust. *Geophysical Research Letters* 39. <http://dx.doi.org/10.1029/2001GL013803>.
- Roeloffs E (1996) Poroelectric techniques in the study of earthquake-related hydrologic phenomena. *Advances in Geophysics* 37: 135–195.
- Rogers D and Dragert H (2003) Episodic tremor and slip on the Cascadia subduction zone: The chatter of slip. *Science* 300: 1942–1943.
- Rowe C, Christensen D, and Carver GA (2004) Preface to the issue dedicated to the 2002 Denali fault earthquake sequence. *Bulletin of the Seismological Society of America* 94: S1–S4.
- Rubinstein JL, Gomberg J, Vidale JE, et al. (2009) Seismic wave triggering of nonvolcanic tremor, episodic tremor and slip, and earthquakes on Vancouver Island. *Journal of Geophysical Research* 114: B00A01. <http://dx.doi.org/10.1029/2008JB005875>.
- Rubinstein JL, La Rocca M, Vidale JE, Creager KC, and Wech AG (2008) Tidal modulation of non-volcanic tremor. *Science* 319: 186–189.
- Rubinstein JL, Shelly DR, and Ellsworth WL (2010) Non-volcanic tremor: A window into the roots of fault zones. In: Cloetingh D and Negendank J (eds.) *New Frontiers in Integrated Solid Earth Science*, pp. 287–314. Springer: Dordrecht.
- Rubinstein JL, Vidale JE, Gomberg J, Bodin P, Creager KC, and Malone SD (2007) Non-volcanic tremor driven by large transient shear stresses. *Nature* 448: 579–582.
- Rybicki K, Kato T, and Kasahara K (1985) Mechanical interaction between neighboring active faults – static and dynamic stress field induced by faulting. *Bulletin of the Earthquake Research Institute, University of Tokyo* 60: 1–21.
- Sahagian DL and Proussevitch AA (1992) Bubbles in volcanic systems. *Nature* 359: 485.
- Sanchez JJ and McNutt SR (2004) Intermediate-term declines in seismicity at Mt. Wrangell and Mt. Veniaminof volcanoes, Alaska, following the 3 November 2002 Mw 7.9 Denali Fault earthquake. *Bulletin of the Seismological Society of America* 94: S370–S383.
- Savage JC and Clark MM (1982) Magmatic resurgence in Long Valley Caldera, eastern California. *Science* 217: 531–533.
- Savage HM and Morone C (2008) Potential for earthquake triggering from transient deformations. *Journal of Geophysical Research* 113: B05302. <http://dx.doi.org/10.1029/2007JB005277>.
- Scholz CH (1998) Earthquakes and friction laws. *Nature* 391: 37–42.
- Shapiro SA, Huenges E, and Born G (1997) Estimating the crust permeability from fluid-injection-induced seismic emission at the KTB site. *Geophysical Journal International* 131: F15–F18.
- Shelly DR, Beroza GC, and Ide S (2007) Complex evolution of transient slip derived from precise tremor locations in western Shikoku, Japan. *Geochemistry, Geophysics, Geosystems* 8: Q10014. <http://dx.doi.org/10.1029/2007GC001640>.
- Shelly DR, Beroza GC, Ide S, and Nakamura S (2006) Low-frequency earthquakes and their relation to episodic tremor and slip. *Nature* 442: 188–191.
- Shelly DR, Moran SC, and Thelen WA (2013) Evidence for fluid-triggered slip in the 2009 Mount Rainier, Washington, earthquake swarm. *Geophysical Research Letters* 40. <http://dx.doi.org/10.1029/grl.50354>.
- Shelly DR, Peng Z, Hill DP, and Aiken C (2011) Triggered creep as a possible mechanism for delayed dynamic triggering of tremor and earthquakes. *Nature Geoscience* 4: 384–388. <http://dx.doi.org/10.1038/NGE0114>.
- Shimomura Y, Nishimura T, and Sato H (2006) Bubble growth processes in magma surrounded by an elastic medium. *Journal of Volcanology and Geothermal Research* 155: 307–322.
- Sibson RH (1982) Fault zone models, heat flow, and the depth distribution of earthquakes in the continental crust of the United States. *Bulletin of the Seismological Society of America* 72: 151–163.
- Singh SK, Anderson JG, and Rodriguez M (1998) Triggered seismicity in the Valley of Mexico from major Mexican earthquakes. *Geofísica Internacional* 37: 3–15.
- Spudich P, Steck LK, Hellweg M, Fletcher JB, and Baker LM (1995) Transient stresses at Parkfield, California, produced by the M 7.4 Landers earthquake of June 28, 1992: Observations from the UPSAR dense seismograph array. *Journal of Geophysical Research* 100: 675–690.
- Stark MA and Davis SD (1995) Remotely triggered microearthquakes at The Geysers geothermal field. *California Geophysical Research Letters* 23: 945–948.
- Stacey S, Gomberg J, and Cocco M (2005) Introduction to special section: Stress transfer, earthquake triggering, and time-dependent seismic hazard. *Journal of Geophysical Research* 110. <http://dx.doi.org/10.1029/2005JB003692>.
- Steeple DW and Steeples DD (1996) Far field aftershocks of the 1906 earthquake. *Bulletin of the Seismological Society of America* 86: 921–924.
- Stein RS (1999) The role of stress transfer in earthquake occurrence. *Nature* 402: 605–609.
- Stein RS and Lisowski M (1983) The 1979 Homestead Valley earthquake sequence, California: Control of aftershocks and postseismic deformation. *Journal of Geophysical Research* 88: 6477–6490.
- Sturtevant B, Kanamori H, and Brodsky E (1996) Seismic triggering by rectified diffusion in geothermal systems. *Journal of Geophysical Research* 101: 25269–25282.
- Surve G and Mohan G (2012) Possible evidence of remotely triggered and delayed seismicity due to the 2001 Bhuj earthquake ( $M_w=7.6$ ) in western India. *Natural Hazards* 64: 299–310.
- Tanaka S, Ohtake M, and Sato H (2004) Tidal triggering of earthquakes in Japan related to the regional tectonic stress. *Earth, Planets and Space* 56: 511–515.
- Tang C-C, Peng Z, Chao K, Chen C-H, and Lin C-H (2010) Detecting low-frequency earthquakes within the non-volcanic tremor in southern Taiwan triggered by the 2005  $M_w$  8.6 Nias earthquake. *Geophysical Research Letters* 37: L16307.
- Tang C-C, Peng Z, Lin C-H, Chao K, and Chen C-H (2013) Statistical properties of low-frequency earthquakes triggered by large earthquakes in Southern Taiwan. *Earth and Planetary Science Letters* 373: 1–7, j.epsl.2013.04.039.
- Tape C, West M, Silwal V, and Ruppert N (2013) Earthquake nucleation and triggering on an optimally oriented fault. *Earth and Planetary Science Letters* 363: 231–241.
- Thomas AM, Burgmann R, Shelly DR, Beeler NM, and Rudolph ML (2012) Tidal triggering of low frequency earthquakes near Parkfield, California: Implications for fault mechanics within the brittle-ductile transition. *Journal of Geophysical Research* 117: B05301. <http://dx.doi.org/10.1029/JB009036>.
- Thomas AM, Nadeau RM, and Burgmann R (2009) Tremor-tide correlations and near-lithostatic pore pressure on the deep San Andreas fault. *Nature* 462: 1048–1052.
- Tibi R, Wiens DA, and Inoue H (2003) Remote triggering of deep earthquakes in the 2002 Tonga sequence. *Nature* 424: 921–925.
- Toda S, Stein R, Beroza G, and Marsan D (2012) Aftershocks halted by static stress shadows. *Nature Geoscience* 5(6): 410–413.
- Toda S, Stein RS, and Lin J (2011) Widespread seismicity excitation throughout central Japan following the 2011  $M=9.0$  Tohoku earthquake and its interpretation by

- Coulomb stress transfer. *Geophysical Research Letters* 38: L00G03. <http://dx.doi.org/10.1029/2011GL047834>.
- Tolstoy M, Vernon FL, Orcutt JA, and Wyatt FK (2002) Breathing of the seafloor: Tidal correlations of seismicity at Axial volcano. *Geology* 30: 503–506.
- Ukawa M, Fujita E, and Kumagai T (2002) Remote triggering of microearthquakes at the Iwo-Jima volcano. *Journal of Geography* 111: 277–286.
- van der Elst NJ and Brodsky EE (2010) Connecting near-field and far-field earthquake triggering to dynamic strain. *Journal of Geophysical Research* 115. <http://dx.doi.org/10.1029/2009JB006681>.
- van der Elst NJ, Brodsky EE, Le Bas P-Y, and Johnson PA (2012) Acoustic compaction in steady shear flow: Experimental evidence for suppression of shear dilatancy by internal acoustic vibrations. *Journal of Geophysical Research* 117: B09314. <http://dx.doi.org/10.1029/2011B008927>.
- Velasco AA, Hernandez S, Parsons T, and Pankow K (2008) Global ubiquity of dynamic earthquake triggering. *Nature Geoscience* 1: 375–379.
- Vohis RC (1967) *Hydrologic Effects of the Earthquake of March 27, 1964, Outside Alaska*. Washington, DC: US Geological Survey.
- Voisin C, Campillo M, Ionescu IR, Cotton F, and Scotti O (2000) Dynamic versus static stress triggering and friction parameters: Inferences from the November 23, 1980, Irpinia earthquake. *Journal of Geophysical Research* 105: 21647–21658.
- Voisin C, Cotton F, and Di Carli S (2004) A unified model for dynamic and static stress triggering of aftershocks, antishocks, remote seismicity, creep events, and multisegmented rupture. *Journal of Geophysical Research* 109. <http://dx.doi.org/10.1029/2003JB002886>.
- Walter TR (2007) How a tectonic earthquake may wake up volcanoes: Stress transfer during the 1996 earthquake-eruption sequence at the Karymsky volcanic group, Kamchatka. *Earth and Planetary Science Letters* 264: 347–359.
- Walter TR, Wang R, Acocella V, Neri M, Grosser H, and Zschau J (2009) Simultaneous magma and gas eruptions at three volcanoes in southern Italy: An earthquake trigger? *Geology* 37: 251–254.
- Wang T-H, Cochran ES, Agnew D, and Oglesby DD (2013) Infrequent triggering of tremor along the San Jacinto Fault near Anza, California. *Bulletin of the Seismological Society of America* 102: 2482–2497.
- Wang C-Y and Manga M (2009) Hydrologic response to earthquakes and a general metric. *Geofluids* 10: 206–216.
- Wang C-Y and Manga M (2010) *Earthquakes and Water*, 218 pp. Springer.
- Wech AG, Boose CM, Stern TA, and Townsend J (2012) Tectonic tremor and deep slow slip on the Alpine Fault. *Geophysical Research Letters* 39: L10303. <http://dx.doi.org/10.1029/2012GL051751>.
- Wen K-L, Beresnev IA, and Cheng S (1996) Moderate-magnitude seismicity remotely triggered in the Taiwan region by large earthquakes around the Philippine Sea Plate. *Bulletin of the Seismological Society of America* 86: 843–847.
- West M, Sanchez JJ, and McNutt SR (2005) Periodically triggered seismicity at Mount Wrangell, Alaska, after the Sumatra earthquake. *Science* 308: 1144–1146.
- Wiemer S (2001) A software package to analyze seismicity: ZMAP. *Seismological Research Letters* 72: 373–380.
- Wilcock WS (2001) Tidal triggering of microearthquakes on the Juan de Fuca Ridge. *Geophysical Research Letters* 28: 3999–4002.
- Wu P and Johnston P (2000) Can deglaciation trigger earthquakes in North America? *Geophysical Research Letters* 27: 1323–1326.
- Wu C, Peng Z, Wang W, and Chen Q-F (2011) Dynamic triggering of shallow earthquakes near Beijing, China. *Geophysical Journal International* 185: 1321–1334.
- Wu J, Peng Z, Wang W, Gong X, Chen Q, and Wu C (2012) Comparisons of dynamic triggering near Beijing, China following the recent Sumatra earthquakes. *Geophysical Research Letters* 39: L21310. <http://dx.doi.org/10.1029/2012GL053515>.
- Yamazaki K, Teraishi M, Komatsu S, Sonoda Y, and Kano Y (2011) On the possibility of the 2011 Tohoku-oki earthquake reactivating Shimoe-dake volcano, southwest Japan: Insight from strain data measured in vaults. *Natural Hazards and Earth System Science* 11: 2655–2661.
- Yang H and Peng Z (2013) Lack of additional triggered tectonic tremor around the Simi Valley and the San Gabriel Mountain in Southern California. *Bulletin of the Seismological Society of America* 103: 3372–3378.
- Yukutake Y, Honda R, Harada M, Aketagawa T, Ito H, and Yoshida A (2011) Remotely triggered seismicity in the Hakone volcano following the 2011 off the Pacific coast of Tohoku earthquake. *Earth, Planets and Space* 63: 737–740. <http://dx.doi.org/10.5047/eps.2011.05.004>.
- Yukutake Y, Miyazawa M, Honda R, et al. (2013) Remotely triggered seismic activity in Hakone volcano during and after the passage of surface waves from the 2011 M 9.0 Tohoku-Oki earthquake. *Earth and Planetary Science Letters* 373(1): 205–216.
- Zigone D, Rivet D, Radiguest M, et al. (2012) Triggering of tremors and slow slip event in Guerrero, Mexico, by the 2010 Mw 8.8 Maule, Chile, earthquake. *Journal of Geophysical Research* 117: B09304. <http://dx.doi.org/10.1029/2012JB009160>.
- Ziv A (2006) On the role of multiple interactions in remote aftershock triggering: The Landers and the Hector Mine case studies. *Bulletin of the Seismological Society of America* 96: 80–89.
- Zoback MD and Zoback ML (2002) State of stress in the Earth's lithosphere. In: Lee WHK, Kanamori H, Jennings PC, and Kisslinger C (eds.) *International Handbook of Earthquake and Engineering Seismology, Part A*, pp. 559–568. Amsterdam: Academic Press.